Hindawi
Adsorption Science & Technology
Volume 2022, Article ID 3030519, 50 pages
https://doi.org/10.1155/2022/3030519

Review Article

Review of the Pressure Swing Adsorption Process for the Production of Biofuels and Medical Oxygen: Separation and Purification Technology

Jesse Y. Rumbo Morales,[1] **Gerardo Ortiz-Torres**,[1] **Rodolfo Omar Domínguez García**,[1] **Carlos Alberto Torres Cantero**,[2,3] **Manuela Calixto Rodriguez**,[4] **Estela Sarmiento-Bustos**,[4] **Edén Oceguera-Contreras**,[1] **Alberto Arturo Flores Hernández**,[5] **Julio César Rodríguez Cerda**,[1] **Yehoshua Aguilar Molina**,[1] **and Mario Martínez García**[1]

[1]*Departamento de Ciencias Computacionales e Ingenierías, Universidad de Guadalajara, Centro Universitario de los Valles, Carretera Guadalajara-Ameca Km.45.5 C.P. 46600, Ameca, Jalisco, Mexico*
[2]*Tecnológico Nacional de México Campus Colima, Mexico*
[3]*Universidad de Colima; Facultad de Ingeniería Mecánica y Eléctrica; Carretera Colima-Coquimatlan Km 9, Valle de las Huertas, Coquimatlán 28400, Colima, Mexico*
[4]*División Académica de Mecánica Industrial, Universidad Tecnológica Emiliano Zapata del Estado de Morelos, Av. Universidad Tecnológica No. 1, Col. Palo Escrito, C.P. 62760, Emiliano Zapata, Morelos, Mexico*
[5]*Tecnológico Nacional de México/Instituto Tecnológico de Matamoros, Mexico*

Correspondence should be addressed to Rodolfo Omar Domínguez García; odomi@academicos.udg.mx

Received 10 June 2022; Revised 24 August 2022; Accepted 6 October 2022; Published 29 October 2022

Academic Editor: Eloy S. Sanz

The production of biofuels has had a great impact on climate change and the reduction of the use of fossil fuels. There are different technologies used for the separation and production of biofuels, which allow having compounds such as ethanol, methane, oxygen, and hydrogen, one of these promising technologies is the Pressure Swing Adsorption process (PSA). The objectives of this article focus on the production and purification of compounds that achieve purities of 99.5% bioethanol, 94.85% biohydrogen, 95.00% medical oxygen, and 99.99% biomethane through the PSA process; also, a significant review is contemplated to identify the different natural and synthetic adsorbents that have greater adsorption capacity, the different configurations in which a PSA operates are studied and identified, and the different mathematical models that describe the dynamic behavior of all the variables are established that interact in this PSA process, parametric studies are carried out in order to identify the variables that have the greatest effect on the purity obtained. The results obtained in this review allow facilitating the calculation of parameters, the optimization of the process, the automatic control to manipulate certain variables and to achieve the rejection of disturbances to have a recovery and production of biofuels with a high degree of purity.

1. Introduction

Currently, PSA processes are displacing other distillation technologies that aim to separate chemical compounds from a mixture at the nanomolecular level, these present a significant contribution in obtaining compounds such as oxygen (O_2), nitrogen (N_2), hydrogen (H_2), carbon dioxide (CO_2), ethanol (C_2H_5OH), and methane (CH_4). The PSA process contemplates at least 2 columns refilled with adsorbents (natural or synthetic), to be able to carry out the adsorption stage (production) and the regeneration stage (release of the active sites of the adsorbent) synchronously. These 2 stages

are carried out through steps, which can be adsorption, depressurization, purge, equalization, and repressurization. The PSA process has a cyclical nature, therefore the pressure, temperature, and molar composition profiles will have an oscillatory dynamic generated by the pressure changes inside the columns. Pressure changes can go from a high pressure (200 kPa 4000 kPa) and down to a vacuum pressure between the ranges of 100 kPa and 10 kPa. The approach of these pressure ranges is derived from experimental tests that show that at high pressure, a greater number of molecules or atoms are adsorbed, being retained on the surfaces of the adsorbents (selectivity over the adsorbed molecules or atoms), and at low pressure that can easily break the weak bond that has formed between the adsorbent and the adsorbed molecules or atoms, resulting in a release of the active sites of the adsorbent. These adsorbents can be zeolites, silica gel, activated carbon, clays, porous glass, montmorillonite, halloysite, silicon dioxide, mesoporous silica, etc. These materials contain nanomolecular pores ranging from 1 to 24 Armstrong (Å); the more contact surface they have, the greater adsorption capacity they will present. Metal-Organic Frameworks (MOFs) have emerged as novel fabulous materials for applications in numerous fields, doing to their exceptional physicochemical characteristics such as high surface area, large porosity with tunable pore properties, presence of abundant active sites, and ease of functionalization [1, 2].

For the PSA process to work synchronously and autonomously, it is necessary to contemplate valves (on-off and proportional) that connect all the columns to achieve the operational cyclical functioning of the process, obtaining separations of chemical compounds with a high degree of purity. Likewise, it is necessary to implement pressure, temperature, flow, and purity sensors along with the columns to acquire as much information or data as possible about these important variables that influence the PSA process.

PSA processes have been involved in several alternatives; one of them is the production of biofuel from renewable raw materials and biomass. Another use of this process is the purification of oxygen, separating it from the gases that pollute the environment (CO and CO_2), which are generated by automobiles and industries. For these reasons, the PSA process is considered a solution to climate change. Currently, with what is being experienced on COVID-19, the design and development of oxygen purifiers-generators are necessary due to the demand that is currently being met and the use of this PSA process is necessary to be used as a separator and gas purifier, and to produce 99% oxygen or according to the user's need.

One of the works found related to the PSA process is the one presented in [3], which reviewed the principles of the PSA process for the capture of carbon dioxide. Wiheeb et al. presented previous works on modeling and comparisons with experimental development of the PSA process. Mention is made of the importance of the steps that contemplate the adsorption and regeneration stages, as well as maintaining stable high temperatures since it favors the regeneration of the adsorbent.

Later in [4], advanced technologies related to hot gas carbon capture and hydrogen production from carbon-based fuels using the PSA process are reviewed. Zhu et al. presented important advances in the development of adsorption kinetic models, the study of adsorption mechanisms, synthesis of efficient CO_2 adsorbents, design, and optimization of adsorption/desorption reactor processes, and integration of purification systems, as well as main challenges and perspectives for the fundamental and pilot study. The development of the system at scale is discussed. Recent advances in the development of high temperature CO/CO_2 purification technologies for hydrogen-rich gas were summarized.

Likewise in [5], Abd et al. described the fundamentals of the PSA process by investigating the main innovative process engineering approaches that improved the performance of the PSA process. Previous research on PSA, simulation, and experimental development for biogas upgrading (biomethane purification) exists and highlights significant findings. In addition, their work analyzes the impact of some parameters on the performance of the PSA process, such as bed porosity, adsorption pressure and time, PSA unit size, and purge/feed ratio.

In [6], Luberti et al. performed a systematic review of the Polybed H_2 PSA process, which includes more than six beds and a complex cycle configuration, showing that it can maximize H_2 recovery and yield, exceeding 90%. A bespoke Polybed PSA process designed for the simultaneous production of high purity hydrogen and carbon dioxide (CO_2) was also reviewed in light of recent international directives aimed at reducing CO_2 emissions and producing blue hydrogen.

Likewise in [7], the progress made in the implementation of mathematical models, simulation, and optimization methods for the improvement of biogas with emphasis on processes based on adsorption are presented. In their work, Hosseini et al. described strategies and methodologies for the development of mathematical models and process simulations based on transport mechanisms, considering the PSA, VPSA (Vacuum Pressure Swing Adsorption), TSA (Temperature Swing Adsorption) process, and fixed adsorption beds for trace removal. Based on studies to date, these processes have offered methane purity and recovery within an adjustable range of 50 to 99% and 75 to 99.4%, respectively.

Later in [8], Zhang et al. carried out a review of the literature on the analytical part of the PSA process, focused on the numerical development to carry out the modeling, optimization, and control of the PSA process. It was determined that the combination of deep learning technology with optimization algorithms based on artificial intelligence and advanced control strategies is of great importance.

This work has several contributions, one of them focuses on providing relevant data on adsorbents for the separation and purification of bioethanol, biohydrogen, medical oxygen, and biomethane; another of the contributions is to present the current reports of parameters to configure and model a PSA process, depending on the compound to be purified. Another important contribution

Table 1: Nomenclature.

Parameter	Description	Units
a	Specific particle surface	m^2m^{-3}
a_{Hi}	Specific heat exchanger surface	m^2m^{-3}
a_p	Specific particle surface per unit volume bed	m^2m^{-3}
A	Area	
AA	Placeholder variable used for Dubinin-Astakhov isotherm evaluation	
b	Kinetic Langmuir factor	bar^{-1}
c_{bi}	Bulk gas phase concentration	$kmolm^{-3}$
c_i	Molar concentration of component i	$kmolm^{-3}$
c_{msi}	Macropore gas phase concentration	$kmolm^{-3}$
c_{sol}	Concentration of solid phase reactant	$kmolkg^{-1}$
c_{pai}	Specific heat capacity of adsorbed phase	$MJkmol^{-1}K^{-1}$
c_{pcat}	Specific heat capacity of catalyst	$MJkg^{-1}K^{-1}$
c_{pg}	Specific gas phase heat capacity at constant pressure	$MJkmol^{-1}K^{-1}$
c_{ps}	Specific heat capacity of adsorbent	$MJkg^{-1}K^{-1}$
c_{pW}	Specific heat capacity of column wall	$MJkg^{-1}K^{-1}$
c_{vg}	Specific gas phase heat capacity at constant volume	$MJkmol^{-1}K^{-1}$
D_B	Bed diameter	m
D_{efc}	Effective micropore diffusion coefficient	m^2s^{-1}
D_{efp}	Effective macropore diffusion coefficient	m^2s^{-1}
D_{ek}	Effective adsorbed phase diffusivity of component *i*	m^2s^{-1}
D_{ki}	Knudsen diffusion coefficient of component *i*	m^2s^{-1}
D_{mi}	Mean molecular diffusion coefficient of component *i*	$MJkmol^{-1}$
E_{act}	Activation energy for Arrhenius relationship	$MJkmol^{-1}$
E_{ii}	Radial dispersion coefficient of component *i*	m^2s^{-1}
E_{zi}	Axial dispersion coefficient of component *i*	m^2s^{-1}
H_{amb}	Wall-ambient heat transfer coefficient	MWm^2K^{-1}
H_B	Height of adsorbent layer	m
H_i	Rate of change of heat of adsorbed phase	$MJm^{-3}s^{-1}$
H_R	Combined heats of homogenous and heterogeneous reactions	$MJm^{-3}s^{-1}$
H_{Rcat}	Heat of catalytic reaction	$MJkmol^{-1}$
H_{Rgas}	Gas phase heat of reaction	$MJkmol^{-1}$
H_{Ti}	Heat of adsorption contribution to solid phase energy balance	$MJm^{-3}s^{-1}$
H_W	Gas-wall heat transfer coefficient	$MJm^{-3}s^{-1}$
ΔH_i	Heat of adsorption of component *i*	$MJkmol^{-1}$
HTC	Gas-solid heat transfer coefficient	$MJm^{-3}s^{-1}$
IP	Isotherm parameter, units depend on isotherm	
j	Colburn j-factor for heat or mass transfer	
$J_{ads,i}$	Mass transfer rate of component *i* owing to adsorption	$kmolm^{-3}s^{-1}$
$J_{cat,reac,i}$	Mass transfer rate of component *i* owing to heterogeneous catalytic reactions	$kmolm^{-3}s^{-1}$
$J_{gas,\ reac\ ,i}$	Mass transfer rate of component *i* owing to homogenous, gas phase reactions	$kmolm^{-3}s^{-1}$
J_i	Mass transfer rate of component *i* to/from adsorbent	$kmolm^{-3}s^{-1}$
$k_{0,i}$	Pre-exponential factor for Arrhenius relationship	ms^{-1}
$k_{0P,i}$	Pre-exponential factor for pressure dependent Arrhenius relationship	ms^{-1}
k_{fi}	Film mass transfer coefficient of component *i*	ms^{-1}
k_{fi}	Gas phase thermal conductivity	$MWm^{-1}K^{-1}$
k_{gr}	Effective radial gas phase thermal conductivity	$MWm^{-1}K^{-1}$
k_i	Effective, lumped mass transfer coefficient of component *i*	s^{-1}

Table 1: Continued.

Parameter	Description	Units
k_s	Solid thermal conductivity	$MWm^{-1}K^{-1}$
k_{gs}	Effective axial gas phase thermal conductivity	$MWm^{-1}K^{-1}$
k_{sr}	Effective radial solid phase thermal conductivity	$MWm^{-1}K^{-1}$
k_{sg}	Effective axial solid phase thermal conductivity	$MWm^{-1}K^{-1}$
k_W	Thermal conductivity of column wall	$MWm^{-1}K^{-1}$
K_{mac}	Macropore mass transfer coefficient	s^{-1}
K_{mic}	Micropore mass transfer coefficient	s^{-1}
K_p	Darcy's constant	$barsm^{-2}$
K_{pi}	Macropore diffusion coefficient	m^2s^{-1}
L	Length of horizontal bed	m
M	Molecular weight	$kgkmol^{-1}$
MTC_g	Gas film mass transfer coefficient	s^{-1}
MTC_s	Solid film mass transfer coefficient	s^{-1}
P	Pressure	bar
P_{sat}	Saturation pressure	bar
Q_{Hi}	Heat transfer rate to internal heat exchanger	$MJm^{-2}s^{-1}$
r	Radial coordinate (in packed bed or particle)	m
r_c	Microparticle (crystal) radius	m
r_p	Particle radius	m
R	Universal gas constant	$barm^{-3}kmol^{-1}K^{-1}$
R_{cat}	Catalytic reaction rate	$kmolkg^{-1}s^{-1}$
R_{gas}	Gas phase reaction rate	$kmolm^{-3}s^{-1}$
R_{sol}	Solid phase reaction rate	$kmolkg^{-1}s^{-1}$
t	Time	s
t_{cycle}	Adsorption cycle time	s
T	Temperature	K
T_0	Initial temperature	K
T_{amb}	Ambient temperature	K
T_c	Critical temperature	K
T_s	Solid phase temperature	K
T_g	Gas phase temperature	K
T_{Hi}	Heat exchange medium temperature	K
T_W	Wall temperature	K
Tort	Adsorbent tortuosity	
v_g	Gas phase superficial velocity	ms^{-1}
W_i	Loading	$kmolkg^{-1}$
W_i^0	Pure component loading of component *i*	$kmolkg^{-1}$
y_i	Mole fraction of component *i* in the gas phase	$kmolkg^{-1}$
z	Axial coordinate	m
Greek symbols		
ϵ_i	Bed (interparticle) voidage	$m^3\,m^{-3}$
ϵ_p	Intraparticle voidage	$m^3\,m^{-3}$
μ	Dynamic viscosity	$N\,s\,m^{-2}$
Ω	Parameter in Glueckauf expression	
ψ	Particle shape factor	
ρ_b	Bed packing density	$kg\,m^{-3}$
ρ_g	Gas phase molar density	$kmol\,km^{-3}$
ρ_p	Particle density	$kmol\,km^{-3}$

Table 1: Continued.

Parameter	Description	Units
ρ_s	Adsorbent bulk density	kg m^{-3}
Subscripts		
b	Bulk or packed bed	
F	Feed stream	
g, s	Gas and solid phase	
i	Component water (w) or ethanol (e)	
p	Particle	

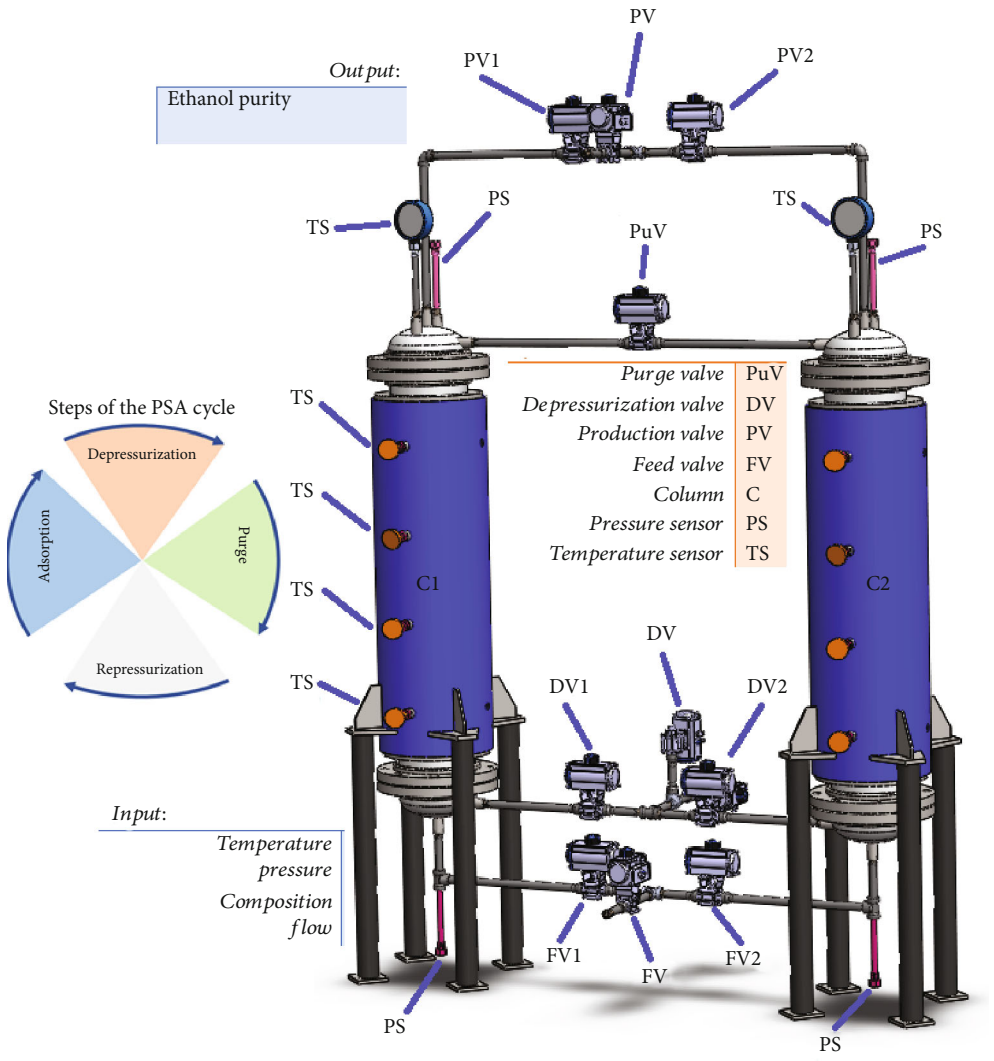

Figure 1: Schematic diagram of the PSA process.

is the parametric study that demonstrates the possible input variables that can affect the purity obtained as a final product, which can also be defined as manipulated variables that can control the desired purity in the face of disturbances, with the aim of being able to keep the purity stable and meet international standards for the use as fuel or medical oxygen. The parametric study will allow defining optimal parameters that favor the start-up of the PSA process to have greater production and recovery. Likewise, obtaining input and output data is very useful for designing neural network structures with the aim of predicting the dynamic behavior of the PSA process.

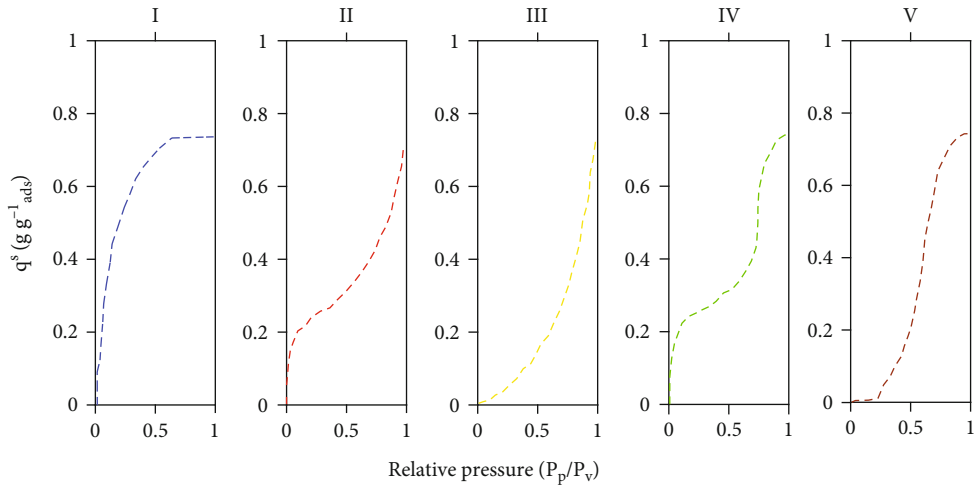

Figure 2: Adsorption isotherms.

Table 1 shows the nomenclature that will be used for this work, which has a great contribution to PSA processes for the production of biofuels and medical oxygen.

This work is presented as follows. In Section 2, the complete model of a PSA process is shown, which includes equations of pressure, temperature, flow, and mole fraction in function of time and space (axial and radial part). In Sections 3–6, the results of the works found on the purification and production of bioethanol, biohydrogen, medical oxygen, and biomethane are shown, and the different works that use the PSA process are visualized in comparative tables taking into account the sizing, the number of columns, the type of adsorbent, the pressure and temperature ranges, the feed composition, and the number of PDEs that are considered to obtain approximate solutions to the PSA process. Likewise, simulations and a demonstrative table (parametric study) are presented that allow defining the possible input variables that can affect the purity of bioethanol, biohydrogen, medical oxygen, and biomethane obtained as a final product.

2. Schematic and Modeling of the PSA Process

Gas-phase adsorption is currently being used to purify and separate chemical compounds, natural gas, and petrochemicals since they present better-operating conditions and reduce energy and equipment costs.

The adsorbent must have selectivity over the molecule or atom to be retained on its surface, allowing the separation and purification of the other compounds that passes through it. Adsorbents must withstand high temperatures and work under different pressure conditions (high and low).

For PSA processes, there may be variations in your mathematical model, this will depend on the need for the data that is required to be obtained, that is, the following assumptions can be considered:

(1) They can work in isothermal or nonisothermal conditions

(2) Heat exchange with environment

(3) Gas-solid heat transfer

(4) Enthalpy of mixing is negligible

(5) Include wall energy data

(6) Heat of adsorption

(7) Thermal conductivity of gas and thermal conductivity of solid

(8) Compression

(9) The system is fully mixed in the radial direction

(10) Plug flow with axial dispersion occurs

(11) The gas phase is ideal or nonideal

(12) The driving force is based on a gas or solid film, and is either linear or quadratic

(13) Gas phase pressure is either constant or the pressure varies according to a laminar or turbulent flow momentum balance

(14) Mass transfer coefficients are either constant or vary with local conditions

(15) Mass transfer is described using a lumped overall resistance, or by a model that accounts separately for micro- and macropore effects

(16) Adsorption isotherms are either applicable for single or multicomponent adsorption

The cyclical nature of the PSA process and its operating conditions determine the type of model to use. For example, a separation process for producing pure oxygen from air

Table 2: Comparison of the thermodynamic values of various adsorbents as a function of temperature.

Reference	Adsorbents	Temperature K	Maximum adsorption capacity Q ($g_{water}\ g_{ads}^{-1}$)	Langmuir constant	Adsorption time
[19]	Cornmeal	333.15	0.029	—	—
		364.15	0.025	—	300 min
[20]	ZSG-1	303.15	0.1046	—	—
	ZSG-1	352.15	0.1241	—	—
	ZSG-1	357.15	0.1499	—	—
	ZSG-1	362.15	0.1511	—	—
	ZSG-1	370.15	0.1529	—	80 min
[21]	Silicalite	298	0.116	—	9 min
[10]	Clinoptilolite	373	0.198	—	—
[11]	Zeolite 3A	348	0.18	25	—
	3A	373	0.171	8	—
	3A	398	0.162	2.9	—
	3A	423	0.135	1.19	—
	3A	448	0.108	0.54	—
[12]	LTA-K	298	0.130	0.735	—
	LTA-Na	298	0.150	0.563	—
	LTA-ca	298	0.094	0.589	—
	FAU-Na	298	0.166	0.611	—
	MOR-Na	298	0.045	0.403	—
[14]	Zeolite 3A	323.15	0.1915	0.00791	200 min
	3A	343.158	0.180	0.00655	180 min
	Heulandite-Sonora	323.15	0.1	0.00925	185 min
	Heulandite-Sonora	343.158	0.097	0.00345	150 min
	Clinoptilolite-Potosí	323.15	0.097	0.00491	180 min
	Clinoptilolite-Potosí	343.158	0.094	0.00253	145 min
[13]	Clinoptilolite	293.15	0.161	—	24 h
[22]	Clinoptilolite	283	0.13428	0.0179	—
	Clinoptilolite	298	0.12618	0.0156	—
	Clinoptilolite	313	0.12402	0.0125	24 h
	Clinoptilolite	328	0.11916	0.0113	—
	Clinoptilolite	343	0.11304	0.0106	—
[23]	Sylobead 3A	373.15	0.198	—	—
[24]	Zeolite 3A	393.15	0.085	0.1006	135 min
	3A	413.15	0.065	0.0828	75 min
[25]	Zeolita NaA	378	0.155	—	
[15]	Philipsita	326.3	0.0432	0.76	57 min
	Philipsita 0.5 M	326.3	0.0800	0.81	34 min
	Philipsita 0.75 M	326.3	0.0770	0.83	35 min
	Philipsita 1 M	326.3	0.1054	1.2	55 min
	Philipsita 2 M (natural)	326.3	0.1016	0.93	41 min

Table 2: Continued.

Reference	Adsorbents	Temperature K	Maximum adsorption capacity Q $(g_{water}\, g_{ads}^{-1})$	Langmuir constant	Adsorption time
[16]	ACF	298.15	0.1571	0.58	600 s
	ACF	308.15	0.1567	0.30	—
	ACF	318.15	0.1576	0.15	1800 s
	ACF-850	298.15	0.2266	0.22	680 s
	ACF-850	308.15	0.2244	0.12	—
	ACF-850	318.15	0.2264	0.06	700 s
	ACF-750	298.15	0.1488	0.59	200 s
	ACF-750	308.15	0.1477	0.29	—
	ACF-750	318.15	0.1456	0.16	450 s
[17]	ZIF-8	298.15	0.45661	5.30	5 min
	ZIF-67	298.15	0.4633	5.35	5 min
[26]	Zeolita 4A	336.15	0.1030	—	57 min
	3A	298.15	0.249	0.317	40 min
	3A	313.15	0.238	0.153	30 min
	3A	323.15	0.220	0.090	22 min
	3A Sintética)	333.15	0.200	0.052	20 min
[18]	Clinoptilolite (1-2 mm)	298.15	0.405	2019.56	540 s
	Clinoptilolite (3 mm)	298.15	0.31	1386.20	720 s
	Clinoptilolite (5 mm)	298.15	0.29	3521.28	180 s
	LV-NENG	298.15	0.275	1353.44	720 s
	Sorbead	298.15	0.26	1053.11	540 s

Table 3: Works reported on the different configurations of PSA processes for purification of bioethanol.

Reference	Experimental /simulated	PSA cycles	Pressure swing (kPa)	Bed regeneration time (min)	Ethanol feed (% wt)
[32]	Simulated	2 beds 4 steps	200 to 13	5.3	90
[33]	Experimental	2 beds 4 steps	(200-240) to 20	7	95
[34]	Experimental	2 beds 5 steps	379.79 to 13.8	5.4	92
[35]	Experimental	2 beds 4 steps	120 to 20	3.8	93.2
[36]	Experimental	3 beds 4 steps	(120, 130) to 20	6.6	87
[37]	Experimental	2 beds 4 steps	303 to 30	45	88.57
[14]	Simulated	2 beds 4 steps	204.5 to 13.4	2.91	90
[30]	Simulated	2 beds 2 steps	340 to 30	—	86

requires a different model to that for a purification process for the production and separation of dehydrated ethanol. PSA process models use a set of partial differential equations to represent moment balance, energy balance, and material balances across the column.

From all this analysis, a general mathematical model of the PSA process is established, this involves most of the equations necessary to determine the important dynamics that characterize the PSA process, this detailed general model is shown in the following:

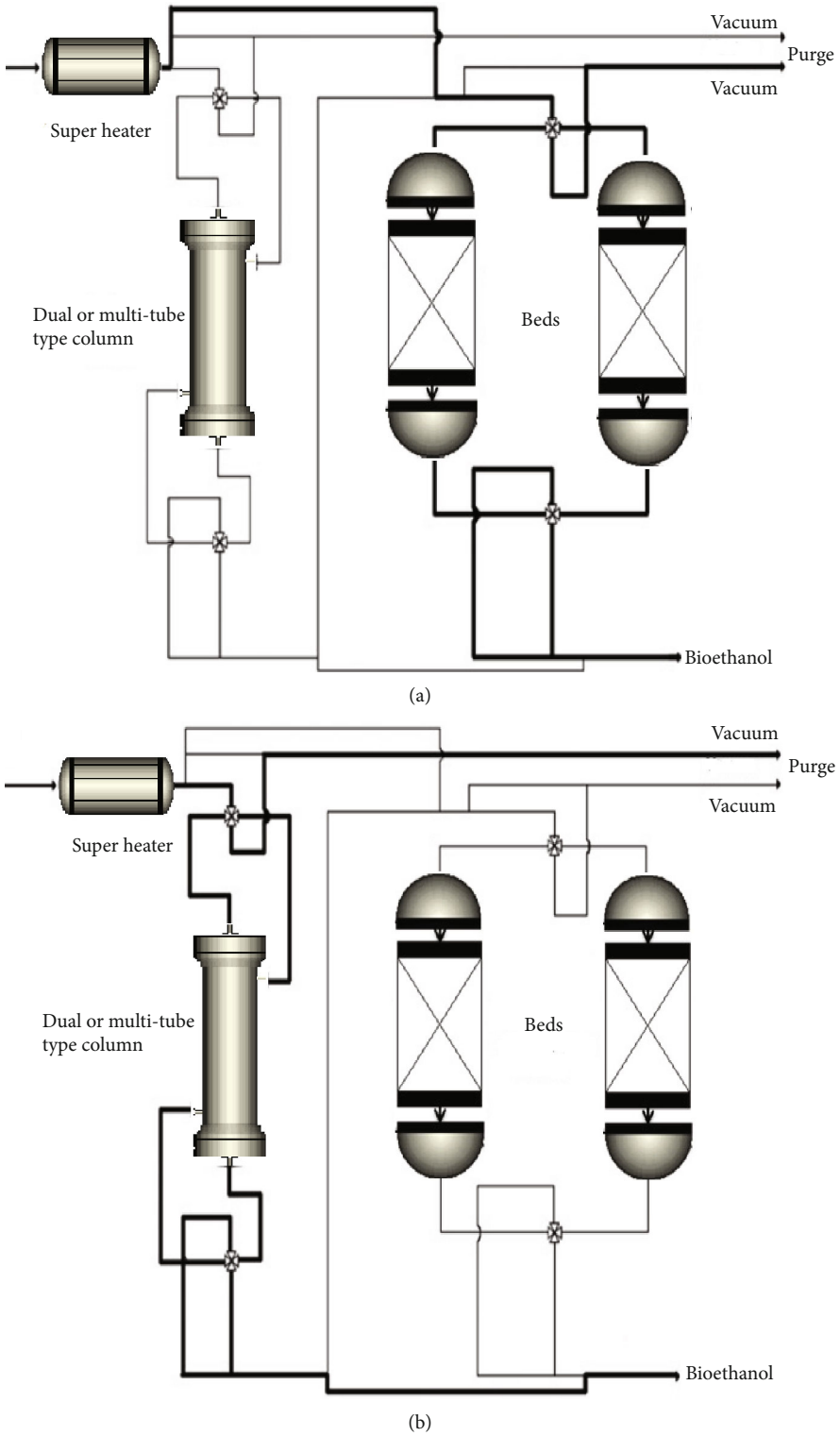

Figure 3: Continued.

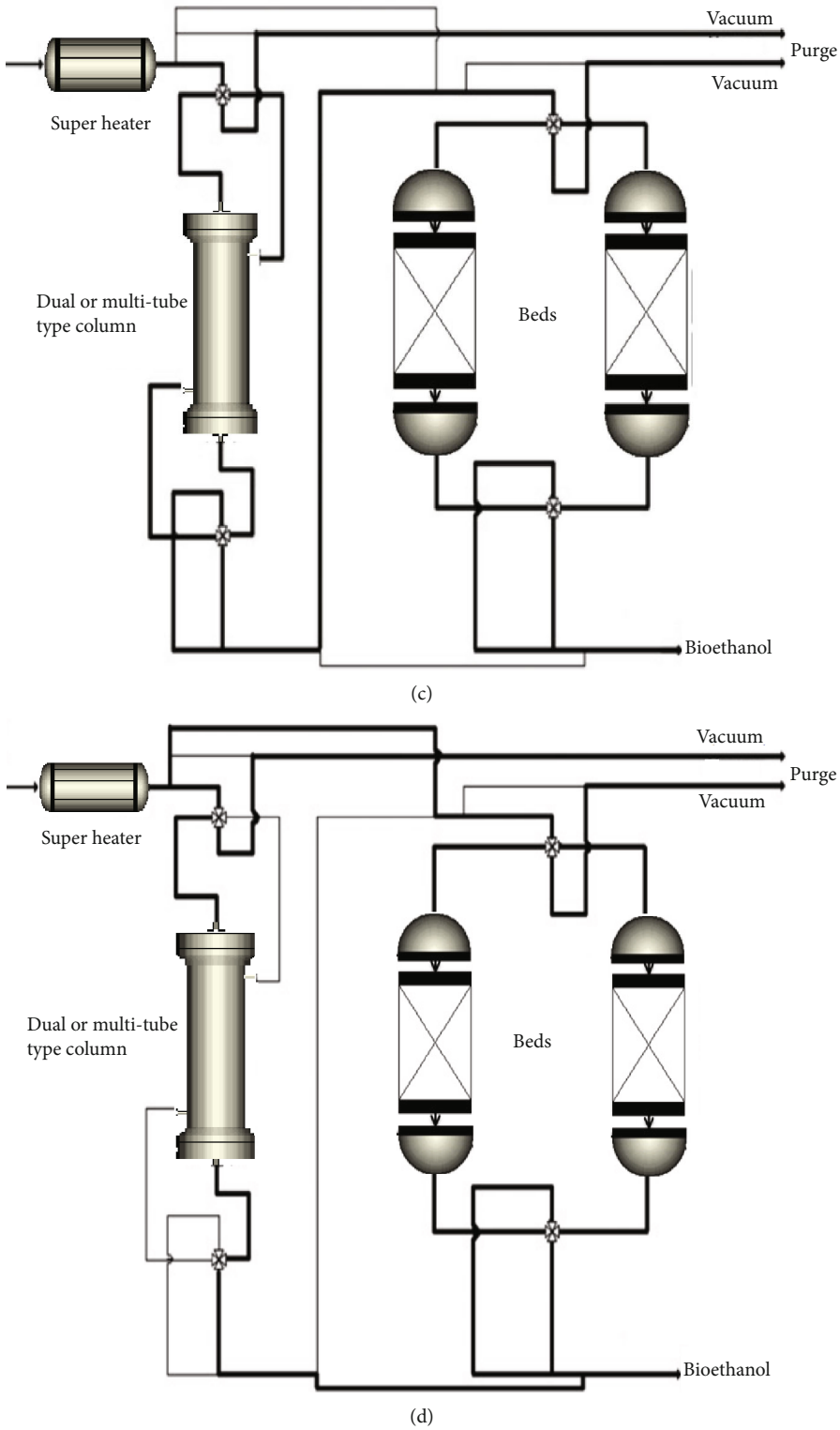

Figure 3: Schematic diagram of the PSA process using different types of connection configurations: (a) two beds, (b) multiple tubes, (c) two-pass beds, and (d) three beds.

Table 4: Distributed parameter models of the PSA processes for bioethanol production.

Reference	Equations governing the PSA process (nonlinear model)	Temperature effects	Pressure effects
[34]	6 PDE	Consider adsorption isotherms	Consider pressure gradient
[37]	5 PDE	Consider adsorption isotherms	Consider pressure gradient
[29]	6 PDE	Consider adsorption isotherms	No pressure gradient
[23]	3 PDE	Does not present adsorption isotherms	Consider pressure gradient
[39]	6 PDE	Consider adsorption isotherms	Consider pressure gradient
[40]	3 PDE	Does not present adsorption isotherms	Consider pressure gradient

Table 5: Governing equations and simplifications for production and purification of bioethanol.

Mass balance for adsorbing component	$\frac{\partial Y_i}{\partial t} = D_{\text{ax}} \frac{\partial^2 Y_i}{\partial z^2} - \frac{u \partial Y_i}{\epsilon \partial z} - \frac{(1-\epsilon)}{\epsilon} \rho_s \frac{\text{RT} \partial q_i}{P \partial t} (1 - Y_i)$
Overall mass balance	$\frac{1 \partial P}{P \partial t} - \frac{1 \partial T}{T \partial t} = -\frac{1 \partial u}{\epsilon \partial z} - \frac{1 u \partial P}{\epsilon P \partial t} + \frac{1 u \partial T}{\epsilon T \partial t} - \frac{(1-\epsilon)}{\epsilon} \rho_s \frac{\text{RT}}{P} \sum_i^n \frac{\partial q_i}{\partial t}$
LDF rate	$\frac{\partial q_i}{\partial t} = k_{\text{LDF}} (q_i^* - q_i)$
Energy balance	$\left[\rho_g c_{\text{pg}} + \frac{1-\epsilon}{\epsilon} \rho_s c_{\text{ps}}\right] \frac{\partial T}{\partial t} = K_{\text{ef}} \frac{\partial^2 T}{\partial z^2} - \frac{u}{\epsilon} C_{\text{pg}} \rho_g \frac{\partial T}{\partial z} + Q \frac{(1-\epsilon)}{\epsilon} \rho_s \frac{\partial q_i}{\partial t}$
Pressure drop	$-\frac{\partial P}{\partial z} = \left(\frac{150 \times 10^{-5} \mu_g (1-\epsilon_i)^2}{(2 r_p \psi)^2 \epsilon_i^3} v^g + \frac{1.75 \times 10^{-5} M_w \rho_g (1-\epsilon_i)}{(2 r_p \psi) \epsilon_i^3} v_g^2 \right)$
Equilibrium	$q_i^* = q_i^s \frac{K(T) P_i}{1 + K(T) P_i} \text{in} \left(\frac{K}{K_0} \right) = \frac{Q}{R} \left(\frac{1}{T} - \frac{1}{T_0} \right)$
Cycle steps	
I. Adsorption	
(i) $t = 0$	$y = W = 0, T = T_F, P = P_F, y = Y^{(\text{IV})} W = W^{(\text{IV})}$ $T = T^{(\text{IV})}, P = P^{(\text{IV})}$
(ii) $z = 0$	$y = y_F, T = T_F, P = P_F, F = F_F$
(iii) $z = L$	$\frac{\partial y}{\partial z} = 0, \frac{\partial T}{\partial z} = 0$
II. Depressurization	
(i) $t = 0$	$y = y^{(I)}, W = W^{(I)}, T = T^{(I)}, P = P^{(I)}$
(ii) $z = 0$	$\frac{\partial y}{\partial z} = 0, \frac{\partial T}{\partial z} = 0$
(iii) $z = L$	$\frac{\partial y}{\partial z} = 0, \frac{\partial T}{\partial z} = 0, \text{F} = F(\text{valve})$
III. Purge	
(i) $t = 0$	$y = y^{(\text{II})}, W = W^{(\text{II})}, T = T^{(\text{II})}, P = P^{(\text{II})}$
(ii) $z = 0$	$Y = Y_P, T = T_P, \text{F} = \text{F}_P$
(iii) $z = L$	$P = P_P, \frac{\partial y}{\partial z} = 0, \frac{\partial T}{\partial z} = 0$
IV. Repressurization	
(i) $t = 0$	$y = y^{(\text{III})}, W = W^{(\text{III})}, T = T^{(\text{III})}, P = P^{(\text{III})}$
(ii) $z = 0$	$y = y_P, T = T_P, F = F(\text{valve})$
(iii) $z = L$	$\frac{\partial y}{\partial z} = 0, \frac{\partial T}{\partial z} = 0$

Table 6: Start-up parameters of the PSA process for the purification and production of bioethanol.

FEED		
Flow	512	$kmolh^{-1}$
Ethanol	0.818	$kmolkmol^{-1}$
Water	0.182	$kmolkmol^{-1}$
Temperature	440	K
Production pressure	379	kPa
Purge pressure	13.5	kPa
SIZING		
Bed height	7.3	m
Bed diameter	2.4	m
Zeolite type 3A particle radius	0.0015875	m
Bulk solid density	729.62	$kg\,m^{-3}$

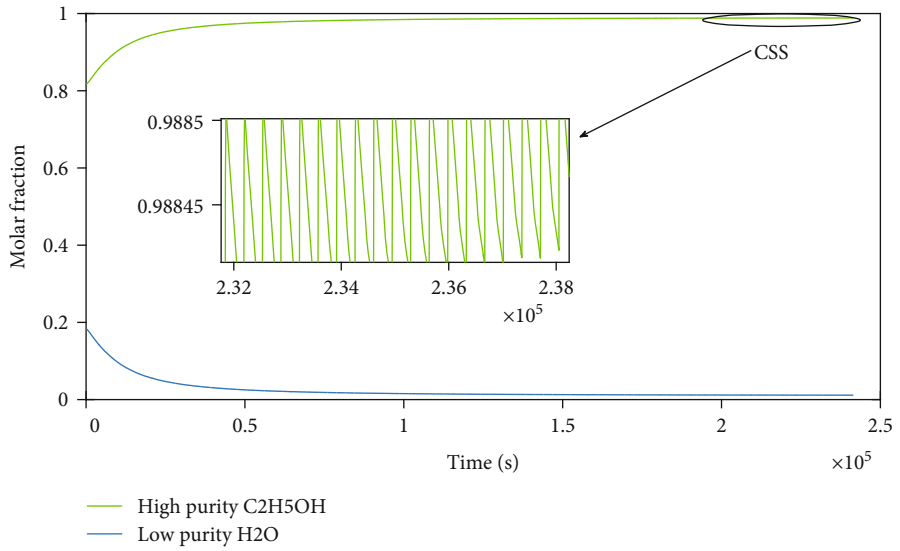

Figure 4: Purification and production of bioethanol from the start-up.

2.1. Mass Balance.

$$-\epsilon_i E_{zi}\frac{\partial^2 c_i}{\partial z^2} - \epsilon_i E_{ri}\frac{1}{r}\frac{\partial}{\partial_r}\left(r\frac{\partial c_i}{\partial_r}\right) + \frac{\partial\left(c_i v_g\right)}{\partial z} + \epsilon_i\frac{\partial c_i}{\partial t} + J_i = 0. \tag{1}$$

Flow over the solid surface

$$J = -\rho\frac{\partial W_i}{\partial t}. \tag{2}$$

The convection $(\partial(C_i V_g)/\partial z)$ with estimated dispersion $(-\epsilon_i E_{zi}\partial^2 c_i/\partial z^2)$ option assumes that the dispersion coefficient varies along the length of the bed.

2.2. Solid Phase Energy Balance.

$$\begin{aligned} &-k_{sa}\frac{\partial^2 T_s}{\partial^2 z^2} - k_{sr}\frac{1}{r}\frac{\partial}{\partial_r}\left(\frac{1}{r}\frac{\partial T_s}{\partial_r}\right) + C_{ps}\rho_s \\ &+ \rho_s\frac{\partial T_s}{\partial t}\sum_{i=1}^{n}\left(C_{pai}W_i\right)\frac{\partial T_s}{\partial t} + \rho_s\sum_{i}^{n}\left(\Delta H_i\frac{\partial W_i}{\partial t}\right) \\ &- \mathrm{MTC}_{ap}\left(T_g - T_s\right) = 0. \end{aligned} \tag{3}$$

The energy balance (solid phase) represents the heat of adsorption $(\rho_s\sum_i^n(\Delta H_i\partial W_i/\partial t))$, accumulation of heat $(C_{ps}\rho_s + \rho_s\partial T_s/\partial t)$, and gas-solid heat transfer $(\mathrm{MTC}_{ap}(T_g - T_s))$.

2.3. Wall Energy Balance.

$$\begin{aligned} &-k_w\frac{\partial^2 T_w}{\partial_z^2} + \rho_w c_{pw}\frac{\partial T_w}{\partial_t} - H_w\frac{4D_B}{\left(D_B + w_r\right)^2 - D_B^2}\left(T_g - T_w\right) \\ &+ H_{amb}\frac{4\left(D_B + w_r\right)^2}{\left(D_B + w_r\right)^2 - D_B^2}\left(T_w - T_{amb}\right) = 0. \end{aligned} \tag{4}$$

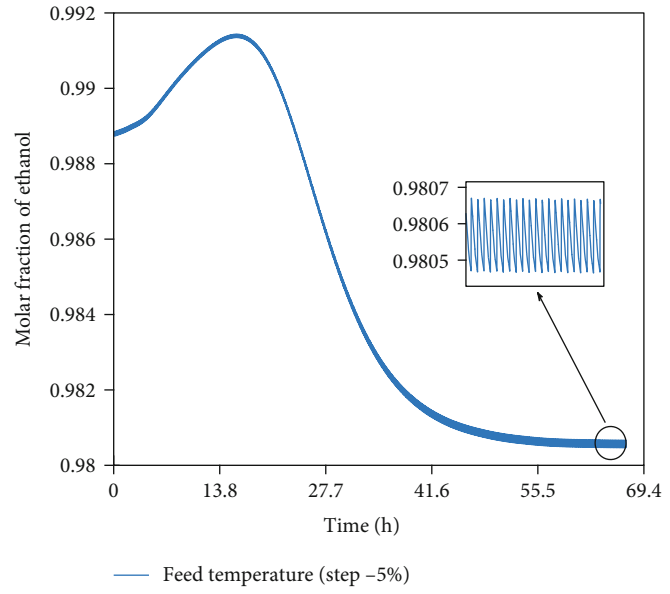

(a) Temperature: 440 K to 418 K; Flow: 512 kmolh^{-1}; Pressure: 379 kPa; Molar fraction: 0.182 (water) and 0.818 (ethanol)

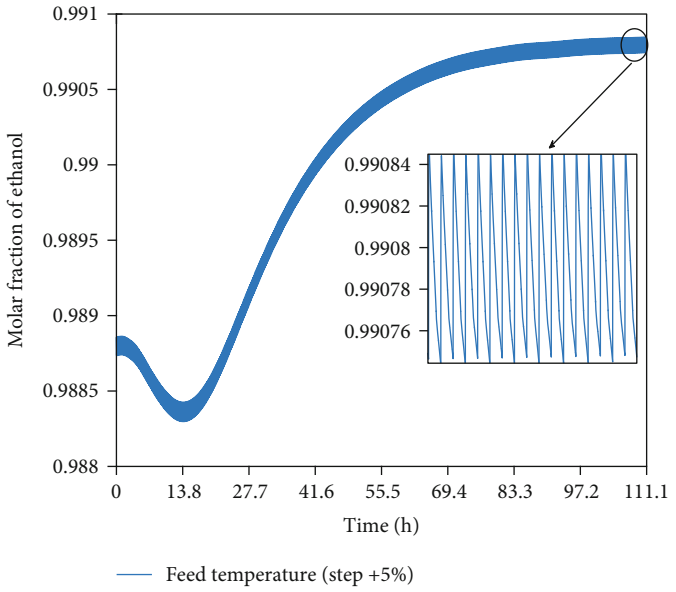

(b) Temperature: 440 K to 462 K; Flow: 512 kmolh^{-1}; Pressure: 379 kPa; Molar fraction: 0.182 (water) and 0.818 (ethanol)

Figure 5: Continued.

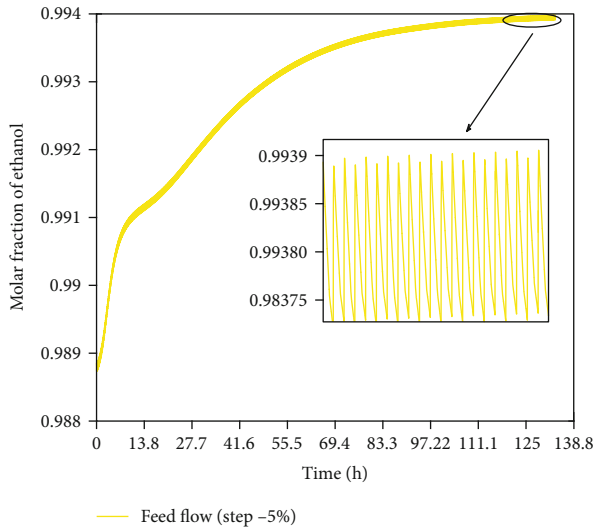

(c) Flow: 512 kmolh^{-1} to 486 kmolh^{-1}; Temperature: 440 K; Pressure: 379 kPa; Molar fraction: 0.182 (water) and 0.818 (ethanol)

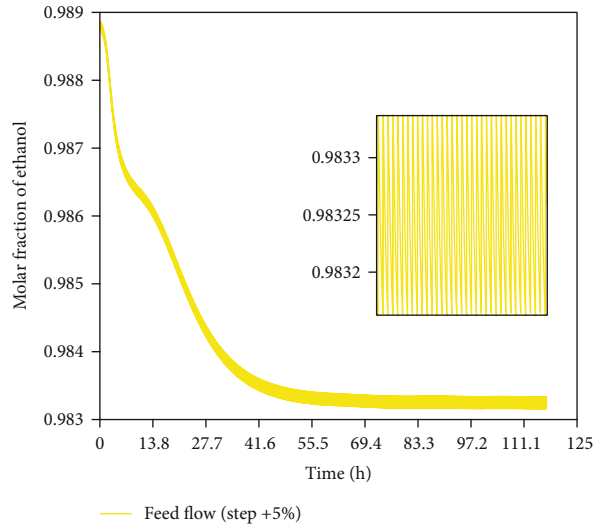

(d) Flow: 512 kmolh^{-1} to 537 kmolh^{-1}; Temperature: 440 K; Pressure: 379 kPa; Molar fraction: 0.182 (water) and 0.818 (ethanol)

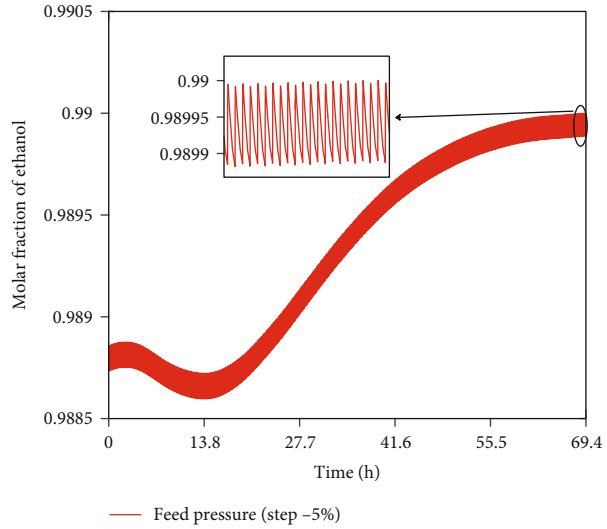

(e) Pressure: 379 kPa to 360 kPa; Flow: 512 kmolh^{-1}; Temperature: 440 K; Molar fraction: 0.182 (water) and 0.818 (ethanol)

Figure 5: Continued.

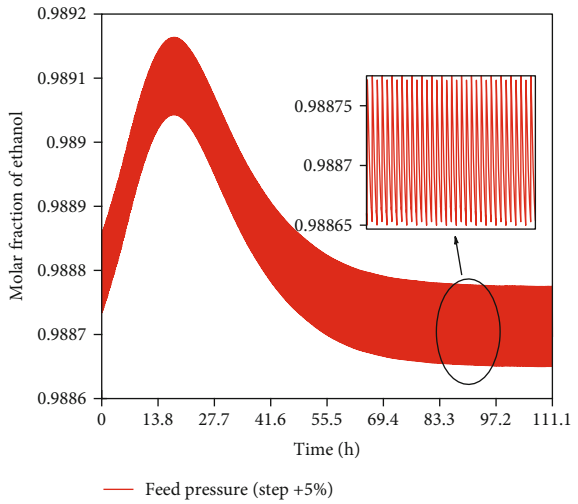

(f) Pressure: 379 kPa to 398 kPa; Flow: 512 kmolh^{-1}; Temperature: 440 K; Molar fraction: 0.182 (water) and 0.818 (ethanol)

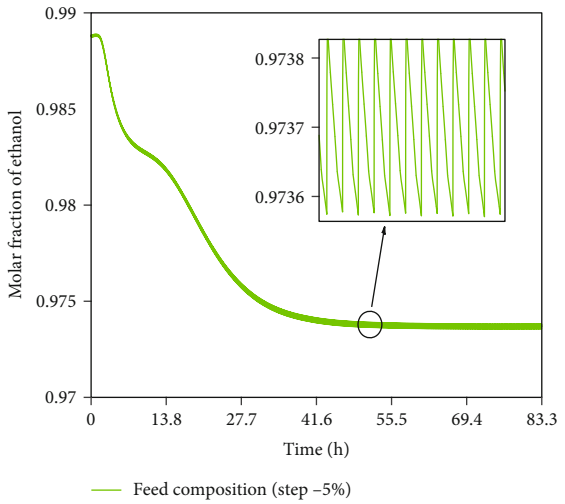

(g) Molar fraction: 0.182 (water) and 0.818 (ethanol) to 0.2229 (water) and 0.7771 (ethanol), Pressure: 379 kPa; Flow: 512 kmolh^{-1}; Temperature: 440 K

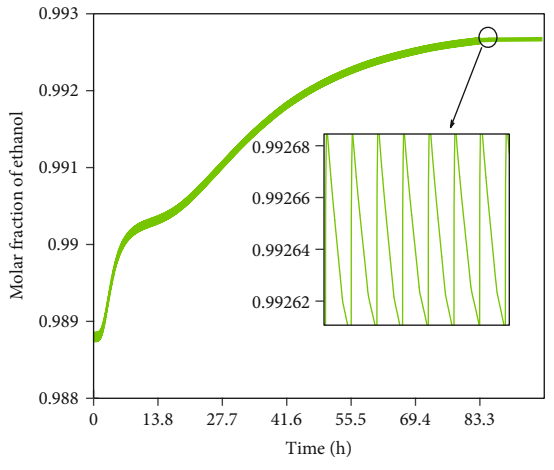

(h) Molar fraction: 0.182 (water) and 0.818 (ethanol) to 0.1411 (water) and 0.8589 (ethanol), Pressure: 379 kPa; Flow: 512 kmolh^{-1}; Temperature: 440 K

Figure 5: Sensitivity analysis applied to the PSA process for the production of bioethanol [41].

Table 7: Data obtained in the CSS from the parametric study.

Run	Temperature (K)	Flow kmolh^{-1}	Pressure kPa	Composition water-ethanol	Purity % wt of ethanol	Number of cycles
1	440	512	379	0.182-0.818	99.5	350
2	418	512	379	0.182-0.818	99.23	363
3	462	512	379	0.182-0.818	99.63	579
4	440	486	379	0.182-0.818	99.75	579
5	440	537	379	0.182-0.818	99.33	370
6	440	512	360	0.182-0.818	99.60	362
7	440	512	398	0.182-0.818	99.54	440
8	440	512	379	0.2229-0.7771	98.95	327
9	440	512	379	0.1411-0.8589	99.71	464

2.4. Momentum Balance.

$$-\frac{\partial P}{\partial z} = -\left(\frac{150x10^{-3}(1-\epsilon_i)^2}{(2r_p\Psi)^2\epsilon_i^2}\mu v_g + 1.75\times10^{-5}M\rho_g\frac{(1-\epsilon_i)}{2r_p\Psi\epsilon_i^3}v_g^2\right). \tag{5}$$

We use the Ergun equation, which combines the description of pressure drops by the Karman-Kozeny equation $(-\partial P/\partial z = -(150x10^{-3}(1-\epsilon_i)^2/(2r_p\Psi)^2\epsilon_i^2\mu v_g)$ for laminar flow and the Burke-Plummer equation $(1.75x10^{-5}M\rho_g(1-\epsilon_i)/2r_p\Psi\epsilon_i^3v_g^2)$ for turbulent flow.

2.5. Kinetic Models

(i) Lumped resistance

$$\frac{\partial W_i}{\partial t} = \mathrm{MTC_{si}}(W_i^* - W_i) \tag{6}$$

(ii) Micro- and macropore effects

$$\left(1-\varepsilon_p\right)\rho_s\frac{\partial W_i}{\partial_t} = \left(1-\varepsilon_p\right)\rho_s K_{\mathrm{mic}}(W_i^* - W_i), \tag{7}$$

$$\begin{aligned}(1-\varepsilon_i)\varepsilon_p\frac{\partial c_{\mathrm{msi}}}{\partial_t} + \left(1-\varepsilon_p\right)\rho_s\frac{\partial W_i}{\partial_t} \\ = \left(1-\varepsilon_p\right)\rho_s K_{\mathrm{mac}}(W_i^* - W_i).\end{aligned} \tag{8}$$

(iii) Particle material balance

$$\frac{\partial W_i}{\partial_t} - D_{ei}\left(\frac{2}{r}\frac{\partial W_i}{\partial_r} + \frac{\partial W_i^2}{\partial_r^2}\right) = 0. \tag{9}$$

(a) Mass transfer coefficients: Arrhenius

$$\mathrm{MTC_{si}} = k_{0i}\exp\left(\frac{-E_{\mathrm{acti}}}{\mathrm{RT}}\right). \tag{10}$$

(b) Mass Transfer Coefficients: Lumped Resistance, Micro-, and Macropore

$$\mathrm{MTC_{si}} = \frac{\Omega D_{\mathrm{ei}}}{r_p^2}. \tag{11}$$

Ω is the parameter in the Glueckauf expression

$$\mathrm{MTC_{mic}} = 15\frac{D_{\mathrm{mic}}}{r_m^2}, \tag{12}$$

$$\mathrm{MTC_{mac}} = 15\frac{D_{\mathrm{mac}}}{r_p^2}. \tag{13}$$

(c) Mass Transfer Coefficients: Pressure Dependent Arrhenius

$$\mathrm{MTC_{si}} = \frac{k_{0\mathrm{pi}}}{P}\exp\left(\frac{-E_{\mathrm{acti}}}{\mathrm{RT}}\right). \tag{14}$$

2.6. Lumped Resistance

2.6.1. Thermodynamic Equilibrium: Langmuir as a Function of Pressure and Concentration.

$$W_i^* = \frac{Ip_1P_i}{1+Ip_2P_i}, \tag{15}$$

$$W_i^* = \frac{Ip_1c_i}{1+Ip_2c_i}. \tag{16}$$

To solve these PDEs, it is necessary to contemplate initial and boundary conditions, which will allow connecting the adsorption, depressurization, purge, equalization, and repressurization steps, that is, the results obtained in the adsorption step will become the initial and boundary conditions of the depressurization step and this methodology will be repeated for the successive steps. For the last step (repressurization) the results obtained will become the initial and boundary conditions of the first step (adsorption) to contemplate a 1 cycle of production and regeneration of the bed. This continues cyclically until the Cyclic Steady State (CSS) is reached, which is when the pressure, temperature,

Table 8: Comparison of the thermodynamic values of various adsorbents as a function of different temperatures and pressures.

Reference	Adsorbents	Temperature K	Maximum adsorption capacity Q $(g\,g_{ads}^{-1})$	Langmuir constant (bar^{-1})	Pressure Atm
[52]	Carbon molecular sieve	293	0.1170 (CO)	0.130	16
	Carbon molecular sieve	293	0.0736 (CH_4)	0.232	16
[43]	Activated carbon	289.1	0.368 (CO)	9.867×10^6	—
	Activated carbon	289.1	0.350 (CH_4)	1.916×10^7	—
	Activated carbon	289.1	0.411 (CO_2)	3.526×10^7	—
	Zeolite 5A	289.1	0.129 (CO)	2.828×10^7	—
	Zeolite 5A	289.1	0.086 (CH_4)	2.410×10^7	—
	Zeolite 5A	289.1	0.150 (CO_2)	3.229×10^8	—
[53]	CMS-T3A	293	0.044 (N_2)	0.105	16
	CMS-T3A	293	0.060 (O_2)	0.088	15
	CMS-T3A	293	0.140 (Ar)	0.093	16
	CMS-T3A	293	0.073 (CO)	0.179	14.85
	CMS-T3A	293	0.161 (CO_2)	0.983	15.5
	CMS-T3A	293	0.050 (CH_4)	0.351	15
	CMS-T3A	293	0.378 (SO_2)	2.253	4.5
	CMS-T3A	303	0.040 (N_2)	0.102	15
	CMS-T3A	303	0.056 (O_2)	0.076	14.6
	CMS-T3A	303	0.128 (Ar)	0.082	15
	CMS-T3A	303	0.073 (CO)	0.150	14.2
	CMS-T3A	303	0.158 (CO_2)	0.764	15.6
	CMS-T3A	303	0.045 (CH_4)	0.329	15
	CMS-T3A	303	0.365 (SO_2)	2.170	4.8
	CMS-T3A	313	0.035 (N_2)	0.097	14.5
	CMS-T3A	313	0.055 (O_2)	0.065	16
	CMS-T3A	313	0.118 (Ar)	0.079	14.4
	CMS-T3A	313	0.071 (CO)	0.137	15.8
	CMS-T3A	313	0.154 (CO_2)	0.583	15
	CMS-T3A	313	0.043 (CH_4)	0.269	15
	CMS-T3A	313	0.349 (SO_2)	2.163	4.7
[50]	PCB-activated carbon	295	0.088 (CH_4)	0.0155	68.04
	PCB-activated carbon	295	0.148 (CO)	0.0056	51.03
	PCB-activated carbon	295	0.392 (CO_2)	0.0227	37.42
	PCB-activated carbon	295	0.335 (H_2S)	0.0479	13.60
[54]	Activated carbon	293.15	0.102 (CO)	9.075×10^6	20
	Activated carbon	293.15	0.080 (CH_4)	1.812×10^7	18
	Activated carbon	293.15	0.308 (CO_2)	3.356×10^7	10
	Activated carbon	293.15	0.014 (N_2)	1.657×10^7	15
	Zeolite 5A	293.15	0.049 (CO)	2.727×10^7	17
	Zeolite 5A	293.15	0.030 (CH_4)	2.386×10^7	18
	Zeolite 5A	293.15	0.202 (CO_2)	3.197×10^4	17
	Zeolite 5A	293.15	0.238 (N_2)	1.055×10^7	20

Table 8: Continued.

Reference	Adsorbents	Temperature K	Maximum adsorption capacity Q $(g\,g_{ads}^{-1})$	Langmuir constant (bar^{-1})	Pressure Atm
[55]	AC5-KS	303	0.147 (CO)	1.428×10^9	—
	AC5-KS	303	0.582 (CO_2)	3.937×10^9	—
	AC5-KS	303	0.0116 (N_2)	9.797×10^8	—
	AC5-KS	303	0.0973 (CH_4)	2.986×10^9	—
[56]	CuBTC (KRICT)	303	0.022 (N_2)	0.0386	7
	CuBTC (KRICT)	303	0.019 (CO)	0.2443	1
	CuBTC (KRICT)	308	0.444 (CO_2)	0.2963	7
	CuBTC (KRICT)	308	0.056 (CH_4)	0.0861	7
	CuBTC (KRICT)	343	0.014 (N_2)	0.0216	7
	CuBTC (KRICT)	343	0.008 (CO)	0.0901	1
	CuBTC (KRICT)	343	0.290 (CO_2)	0.1185	7
	CuBTC (KRICT)	343	0.036 (CH_4)	0.0657	7
	CuBTC (KRICT)	373	0.009 (N_2)	0.0152	7
	CuBTC (KRICT)	373	0.042 (CO)	0.0491	1
	CuBTC (KRICT)	373	0.187 (CO_2)	0.0619	7
	CuBTC (KRICT)	373	0.024 (CH_4)	0.0410	7
[57]	Cu-BTC	303	0.125 (CO)	2.4433	—
	Cu-BTC	303	0.660 (CO_2)	0.3437	—
	Cu-BTC	303	0.104 (N_2)	0.0386	—
	Cu-BTC	303	0.116 (CH_4)	0.1416	—
[58]	Zeolite 5A	303	0.064 (CO)	0.2363	10
	Zeolite 5A	303	0.034 (CH_4)	0.2003	10
[59]	TDA AMS-19	453.15	0.268 (CO_2)	4.634×10^{-8}	41
	TDA AMS-19	513.15	0.198 (CO_2)	4.349×10^{-8}	18
	TDA AMS-19	573.15	0.158 (CO_2)	4.135×10^{-8}	18
[60]	BPL 4X10 activated carbon	293.15	0.311 (CO_2)	0.4	12
[61]	MG50	623.15	0.085 (CO_2)	64.8	—
[62]	MG50	523.15	0.043 (CO_2)	7.8×10^{-5}	1
	MG50	623.15	0.034 (CO_2)	7.3×10^{-5}	1
	MG50	723.15	0.032 (CO_2)	5.0×10^{-5}	1
[63]	$K_2CO_3/Mg_3AI - CO_3$	673.15	0.019 (CO_2)	37.4	1
[64]	$K_2CO_3/Mg_3AI - CO_3$	673	0.027 (CO_2)	16.9	0.45
	$K_2CO_3/Mg_3AI - CO_3$	673	0.022 (CO_2)	17.0	0.58
	$K_2CO_3/Mg_3AI - CO_3$	673	0.028 (CO_2)	23.6	0.19
	$K_2CO_3/Mg_3AI - CO_3$	753	0.025 (CO_2)	19.3	0.19
[65]	$K_2CO_3/Mg_3AI - CO_3$	673.15	0.011 (CO_2)	37.4	3
	$K_2CO_3/Mg_3AI - CO_3$	793.15	0.011 (CO_2)	21.2	3
[18]	K-MG30	723.15	0.028 (CO_2)	—	10.85
	K-MG30	673.15	0.022 (CO_2)	—	10.85
	K-MG30	623.15	0.015 (CO_2)	—	10.85
	K-MG30	573.15	0.009 (CO_2)	—	10.85

Table 8: Continued.

Reference	Adsorbents	Temperature K	Maximum adsorption capacity Q $\left(g\, g_{ads}^{-1}\right)$	Langmuir constant (bar^{-1})	Pressure Atm
[2]	CuBTC-OMC (MOF-composite)	298.15	0.191 (CO_2)	—	1
	CuBTC/GO (MOF-composite)	295	0.135 (CO_2)	—	1.1
	CuBTC@MWCNT (MOF-composite)	298.15	0.149 (CO_2)	—	1
	Cu3($BTC)_2$ (MOF-composite)	298.15	0.595 (CO_2)	—	18
	CG-9 (CuBTC-GO-9) (MOF-composite)	273	0.363 (CO_2)	—	1

Table 9: Works reported on the different configurations of PSA processes for purification of biohydrogen.

Reference	Experimental/simulated	PSA cycles	Pressure swing (kPa)	Bed regeneration time (min)	Hydrogen feed (% molar fraction)
[55]	Simulated	2 beds 10 steps	500 to 50	5	79
[67]	Simulated	10 beds 5 steps	(1300-1200) to 20	—	62.57
[56]	Experimental	2 beds 4 steps	350 to 100	7.5	67, 68, 78, and 81
[57]	Experimental	2 beds 4 steps	350 to 100	5.8	67, 68, and 78
[58]	Simulated	6 beds 9 and 12 steps	1100 to 100	6.6	70
[68]	Experimental	4 beds 8 steps	(1400-1600) to (131-50)	—	55
[59]	Simulated	4, 6, 8, and 10 beds 4, 6, 8, and 10 steps	(3450-1730) to 100	4.6	15
[60]	Simulated	4 beds 7 steps	1600 to 100	—	25, 50, and 75
[69]	Experimental	2 beds 5 steps	(1000-4000) to 100	0.8	50
[70]	Experimental	8 beds 12 steps	3500 to 100	4	88.75
[71]	Experimental	2 and 4 beds 6 and 10 steps	(3000-3500) to 110	5 and 6.3	88

and mole fraction profiles have oscillatory cyclic dynamics, resulting in stable behavior at a setpoint.

It is important to mention that the initial and boundary conditions will depend on the number of variables involved in the PDEs.

There are several numerical methods (orthogonal placement, finite element, finite difference, etc.) to discretize the PDEs, which will allow the bed to be sectioned or partitioned into meshes, nodes, points, or areas; this will depend on the numerical method used. Likewise, it is necessary to define the number to be sectioned or partitioned, since the approximation obtained on the real results presented by a PSA plant will depend on that. The software used to simulate these PSA cases is Aspen Adsorption [9].

Figure 1 shows the general scheme of a PSA process contemplating pressure, temperature, flow, purity sensors, valves, metallic structure, and the PSA cycle.

3. Bioethanol Purification by PSA

Bioethanol comes from renewable biological raw material; it is not corrosive or toxic. This product can be used in the pharmaceutical industry, alcoholic beverages, cooking, perfumery, cosmetics, solvents, and mainly as an oxygenating additive (they increase the octane number) or be used as a fuel and reduce the risk of climate change, which is caused by fuels developed from fossils. However, for bioethanol to be used as fuel, it is necessary that its water content be very low and obtains a purity of 99% by weight of ethanol, to avoid the formation of two liquid phases in the mixture and be able to meet standards set by international norms.

One of the important aspects of the study of the PSA process is the selection of the adsorbent or molecular sieves that will allow the separation and purification of an ethanol-water mixture.

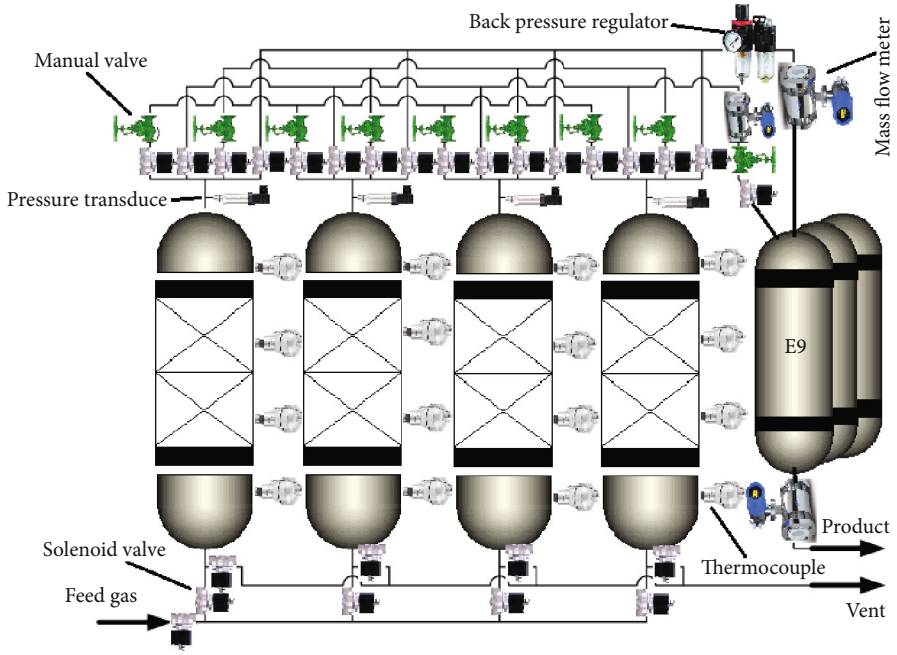

Figure 6: Schematic diagram of the PSA process using 4-beds, 9-steps.

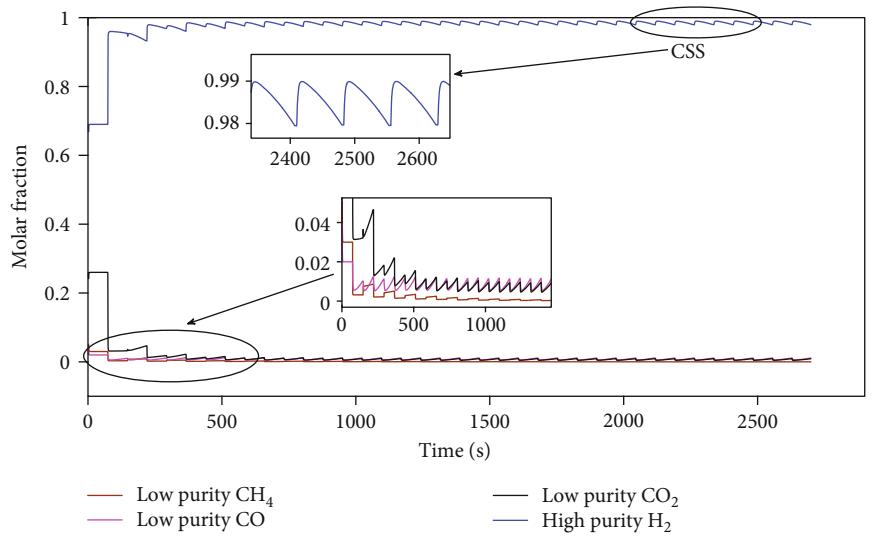

Figure 7: Purification and production of biohydrogen from the start-up.

Table 10: Distributed parameter models of the PSA processes for biohydrogen production.

Reference	Equations governing the PSA process (nonlinear model)	Temperature effects	Pressure effects
[71]	6 PDEs	Consider adsorption isotherms	Consider pressure gradient
[68]	4 PDEs	Consider adsorption isotherms	No pressure gradient
[58]	3 PDEs	Does not present adsorption isotherms	No pressure gradient
[57]	4 PDEs	Does not present adsorption isotherms	Consider pressure gradient
[56]	5 PDEs	Consider adsorption isotherms	Consider pressure gradient
[55]	6 PDEs	Does not present adsorption isotherms	Consider pressure gradient

Table 11: Governing equations and simplifications for production and purification of biohydrogen.

Mass balance equation	$-D_L \dfrac{\partial^2 c_i}{\partial z^2} + \dfrac{\partial (U_z c_i)}{\partial z} + \dfrac{\partial c_i}{\partial t} + \dfrac{(1-\epsilon_b)}{\epsilon_b}\rho_p \dfrac{\partial n_i}{\partial t} = 0$
Energy balance equation	$K_L \dfrac{\partial^2 T}{\partial z^2} + \left[\epsilon_b c C_{\mathrm{pg}} + (1-\epsilon_b)\rho_p C_{\mathrm{ps}}\right] \dfrac{\partial T}{\partial t} - \epsilon_b c C_{\mathrm{pg}} U_z \dfrac{\partial T}{\partial z} = (1-\epsilon_b)\rho_p \sum_{j=1}^{N} \Delta H_j \dfrac{\partial n_j}{\partial t} + \dfrac{2h_{\mathrm{in}}}{R_{\mathrm{in}}}(T_w - T)$
Ergun equation for momentum balance	$-\dfrac{\partial P}{\partial z} = \left(\dfrac{150\mu V_z (1-\epsilon_b)^2}{4R_p^2 \epsilon_b^3} + \dfrac{1.75\rho_g (1-\epsilon_b)}{(2R_p)\epsilon_b^3} v_g^2\right)$
Adsorption isotherms and kinetics	$n_i^* = n_i^s\left(b_i P_i / 1 + \sum_{j=1}^{N} b_j P_j\right)(\partial n_i/\partial t) = k_i (n_i^* - n_i), i = 1, \cdots, N)$
Boundary and initial conditions	
I. Adsorption	
(i) $t = 0$	$c_{H_2}(z,0) = c_0, c_{\mathrm{CO}}(z,0) = 0, c_{\mathrm{CH_4}}(z,0) = 0, c_{\mathrm{CO_2}}(z,0) = 0$ $T(z,0) = T_0, T_w(z,0) = T_0, p(z,0) = p_0, \eta_i(z,0) = \eta_i^*$
(ii) $z = 0$	$-D_L\left(\partial_{c_i}/\partial z\right) = u[c_i(0^-,t) - c_i(0^+,t)], p = p_0, U_z = U_{\mathrm{zo}}$ $-K_L(\partial T/\partial t) = \epsilon_b c C_{\mathrm{pg}} U_z [T(0^-,t) - T(0^+,t)]$
(iii) $z = L$	$-D_L\left(\partial_{c_i}/\partial z\right) = 0, \partial U_z/\partial z = 0, -K_L(\partial T/\partial t) = 0, \partial p/\partial z = 0$
II. Depressurization	
(i) $t = 0$	$c_{H_2}(z,0) = c_0^{(I)}, c_{\mathrm{CO}}(z,0) = c_{\mathrm{CO}}^{(I)}, c_{\mathrm{CH_4}}(z,0) = c_{\mathrm{CH_4}}^{(I)}, c_{\mathrm{CO_2}}(z,0) = c_{\mathrm{CO_2}}^{(I)}$ $T(z,0) = T^{(I)}, T_w(z,0) = T^{(I)}, p(z,0) = p^{(I)}, \eta_i(z,0) = \eta_{i^{(I)}}^*$
(ii) $z = 0$	$\partial_{c_i}/\partial z = 0, \partial p/\partial z = 0, \partial U_z/\partial z = 0, \partial T/\partial t = 0$
(iii) $z = L$	$\partial_{c_i}/\partial z = 0, \partial U_z/\partial z = 0, \partial T/\partial t = 0, \partial p/\partial z = 0, F = F_{\mathrm{valve}}$
III. Purge	
(i) $t = 0$	$c_{H_2}(z,0) = c_0^{(\mathrm{II})}, c_{\mathrm{CO}}(z,0) = c_{\mathrm{CO}}^{(\mathrm{II})}, c_{\mathrm{CH_4}}(z,0) = c_{\mathrm{CH_4}}^{(\mathrm{II})}, c_{\mathrm{CO_2}}(z,0) = c_{\mathrm{CO_2}}^{(\mathrm{II})}$ $T(z,0) = T^{(\mathrm{II})}, T_w(z,0) = T^{(\mathrm{II})}, p(z,0) = p^{(\mathrm{II})}, \eta_i(z,0) = \eta_{i^{(\mathrm{II})}}^*$
(ii) $z = 0$	$\partial_{c_i}/\partial z = 0, \partial p/\partial z = 0, \partial U_z/\partial z = 0, \partial T/\partial t = 0, F = F_{\mathrm{valve}}$
(iii) $z = L$	$\partial_{c_i}/\partial z = 0, \partial U_z/\partial z = 0, \partial T/\partial t = 0, \partial p/\partial z = 0$
IV. Pressurization	
(i) $t = 0$	$c_{H_2}(z,0) = c_0^{(\mathrm{III})}, c_{\mathrm{CO}}(z,0) = c_{\mathrm{CO}}^{(\mathrm{III})}, c_{\mathrm{CH_4}}(z,0) = c_{\mathrm{CH_4}}^{(\mathrm{III})}, c_{\mathrm{CO_2}}(z,0) = c_{\mathrm{CO_2}}^{(\mathrm{III})}$ $T(z,0) = T^{(\mathrm{III})}, T_w(z,0) = T^{(\mathrm{III})}, p(z,0) = p^{(\mathrm{III})}, \eta_i(z,0) = \eta_{i^{(\mathrm{III})}}^*$
(ii) $z = 0$	$\partial_{c_i}/\partial z = 0, \partial p/\partial z = 0, \partial U_z/\partial z = 0, \partial T/\partial t = 0, F = F_{\mathrm{valve}}$
(iii) $z = L$	$\partial_{c_i}/\partial z = 0, \partial U_z/\partial z = 0, \partial T/\partial t = 0, \partial p/\partial z = 0$

3.1. Adsorption and Separation for the Ethanol-Water Mixture with Different Adsorbents. The study of the adsorption phenomenon with molecular sieves makes it possible to determine models capable of predicting the thermodynamic equilibrium of different adsorbents used for the ethanol-water mixture. The thermodynamic equilibrium of each adsorbent is represented by an adsorption isotherm at a constant temperature, which determines the maximum adsorption capacity. The adsorption isotherm is obtained from experimental data. These represent the amount of material (water in this case) adsorbed on the surface of the adsorbent, as a function of the composition of the material (water) present in the gas phase, the latter is expressed as a molar fraction or partial pressure. There are 5 types of adsorption isotherms as shown in Figure 2, they can be monomolecular isotherms (monolayers) or polymolecular isotherms (multilayers). The most common isotherms are types I, II, and III. To describe the adsorption isotherms that are obtained experimentally and can be represented in different mathematical models, each model contemplates a series of considerations.

For the ethanol-water mixture a type I adsorption isotherm is obtained, which is represented by the Langmuir model. This model proposes a constant temperature, localized adsorption only active sites, a homogeneous surface, and the adsorption occurs in a monolayer, assuming that each adsorption site can adhere to only one adsorbate molecule, the adsorption energy is the same for all adsorption sites and there is no interaction between the adsorbed molecules [10–13]. The thermodynamic equilibrium provides a measure of adsorption

Table 12: Start-up parameters of the PSA process for the purification and production of biohydrogen.

FEED		
Flow	0.162	$kmolkmol^{-1}$
CO	0.02	$kmolkmol^{-1}$
CO_2	0.26	$kmolkmol^{-1}$
Hydrogen	0.69	$kmolkmol^{-1}$
Methane	0.03	$kmolkmol^{-1}$
Temperature	298.15	K
Production pressure	980	kPa
Purge pressure	100	kPa
SIZING		
Bed height	1	m
Bed diameter	0.037	m
Zeolite type 5A particle radius	0.0015	m
Bulk solid density	850.0	$kg\,m^{-3}$

efficiency during the removal of specific impurities (water molecules), as well as the maximum adsorption capacity. On the other hand, the kinetic equilibrium data are represented using breakdown curves, in these, the composition of the adsorbed phase is related to the adsorption time to reach the maximum capacity. The increase in temperature favors the adsorbent to retain the molecules or atoms and reach its maximum saturation point in less time, but it does not favor thermodynamic equilibrium since the maximum adsorption capacitance is reduced. The rate of adsorption is proportional to the rate of diffusion in the pores.

Among the adsorbents that have been used to separate the ethanol-water mixture, natural zeolites are good candidates and have an advantage over some types of membranes or natural adsorbents because they remain stable in harsh chemical environments and high temperatures [14–18]. Dehydration of ethanol through adsorption with natural zeolites is acceptable and effective in adsorbing large amount of water, but the use of synthetic zeolites has recently been suggested as a promising alternative. One of the most accepted and studied with good results is the synthetic zeolite 3A. The review of several studies allowed us to make a concentrate on works, in which different adsorbents are applied, useful to separate the ethanol-water mixture. The information is contained in Table 2, which describes the characteristics of thermodynamic equilibrium and the time it reaches its maximum saturation point at different time, these determine the maximum capacity and time with which they adsorb. The results were obtained as a function of temperature since the adsorption capacity depends significantly on this variable. Table 2 shows the different adsorbents used for the separation of the ethanol-water mixture, as well as the constants Q and K, referred to as the maximum adsorption capacity and the Langmuir constant.

Table 2 shows that natural zeolites have disadvantages over synthetic zeolites, specifically compared to 3A zeolites and ZIF, since the latter adsorb a greater amount of water. However, clinoptilolite presents large contributions with a maximum adsorption capacity, between 0.27 and 0.3 $g_{water}g_{ads}^{-1}$.

3.2. Mathematical Models, Characteristics, and Configuration of the PSA Process for the Production of Bioethanol. There are some studies on PSA processes with columns packed with zeolite, specifically designed to dehydrate ethanol [27–29], in which advantages and disadvantages of different operational methods are compared such as the use of two beds, three beds, and multibeds (see Table 3).

It is important to take into account the additional energy required to circulate the mixture, as well as the electricity required to operate the adsorption and desorption beds and the air and vacuum compressor [30, 31]. Table 3 shows the cycle times considered in different articles, regeneration takes between 3 and 45 min.

In the study of Jeong et al. [36], the two-bed process and the multibed process produced 99.5% anhydrous ethanol by weight, with a feed of 87.0% by weight ethanol. However, the multibed process presented lower energy consumption (higher energy efficiency). On the other hand, the two-bed process has the advantage of producing anhydrous ethanol from the input ethanol concentration as low as 81.3% in weight. And lastly, the three-bed process required the longest regeneration time (twice the amount of time) for zeolite, but a very stable process with higher performance was achieved due to less time lost in the change of cycle, so it was concluded that this is the most suitable for a large-scale commercial application. The process flow diagram is shown in Figure 3.

The PSA process is more used than the TSA due to its efficiency and low energy cost, for this reason, there is interest in presenting proposals to improve the operation of PSA processes for different applications [38]. To this end, different analyzes have been carried out based on the mathematical models reported in Table 4.

Table 4 shows a concentration of studies in which different mathematical models for PSA processes are proposed. In this table, the number of PDEs is indicated, if it presents a model for the adsorption isotherms and if they consider pressure variations. The mathematical model of the PSA process or the numerical simulation of the same makes it possible to determine the diameter, the height of the bed, and the amount of zeolite required. On the other hand, they allow establishing nominal operating conditions. The PDEs that represent the behavior of the process, normally consider variations in the axial direction of temperature, pressure, composition, and speed, and neglect variations in other directions. Temporal variations are also considered.

In general, the models of a cyclic PSA process can be curves of the hyperbolic or parabolic type, depending on the assumptions of the modeling. The numerical methods to discretize these PDEs are finite differences, finite elements, and orthogonal placement on finite elements. An example of mathematical modeling of a PSA process is reported by Simo et al. [34] and is shown in Table 5.

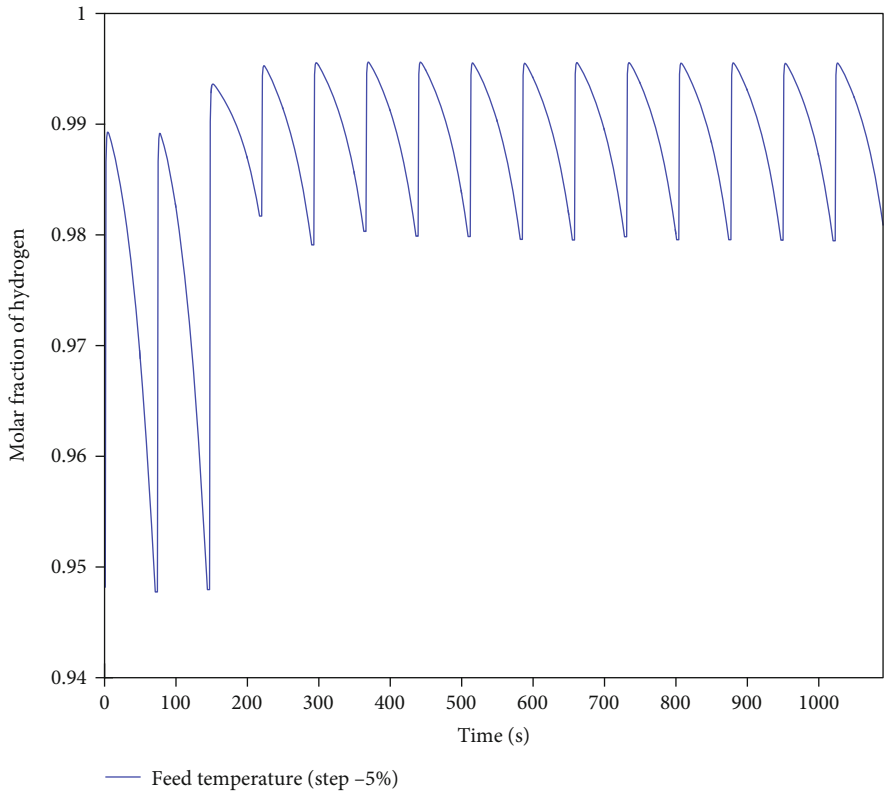

(a) Temperature: 298.15 K to 283.24 K; Flow: 0.162 kmolh^{-1}; Pressure: 980 kPa; Molar fraction: 0.02 (CO), 0.26 (CO_2), 0.69 H_2, and 0.03 CH_4

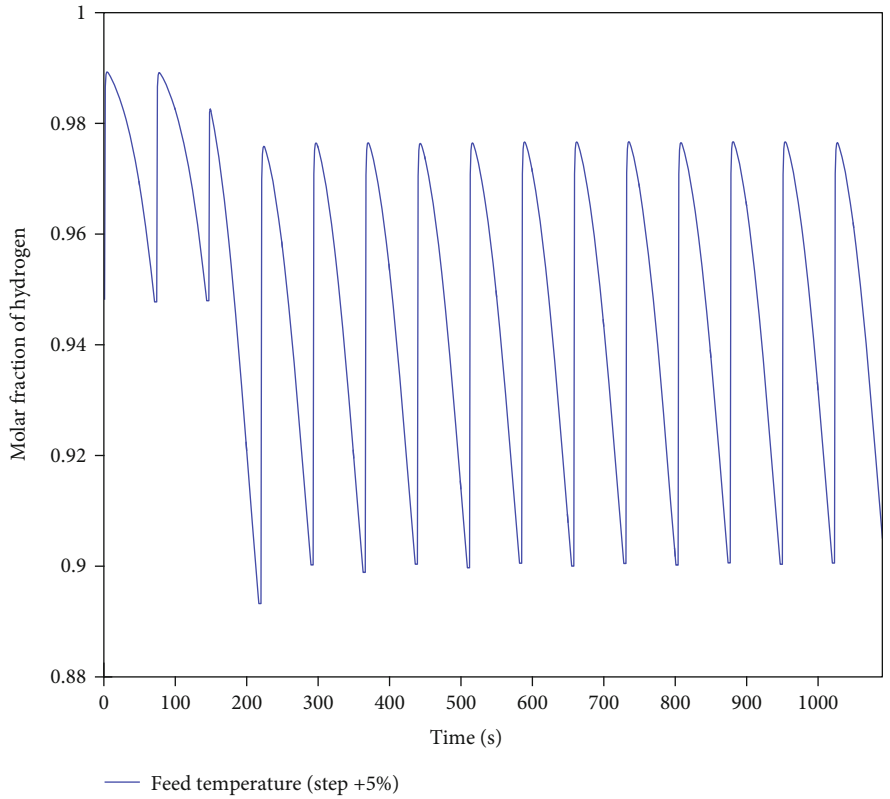

(b) Temperature: 298.15 K to 313.05 K; Flow: 0.162 kmolh^{-1}; Pressure: 980 kPa; Molar fraction: 0.02 (CO), 0.26 (CO_2), 0.69 H_2, and 0.03 CH_4

Figure 8: Continued.

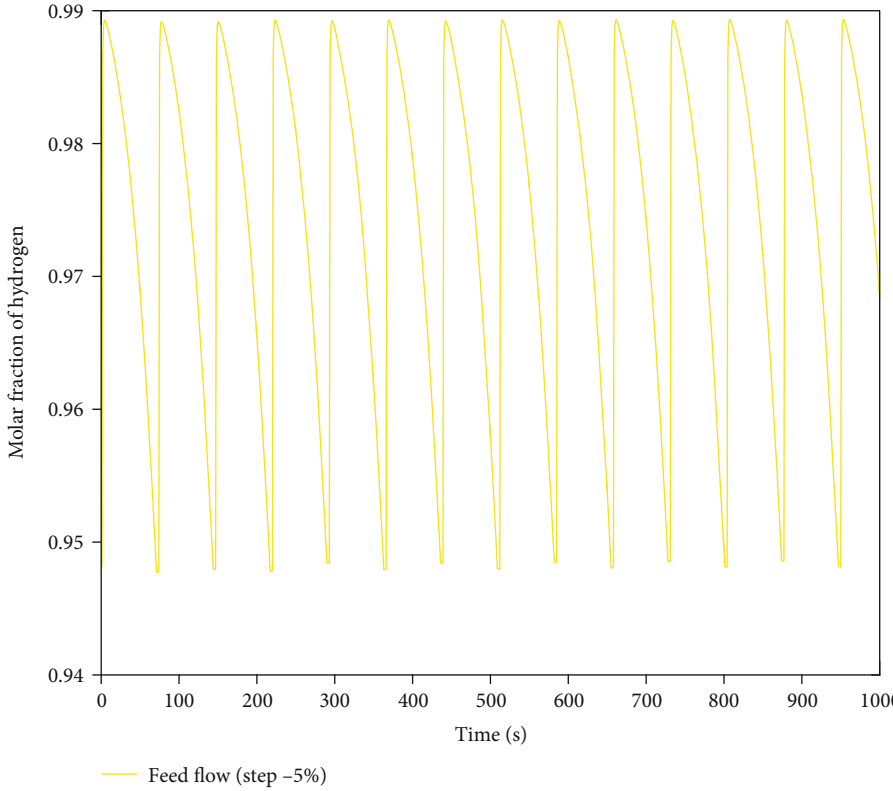

(c) Flow: 0.162 kmolh^{-1} to 0.153 kmolh^{-1}; Temperature: 298.15 K; Pressure: 980 kPa; Molar fraction: 0.02 (CO), 0.26 (CO_2), 0.69 H_2, and 0.03 CH_4

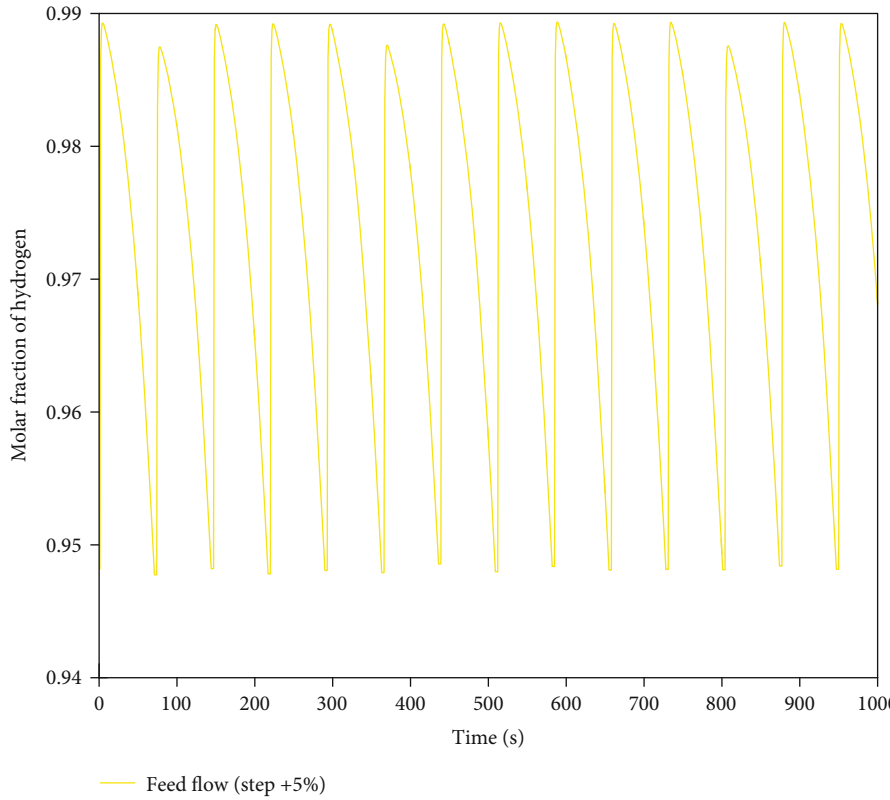

(d) Flow: 0.162 kmolh^{-1} to 0.170 kmolh^{-1}; Temperature: 298.15 K; Pressure: 980 kPa; Molar fraction: 0.02 (CO), 0.26 (CO_2), 0.69 H_2, and 0.03 CH_4

Figure 8: Continued.

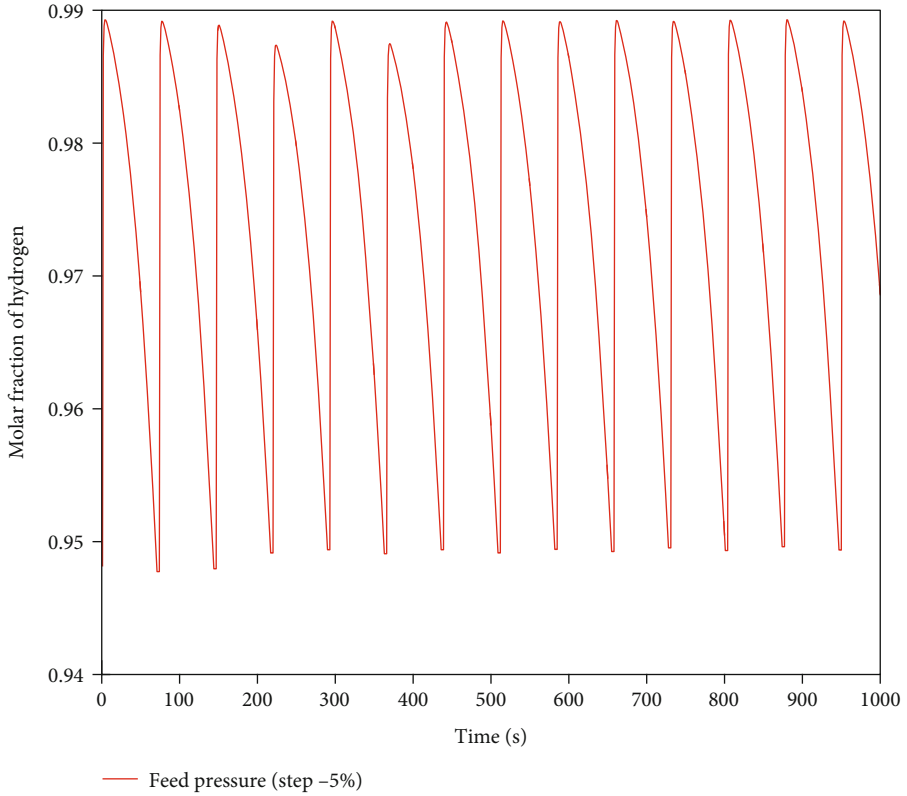

(e) Pressure: 980 kPa to 931 kPa; Flow: 0.162 $kmolh^{-1}$; Temperature: 298.15 K; Molar fraction: 0.02 (CO), 0.26 (CO_2), 0.69 H_2, and 0.03 CH_4

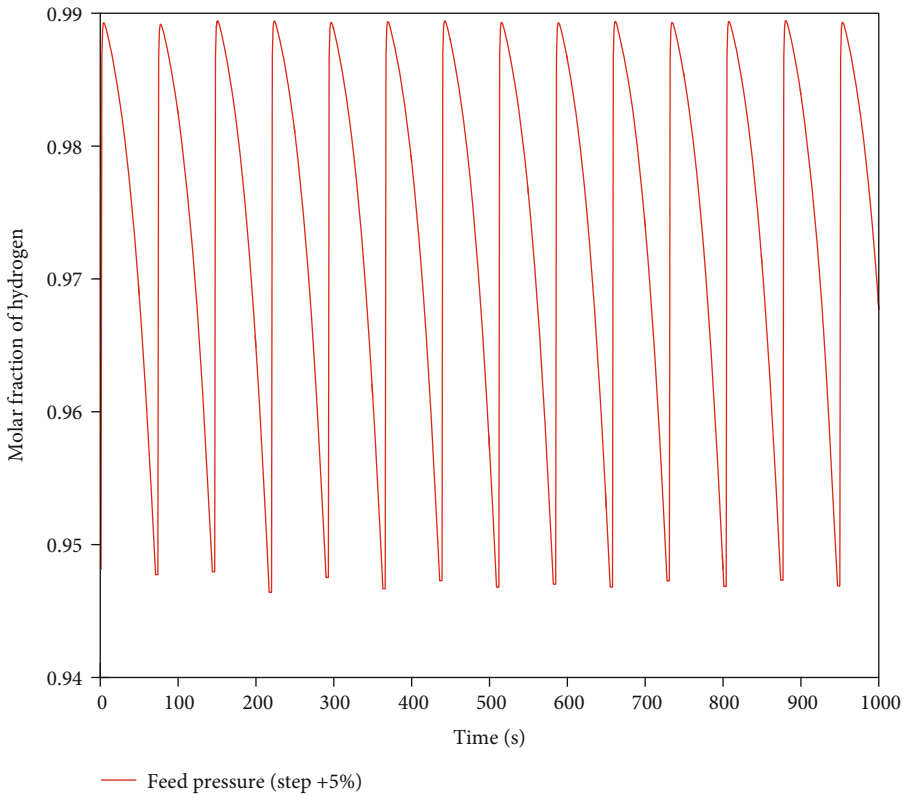

(f) Pressure: 980 kPa to 1029 kPa; Flow: 0.162 $kmolh^{-1}$; Temperature: 298.15 K; Molar fraction: 0.02 (CO), 0.26 (CO_2), 0.69 H_2, and 0.03 CH_4

Figure 8: Continued.

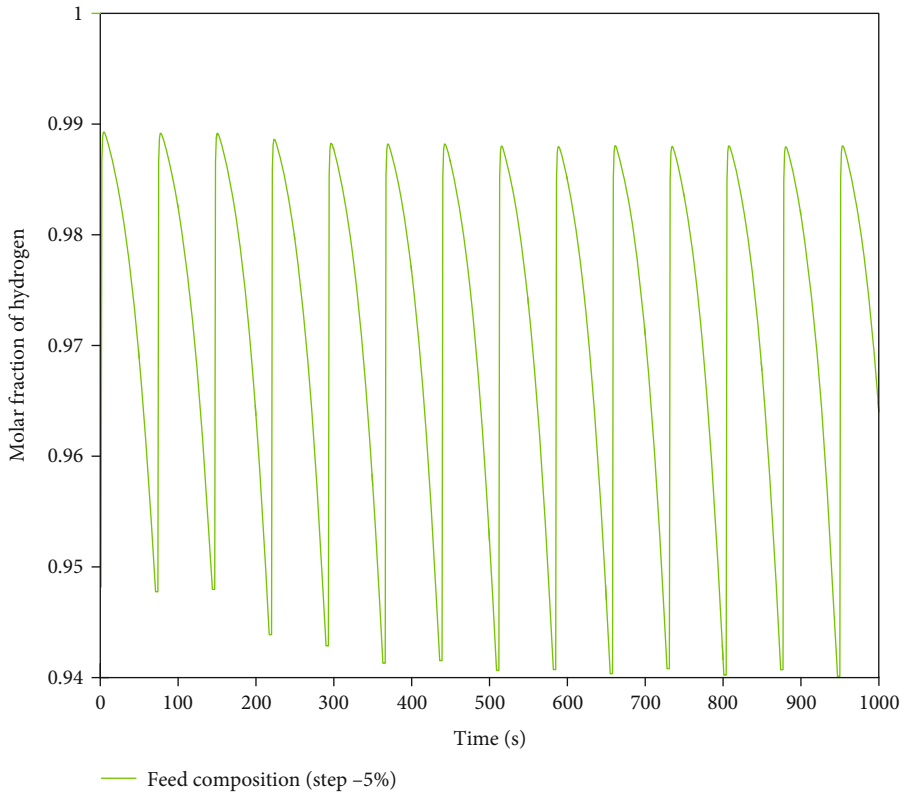

(g) Molar fraction: 0.02 (CO), 0.26 (CO_2), 0.69 H_2 and 0.03 CH_4 to 0.6555 (H_2), 0.2945 (CO_2), 0.03 (CH_4), and 0.02 CO; Pressure: 980 kPa; Flow: 0.162 $kmolh^{-1}$; Temperature: 298.15 K

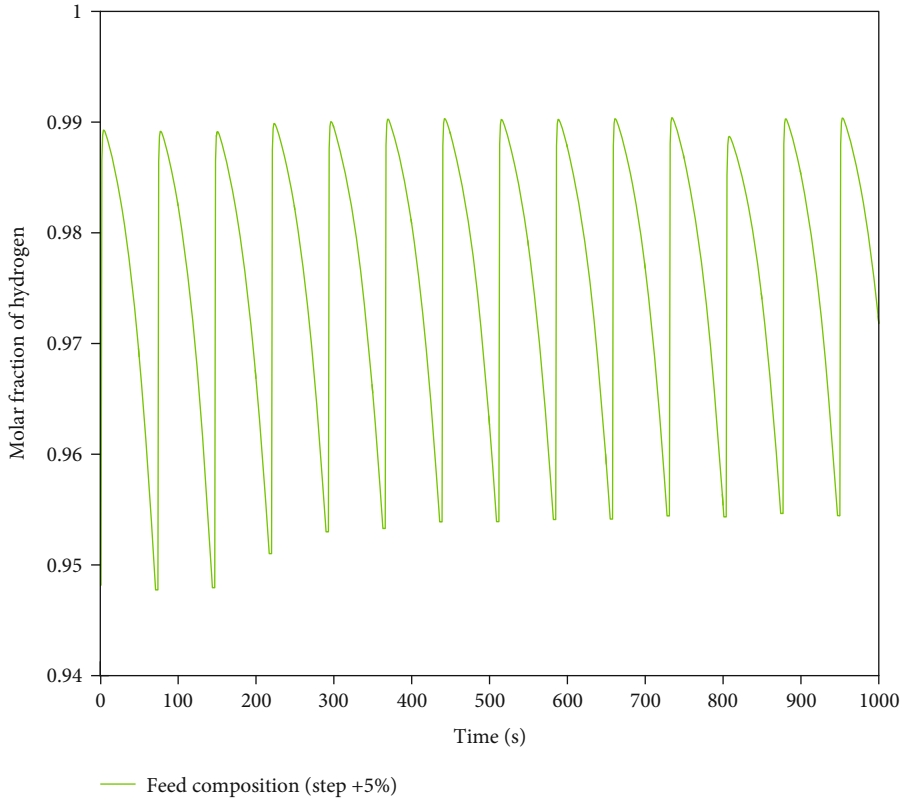

(h) Molar fraction: 0.02 (CO), 0.26 (CO_2), 0.69 H_2, and 0.03 CH_4 to 0.7245 (H_2), 0.2255 (CO_2), 0.03 (CH_4), and 0.02 CO; Pressure: 980 kPa; Flow: 0.162 $kmolh^{-1}$; Temperature: 298.15 K

Figure 8: Sensitivity analysis applied to the PSA process for the production of biohydrogen [72].

Table 13: Analysis of the possible input variables that have the greatest effect on the purity obtained.

Run	Temperature (K)	Flow kmolh^{-1}	Pressure kPa	Composition CO-CO_2-hydrogen-methane	Purity % molar fraction of hydrogen	Number of cycles
1	298.15	0.162	980	0.02-0.26-0.69-0.03	94.85	30
2	283.24	0.162	980	0.02-0.26-0.69-0.03	98.01	2
3	313.05	0.162	980	0.02-0.26-0.69-0.03	90.02	2
4	298.15	0.153	980	0.02-0.26-0.69-0.03	94.95	1
5	298.15	0.170	980	0.02-0.26-0.69-0.03	94.75	1
6	298.15	0.162	931	0.02-0.26-0.69-0.03	95.00	1
7	298.15	0.162	1029	0.02-0.26-0.69-0.03	94.65	1
8	298.15	0.162	980	0.02-0.2945-0.6555-0.03	94.00	2
9	298.15	0.162	980	0.02-0.2255-0.7245-0.03	95.50	2

To solve this type of PDE, initial and boundary conditions are needed in each step of the PSA process, as an example, the conditions established for the model of Simo et al. [34] are shown in Table 5, where the Roman numerals indicate the sequence in how they should be applied successively for each step of the process:

3.3. Parametric Study of the PSA Process for the Production of Bioethanol. To observe the dynamics of the purity achieved from the start and reach the CSS, the case of Simo et al. [34] is proposed. The parameters of this PSA process for the production and purification of bioethanol are shown in the following Table 6.

Figure 4 shows how the purity of ethanol increases and the purity of water decreases, this is due to the conditions established in Table 6 and the selective characteristics of the adsorbent to retain the greatest number of water molecules. The ethanol profile rises as the cycles pass until reaching the CSS and obtaining a purity of 99% by wt of ethanol. CSS is reached after 350 cycles (67 h).

Subsequently, Figure 5 shows the possible input variables that can have a greater and lesser effect on the purity of bioethanol. These tests were done in the CSS.

The results obtained with this analysis show that the temperature, flow, and composition of the feed have a greater effect on the purity of ethanol. On the other hand, the pressure variable has no effect on purity. An important difference between the variables that had the greatest effect on ethanol purity was the convergence time. Due to this criterion, it can be seen that the feed composition has the shortest time compared to the other two variables. For this reason, it is of great importance to have the composition of the feed controlled at the time of entering it at the entrance of the real PSA process, since this can cause decreases in purity, acting as a disturbance (see Table 7).

4. Biohydrogen Purification by PSA

Biohydrogen is a biologically produced gas; it is obtained from algae, bacteria, and archaea. Biohydrogen is a biofuel with great potential that can be obtained through specific cultivation or from organic waste [42, 43]. Biohydrogen can serve as the energy source for gas turbines and fuel cells, or as the raw material for chemical industries [44]. The development of a biohydrogen station system is important to the commercialization of fuel cells and fuel cell-powered vehicles. One of the key challenges for biohydrogen production is the design of an efficient purification process. In conventional hydrogen production plants, the shifted gas should first be precooled to meet the temperature requirement of CO_2 absorption units, and then be reheated after the CO_2 removal [4]. Additional purification units are needed to remove the residual trace CO because of the thermodynamically [45]. Alternatively, the elevated-temperature pressure swing adsorption process based on WGS catalysts and CO_2 and methane adsorbents are able to achieve triple functions: CO catalytic conversion, methane and CO_2 adsorption, and hydrogen purification in a single unit [46].

The main methods for hydrogen production can be categorized as follows:

(i) Fossil fuels as a source of hydrogen production

(ii) Water as a source of hydrogen production

(iii) Utilization of solar energy

(iv) Biological methods of hydrogen production

(v) Fermentative hydrogen production from organic compounds

(vi) Hydrogen production from biomass

Our lab is focused on hydrogen production by mean dark fermentation using different consortia and agroindustrial waste as substrate. Hydrogen production by fermentative processing has been given little attention, while hydrogen production by photosynthetic microorganisms has been studied extensively. The evolution of hydrogen by fermentation has, however, several advantages for industrial production [47–49].

Fermentative bacteria have a very high evolution rate of hydrogen. They can produce hydrogen constantly, day and night, from organic substrates. They can have a growth rate adequate for the supply of microorganisms to the production systems.

Table 14: Comparison of the thermodynamic values of various adsorbents as a function of different temperatures and pressures.

Reference	Adsorbents	Temperature K	Maximum adsorption capacity Q $\left(g\, g_{ads}^{-1}\right)$	Langmuir constant (bar^{-1})	Pressure Atm
[79]	5A	273	0.063 (N_2)	0.073	1.97-5.9
	5A	293	0.049 (N_2)	0.073	1.97-5.9
	5A	313	0.040 (N_2)	1.214	1.97-5.9
	5A	333	0.035 (N_2)	1.214	1.97-5.9
[80]	CMS	283	0.07 (N_2)	20.5	7.8
	CMS	298	0.0588 (N_2)	15.6	7.8
	CMS	308	0.0532 (N_2)	10.7	7.8
[81]	CMS	297	0.8430 (N_2)	4.663×10^4	4-6
	CMS	297	0.4430 (Ar)	714.904	4-6
	CMS	296	0.85 (N_2)	4.741×10^4	4-6
	CMS	296	0.5107 (N_2)	717.548	4-6
[82]	5A	298.15	0.1484 (N_2)	—	1.48-4.35
	CMS	298.15	0.07392 (N_2)	—	2.0-6.7
[77]	Li-LSX	288	0.0392 (N_2)	0.8574	1
	Li-LSX	298	0.0308 (N_2)	0.8574	1
	Li-LSX	308	0.0252 (N_2)	0.8574	1
	Na-LSX	288	0.014 (N_2)	0.1037	1
	Na-LSX	298	0.0112 (N_2)	0.1037	1
	Na-LSX	308	0.0084 (N_2)	0.1037	1
	K-LSX	288	0.0077 (N_2)	0.00479	1
	K-LSX	298	0.0056 (N_2)	0.00479	1
	K-LSX	308	0.00378 (v)	0.00479	1
[83]	5A	298.15	0.146 (N_2)	2813.7	1
	Li-ag-X	298.15	0.089 (N_2)	28613.0	
[84]	NaX	296.15	0.083 (N_2)	8.319×10^{-5}	1-1.4
[85]	Oxysiv 5	293.15	0.0865 (N_2)	0.1006	3-4
	Oxysiv 5	293.15	0.123 (Ar)	0.03365	3-4
	AgLiLSX	293.15	0.0738 (N_2)	0.2581	3-4
	AgLiLSX	293.15	0.2900 (Ar)	0.0230	3-4
[86]	Mordenite	303.15	0.0532 (N_2)	—	3
	A	303.15	0.0252 (N_2)	—	2.5
	X	303.15	0.0259 (N_2)	—	3.5
[87]	LiLSX	289.15	0.0602 (N_2)	2.418×10^{-6}	1
[78]	LiLSX (Zeochem)	273.1	0.07 (N_2)	2.587×10^{-5}	1
	LiLSX (Zeochem)	303.1	0.0476 (N_2)	2.585×10^{-5}	1
	LiLSX (Zeochem)	338.1	0.035 (N_2)	2.577×10^{-5}	1
	LiLSX (Arkema)	273.1	0.063 (N_2)	3.446×10^{-5}	1
	LiLSX (Arkema)	303.1	0.0434 (N_2)	3.406×10^{-5}	1
	LiLSX (Arkema)	338.1	0.0308 (N_2)	3.366×10^{-5}	1
[88]	LSCF1991	773.15	0.0168 (N_2)	0.0693	1
	LSCF1991	873.15	0.014 (N_2)	0.0854	1
	LSCF1991	973.15	0.0112 (N_2)	0.1001	1
	LSCF1991	1073.15	0.0105 (N_2)	0.1082	1

Table 14: Continued.

Reference	Adsorbents	Temperature K	Maximum adsorption capacity Q $\left(g\, g_{ads}^{-1}\right)$	Langmuir constant (bar^{-1})	Pressure Atm
[89]	LiX	288.15	0.042 (N_2)	9.50×10^{-6}	3.5
	LiX	303.15	0.035 (N_2)	9.39×10^{-6}	3.5

Table 15: Works reported on the different configurations of PSA processes for purification of medical oxygen.

Reference	Experimental/simulated	PSA cycles	Pressure swing (kPa)	Bed regeneration time (min)	Oxygen feed (% molar fraction)
[83]	Experimental	1 bed 4 steps	400 to 100	0.016	21
[90]	Simulated	2 beds 5 steps	100 to 90	—	21
[91]	Simulated	4 beds 7 steps	300 to 50	1.3	22
[79]	Experimental	2 beds 6 steps	150 to 50	—	50
[75]	Simulated	6 beds 9 steps	1000 to 100	—	21
[92]	Experimental	2 beds 6 steps	355 to 101	0.33	90
[93]	Simulated	2 beds 5 steps	150 to 100	0.1 to 2.1	—
[94]	Simulated	2 beds 4 steps	250 to 75	0.666	20.8
[95]	Experimental	2 beds 3 steps	250 to 100	0.166	21
[96]	Simulated	1 beds 4 steps	—	0.083	20 to 50
[97]	Experimental	4 and 6 beds 5 steps	250 to 101	0.5, 0.8, and 1	—

Therefore, fermentative evolution is more advantageous than photochemical evolution for the mass production of hydrogen by microorganisms. Fermentative hydrogen production can be maximized through the effective coupling of the following factors:

(i) An accessible and rich source of electron and biochemical electron pump

(ii) An active hydrogenase

4.1. Adsorption and Separation for the CO, CO_2, Nitrogen, Methane, Water, H_2S, and Hydrogen Mixture with Different Adsorbents. In the case of the separation and purification of hydrogen, it is necessary to consider adsorbents (activated carbon, zeolite, silica gel, activated alumina) that have selectivity over the components: CO, CO_2, methane, etc. This makes it possible to use multigas isotherms (without interaction parameters) for multicomponent adsorption modeling [50].

The PSA process for the purification and production of hydrogen is necessary the use of different types of adsorbents with a high degree of selectivity, for this, silica gel can remove moisture and higher hydrocarbons, and the use of activated carbon retains CH_4, CO_2, and H_2S [51]. Finally, it is known that zeolite 5A is one of the adsorbents that have a high selectivity over N_2 and CO. There are several different materials and adsorbents on the market, making it difficult to compare data from the literature.

For this, the different adsorbents that can be used to purify hydrogen have been investigated in detail; the results found are shown in Table 8.

Table 8 shows different types of adsorbents, however, the most outstanding are CMS-T3A, PCB-activated carbon, and activated carbon. These adsorbents show selectivity over a variety of compounds (N_2, O_2, Ar, CO, CO_2, CH_4, and H_2S) and have higher adsorption compared to other natural and synthetic adsorbents. One difference between these three defined adsorbents is the adsorption capacity from temperature change.

4.2. Mathematical Models, Characteristics, and Configuration of the PSA Process for the Production of Biohydrogen. To ensure a continuous separation process, multiple columns are required (see Table 9). H_2 purification is done with the PSA process, using an adsorption pressure of 500 to 4000 kPa and for the purge step, only 100 kPa is

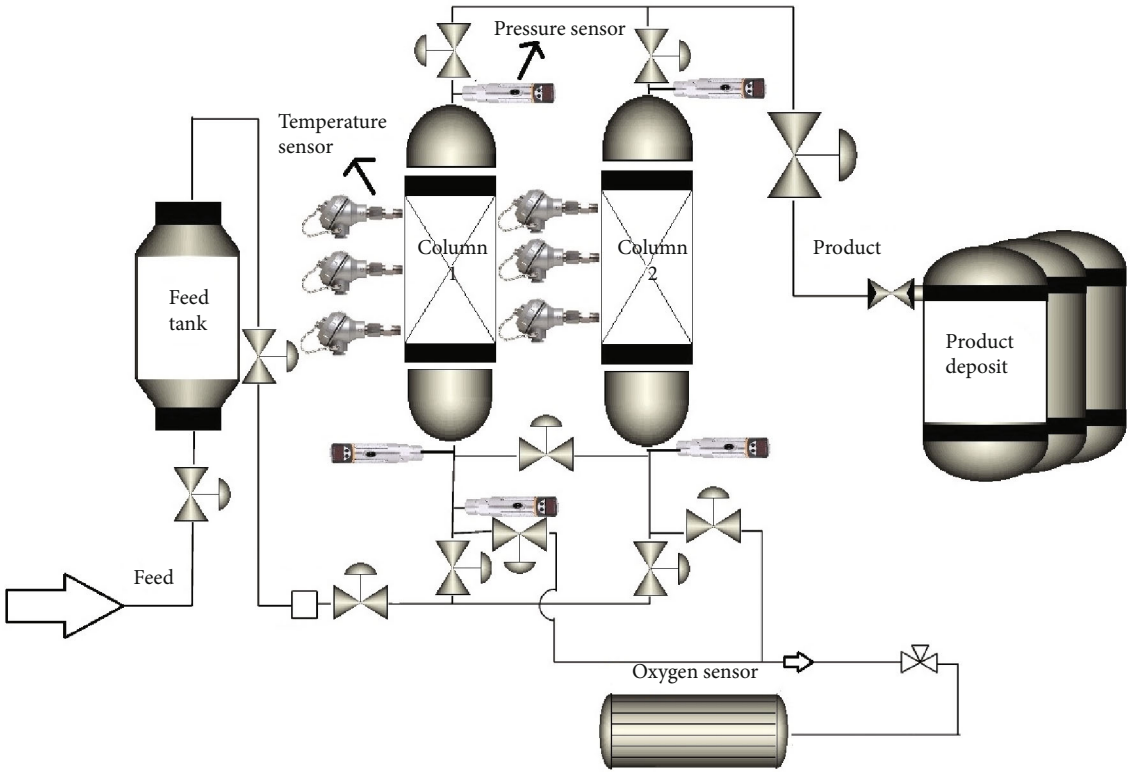

Figure 9: Schematic diagram of the PSA process using 2-beds, 6-steps.

Table 16: Distributed parameter models of the PSA processes for medical oxygen production.

Reference	Equations governing the PSA process (nonlinear model)	Temperature effects	Pressure effects
[98]	4 PDEs	Does not present adsorption isotherms	Consider pressure gradient
[87]	3 PDEs	Consider adsorption isotherms	No pressure gradient
[94]	5 PDEs	Consider adsorption isotherms	Consider pressure gradient
[77]	3 PDEs	Consider adsorption isotherms	No pressure gradient
[88]	4 PDEs	Consider adsorption isotherms	Consider pressure gradient

used. A temperature of 295 K is contemplated in the production and regeneration stages. For the production and purification of biohydrogen, a minimum of 4 columns is used (see Figure 6).

Different types of structures and configurations have been studied with respect to the PSA process, one of them presented a study of the performance of the PSA process using multiple beds to produce high purity biohydrogen from synthesis gas H_2: 72.2%, CH_4: 4.17%, CO: 2.03%, CO_2: 21.6%). In the study of Yang et al. [66], it was an experimental and theoretical work, as a result, they obtained purity of 99.999% of biohydrogen and recovery of 66% of the synthesis gas, with an oscillating pressure of 100 to 800 kPa and ambient temperature.

Table 9 shows the different configurations presented by the PSA processes for the production of biohydrogen.

It can be seen in Table 9 that more beds are used compared to bioethanol production, likewise, the number of steps is greater and the pressure values are high with oscillations between 1000 and 10000 kPa. To do the purge, it is only necessary to handle an atmospheric pressure and it is not necessary to use a vacuum pressure.

In the study of Liemberger et al. and Yang et al. [50, 66], they showed that the recovery of hydrogen increases when the linear speed and the adsorption time increase, however, the purity of the hydrogen decreases. On the other hand, the 4-bed 9-step PSA process could be optimally operated at a linear speed of 3 cms^{-1}, adsorption time of 50 s, and a pressure of 200 kPa in the purge step (see Figure 7).

Table 10 shows the modeling characteristics that describe the PSA process for biohydrogen production and shows that the number of PDEs can vary, depending on the considerations to obtain a less complex model. In some works, the results and profiles of pressure and temperature are considered, and in others only one of these variables that are a function of time and space.

The base mathematical model that was taken from the works of Lee et al. and Xiao et al. [42, 43] (see Table 11).

Table 17: Governing equations and simplifications for production and purification of medical oxygen.

Overall mass balances	$-D_l\left(\partial C_i/\partial_z^2\right) + \left(\partial(\mathrm{uc}_i)/\partial_z\right) + \left(\partial c_i/\partial_t\right) + \rho_p(1-\varepsilon/\varepsilon)\left(\bar{\partial} q_i/\partial_t\right) = 0$
Energy balance equation	$-K_L\dfrac{\partial^2 T}{\partial_z^2} + \varepsilon\rho_g C_{\mathrm{pg}}\dfrac{\partial(uT)}{\partial_z} + \left(\varepsilon_t\rho_g C_{\mathrm{pg}+\rho_B C_{\mathrm{ps}}}\right)\dfrac{\partial T}{\partial t} - \rho_B\sum_{i=1}^{n}(\bar{-}\Delta H)\dfrac{\bar{\partial} q_i}{\partial t} + \dfrac{2h_i}{R_{Bi}}(T-T_W) = 0$
Pressure drop	$-\dfrac{\mathrm{dP}}{\mathrm{dz}} = a\mu u + b\rho u\lvert u\rvert, , a = \dfrac{150\,(1-\varepsilon)^2}{4R_p^2}\dfrac{}{\varepsilon^2}, , b = 1.75\dfrac{(1-\varepsilon)^2}{2R_p^{\varepsilon}}\Bigg)$
Multicomponent adsorption equilibrium	$q_i = \dfrac{q_{\mathrm{mi}B_i P_i^{\mathrm{ni}}}}{1+\sum_{j=1}^{n} B_j P_j^{\mathrm{nj}}}$
LDF model	$\bar{\partial} q_i/\partial t = w_i(q_i^* - \bar{q}_i), , w_i = \mathrm{KD}_{\mathrm{ei}}/R_p^2$
Boundary and initial conditions	
I. Pressurization	
(i) $t = 0$	$c_i(Z,0) = 0, \bar{q}_i(Z,0) = 0, T_i = (Z,0) = T_0, P_i\,(Z,0) = P_p$
(ii) $z = 0$	$-\left(\dfrac{\partial c_i}{\partial Z}\right) = Pe_m U\left(C_i\Big\lvert z_{(=0)} - C_i\Big\lvert z_{=0+1}\right), \bar{q}_i(0,t) = 0, T_i = (0,1) = T_0, P_i(0,t) = P_p$
(iii) $z = L$	$\left(\dfrac{\partial c_i}{\partial Z}\right) = 0, \left(\dfrac{\partial T_i}{\partial Z}\right) = 0, \left(\dfrac{\partial P_i}{\partial Z}\right) = 0$
II. Adsorption	
(i) $t = 0$	$c_i(Z,0) = c_i^{(I)}, \bar{q}_i(Z,0) = q_i^{(I)}, T_i = (Z,0) = T_i^{(I)}, P_i\,(Z,0) = P_i^{(I)}$
(ii) $z = 0$	$\left(\dfrac{\partial c_i}{\partial Z}\right) = 0, \left(\dfrac{\partial T_i}{\partial Z}\right) = 0, \left(\dfrac{\partial P_i}{\partial Z}\right) = 0$
(iii) $z = L$	$\left(\dfrac{\partial c_i}{\partial Z}\right) = 0, \left(\dfrac{\partial T_i}{\partial Z}\right) = 0, \left(\dfrac{\partial P_i}{\partial Z}\right) = 0$
III. First blowdown	
(i) $t = 0$	$c_i(Z,0) = c_i^{(II)}, \bar{q}_i(Z,0) = q_i^{(II)}, T_i = (Z,0) = T_i^{(II)}, P_i(Z,0) = P_i^{(II)}$
(ii) $z = 0$	$\left(\dfrac{\partial c_i}{\partial Z}\right) = 0, \left(\dfrac{\partial T_i}{\partial Z}\right) = 0, \left(\dfrac{\partial P_i}{\partial Z}\right) = 0, F = F_{valve}$
(iii) $z = L$	$\left(\dfrac{\partial c_i}{\partial Z}\right) = 0, \left(\dfrac{\partial T_i}{\partial Z}\right) = 0, \left(\dfrac{\partial P_i}{\partial Z}\right) = 0$
IV. Second blowdown	
(i) $t = 0$	$c_i(Z,0) = c_i^{(III)}, \bar{q}_i(Z,0) = q_i^{(III)}, T_i = (Z,0) = T_i^{(III)}, P_i(Z,0) = P_i^{(III)}$
(ii) $z = 0$	$\left(\dfrac{\partial c_i}{\partial Z}\right) = 0, \left(\dfrac{\partial T_i}{\partial Z}\right) = 0, \left(\dfrac{\partial P_i}{\partial Z}\right) = 0, F = F_{valve}$
(iii) $z = L$	$\left(\dfrac{\partial c_i}{\partial Z}\right) = 0, \left(\dfrac{\partial T_i}{\partial Z}\right) = 0, \left(\dfrac{\partial P_i}{\partial Z}\right) = 0$
V. Purge	
(i) $t = 0$	$c_i(Z,0) = c_i^{(IV)}, \bar{q}_i(Z,0) = q_i^{(IV)}, T_i = (Z,0) = T_i^{(IV)}, P_i(Z,0) = P_i^{(IV)}$
(ii) $z = 0$	$\left(\dfrac{\partial c_i}{\partial Z}\right) = 0, \left(\dfrac{\partial T_i}{\partial Z}\right) = 0, \left(\dfrac{\partial P_i}{\partial Z}\right) = 0, F = F_{valve}$
(iii) $z = L$	$(\partial c_i/\partial Z) = 0, (\partial T_i/\partial Z) = 0, (\partial P_i/\partial Z) = 0$

A semicomplete model is proposed since it does not contemplate the part of the equations of the wall and a general balance. It uses four steps to complete one cycle of the PSA process.

The initial and boundary conditions are contemplated in Table 11, the mathematical model finds solutions of Y, c, T, and P as a function of time and space.

4.3. Parametric Study of the PSA Process for the Production of Biohydrogen. The base model of the works of Lee et al. and Xiao et al. [42, 43] was used. The parameters of this PSA process for the production and purification of biohydrogen are shown in Table 12.

The results found from the start-up to reaching the CSS are shown in Figures 6 and 8.

Figure 6 shows how the purity of hydrogen increases and the purities of CO, CO_2, and methane decreases; this is due to the selectivity of the adsorbent and the nominal star-up conditions shown in Table 12. The hydrogen profile goes up as the cycles pass until reaching the CSS and obtaining a purity of 95%. CSS is reached after 30 cycles (1.2 h).

Figure 8 shows the results obtained from variations of 0.5% on the input variables. In most cases (pressure, flow, and composition), the effects on hydrogen purity were negligible. However, the effect of the temperature variable presented important changes, defined as the main variable that can be used to control the purity of hydrogen. It is important to mention that this variable is limited in its small values since it cannot generate values less than 5° since this would generate energy costs due to the demand to use temperatures less than 0°.

Table 13 shows the detailed data of the results presented in Figure 8. It shows the cycle times, the purities, and the changes generated by each input variable.

5. Medical Oxygen Purification by PSA

Medical oxygen is a mixture of gases that typically has an oxygen percentage equal to or greater than 93%, and is widely prescribed for mechanically ventilated patients in intensive care units [73]. The rest of the compounds of the mixture includes nitrogen and argon, and contain 0.03% CO_2 or 0.001% CO [74]. To achieve that percentage of oxygen, PSA processes are necessary. In them, air from the environment is subjected to filtration and compression stages before passing through a bed of zeolites. The adsorption of the molecules will depend on the pressure and temperature; these zeolites have greater selectivity over nitrogen molecules than oxygen, thus resulting in the air with a higher proportion of oxygen.

The last year has seen an increase in the demand for medical oxygen due to the pandemic generated by COVID-19. That is why it has ventured into the development of portable technologies that generate oxygen, having a resource that provides oxygen supply for anoxic environments, due to its profitability, operating flexibility, and oxygen purification. It may be used in chemical processing, fishing farms, medical applications, combustion enhancement, oxyfuel cutting operations in metal fabrication, bleaching in the paper industry, wastewater treatment, fuel cells, etc. [75, 76]. One of the technological alternatives to purify and produce medical oxygen is the adsorption process with molecular sieves using the pressure swing adsorption method. The PSA can be operated with a pressure range from 1 to 1000 kPa and room temperature for small-scale oxygen production with high purity between 90%, 95%, and 99%. In general, the separation of the air is carried out at relatively high pressure and the nitrogen molecules are retained on the natural or synthetic zeolites [77, 78].

5.1. Adsorption and Separation for the O_2, N_2, and Ar with Different Adsorbents. In the case of the nitrogen and oxygen separation isotherms, it was determined by the energetic homogeneity of the surface of the adsorbents. The isotherms for this type of separation are concave towards the axis of relative pressure or concentrations (see Figure 2), so it is assumed that they correspond to the type I isotherms, which are for adsorption of gases in microporous solids.

Table 18: Start-up parameters of the PSA process for the purification and production of medical oxygen.

FEED		
Flow	0.894	$kmolh^{-1}$
Nitrogen	0.78	$kmolkmol^{-1}$
Oxygen	0.22	$kmolkmol^{-1}$
Temperature	296.15	K
Production pressure	150	kPa
Purge pressure	20	kPa
SIZING		
Bed height	1.8	m
Bed diameter	0.11	m
NaX zeolite		
Particle radius	0.000985	m
Bulk solid density	911.72	$Kg\,m^{-3}$

For this separation of compounds, there are different types of adsorbents; these can be Ca-X, CMS, LiX, 5A or 13X, NaX, or LiLSX. However, the concentration of the product is limited to 95% oxygen, because of the presence of argon in air, since these adsorbents present similar adsorption capacities for oxygen and argon.

For this reason, there are several adsorbents that can be used to adsorb and separate oxygen from argon. Some natural and synthetic zeolites are also identified in the following Table 14.

Table 14 shows varieties of adsorbents with different adsorption capacities on the selective compounds. It will be observed that at lower temperatures, adsorbents tend to adsorb more molecules or atoms. It can be seen that zeolite type 5A and CMS have higher adsorption capacity compared to the other adsorbents. Likewise, it observes that the ranges in which the PSA process works for the production of medical oxygen range from 1 to 4 bar, which are lower compared to the other PSA processes for the production of bioethanol and biohydrogen.

The basic PSA process may be using only one bed, however up to two or three beds may be implemented. These adsorbent-packed columns can release heat energy in the adsorption step and adsorb it in the regeneration step. In this case, the PSA process for the production of medical oxygen does not contemplate very high pressures since it uses the heat produced to improve the regeneration capacity.

For the production of medical oxygen using the PSA process, there is a great variety of structures and configurations, but there is one in particular for the separation of oxygen, which is the Rapid Pressure Swing Adsorption (RPSA), this type of configuration has been shown in several works. Related to the production of medical oxygen and above 99% in purity, the times contemplated by this configuration are very short with very small columns. Table 15 shows the different works that exist.

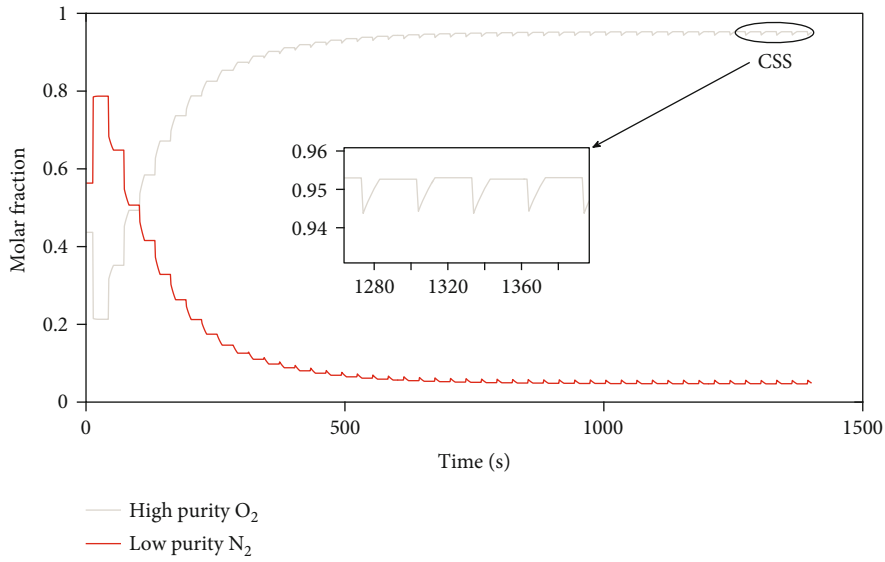

Figure 10: Purification and production of medical oxygen from the start-up.

The scheme of the PSA process for the production of medical oxygen is shown in Figure 9. Two stainless steel columns with a length of 1 m are presented. Temperature sensors (RTD and PT 100) are provided along the column, providing data from the feed end to the top. Two pressure transducers placed on the flanges, the feed flow to the columns is controlled with a tank and regulating valve, concentration variations in the stages are analyzed with oxygen sensors.

A wide variety of works that have developed numerical calculations with different simplifications or considerations applied to PSA processes for medical oxygen production.

Numerical methods techniques have been used to obtain an approximate solution of the PDEs that represent the complex model of the PSA process. Table 16 shows the different works that implement certain conditions to simplify the PSA mathematical model.

The PSA process model used in this section is shown in Table 17. An energy balance equation is included, establishing that the temperatures in the solid and gas are constant and equal. The pressure drop is represented using the Ergun equation; Langmuir model was used to describe the adsorption isotherm. Mass transfer is represented using a linear driving force model based on solid charge. These equations represented by PDEs contemplate their initial and boundary conditions to obtain a solution in each step of the PSA process for medical oxygen production.

The works of Todd et al. and Webley and He [84, 99] were contemplated to structure the PSA model for medical oxygen production, this is shown in Table 17.

5.2. Parametric Study of the PSA Process for the Production of Medical Oxygen. Table 18 shows the parameters with which the process begins until reaching the CSS and obtaining a purity of medical oxygen of 95.00%.

The results found from the start-up to reaching the CSS are shown in Figures 10 and 11.

Figure 10 shows the oxygen and nitrogen profiles. Between cycles 3 and 4, the molar fraction of oxygen experiences a drop, this is due to the fact that both beds start with atmospheric pressure, and this continues until the beds stabilize with the appropriate pressure of 150 kPa. Subsequently, the mole fraction of oxygen begins to rise, and that of nitrogen falls. These continue until reaching the CSS, which is fulfilled at 23 cycles, obtaining a medical oxygen purity of 95.00%.

Table 19 and Figure 11 show the changes made to the input variables and the results obtained on oxygen purity. The variation that was made while in the CSS was 0.5%.

The results shown in Figure 11 demonstrate that all input variables have an effect on oxygen purity. However, the most outstanding variables are feed pressure and composition. A differentiator between these two variables is the purity is obtained. It is observed that by varying the feed composition, higher oxygen purity can be achieved with a shorter cycle time compared to that shown by the pressure variable. It is of great importance to be able to manipulate this variable since it can cause the purity to drop during the production and purification of medical oxygen.

Table 19 shows the detailed data of the results presented in Figure 8. It shows the cycle times, the purities, and the changes generated by each input variable.

6. Biomethane Purification by PSA

Biomethane is a gas generated from renewable resources, produced from organic matter (biomass, agricultural, industrial, urban waste, etc.). This has characteristics similar to natural gas and has great advantages over fossil fuels, which allow the reduction and dependency on external energy. This biogas can be applied in the market for the industry, domestic sector, and electricity generation. However, for this biogas to be used, it is necessary to separate it from the compound CO_2 and

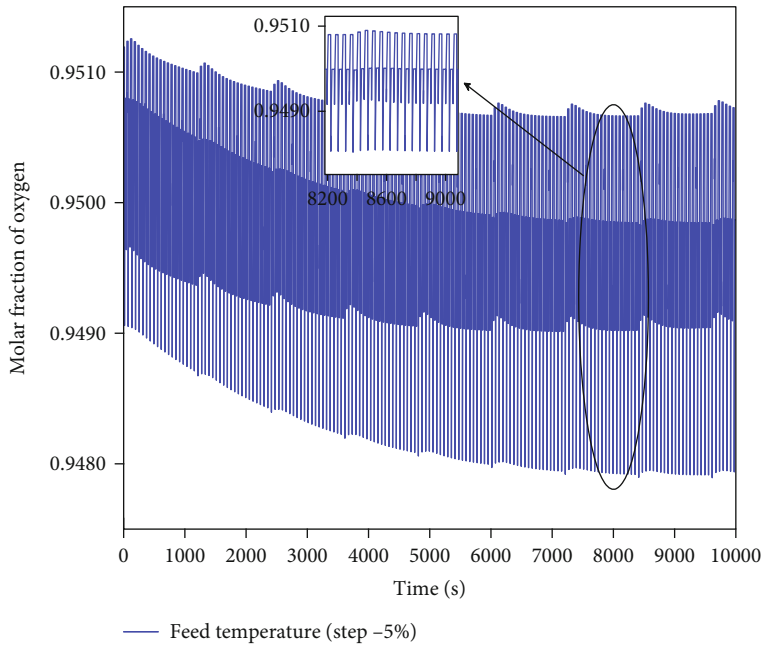

(a) Temperature: 296.15 K to 281.34 K; Flow: 0.89436528 kmolh^{-1}; Pressure: 150 kPa; Molar fraction: 0.78 (N_2) and 0.22 (O_2)

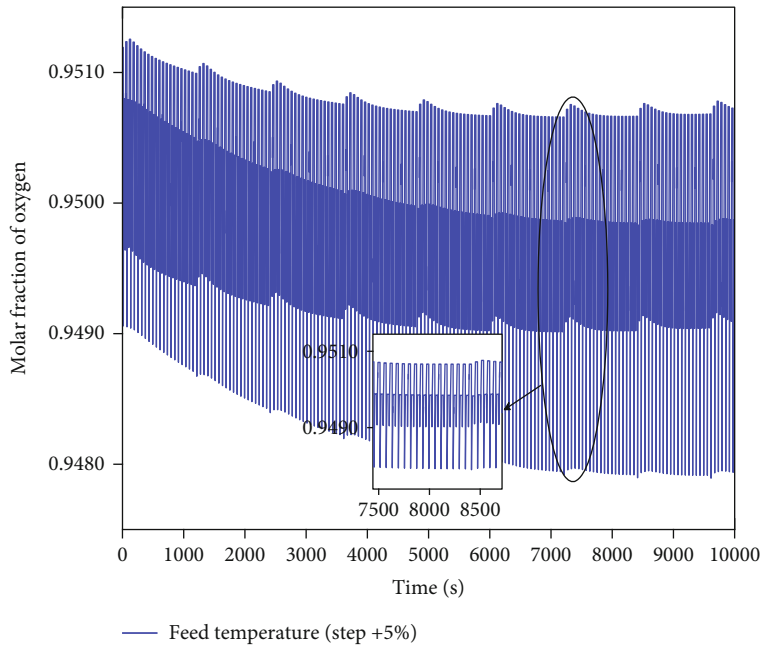

(b) Temperature: 296.15 K to 310.95 K; Flow: 0.89436528 kmolh^{-1}; Pressure: 150 kPa; Molar fraction: 0.78 (N_2) and 0.22 (O_2)

Figure 11: Continued.

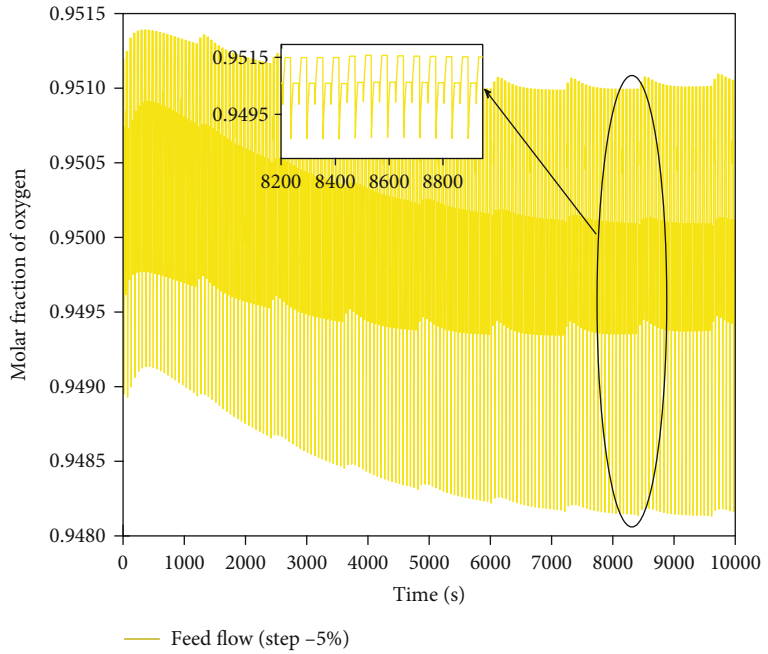

(c) Flow: 0.89436528 kmolh^{-1} to 0.849647016 kmolh^{-1} Temperature: 296.15 K; Pressure: 150 kPa; Molar fraction: 0.78 (N_2) and 0.22 (O_2)

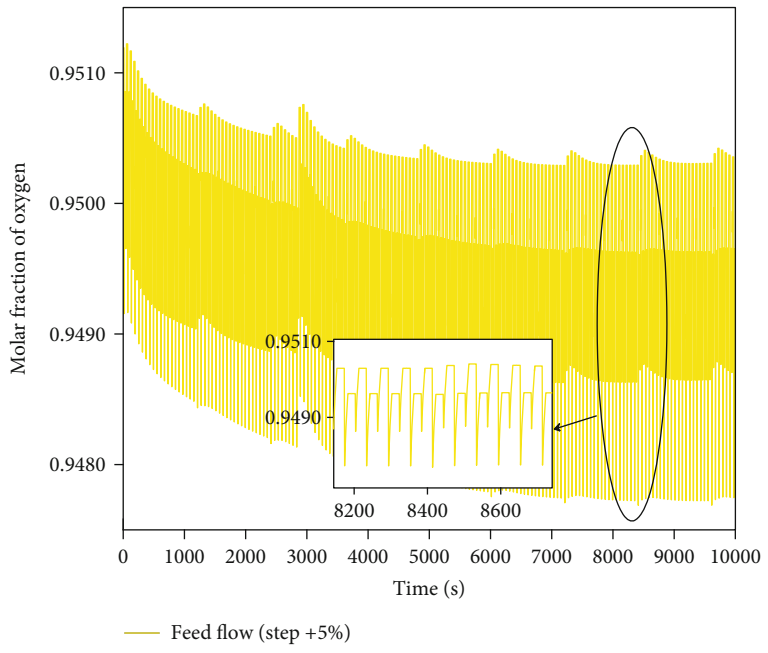

(d) Flow: 0.89436528 kmolh^{-1} to 0.939083544 kmolh^{-1} Temperature: 296.15 K; Pressure: 150 kPa; Molar fraction: 0.78 (N_2) and 0.22 (O_2)

Figure 11: Continued.

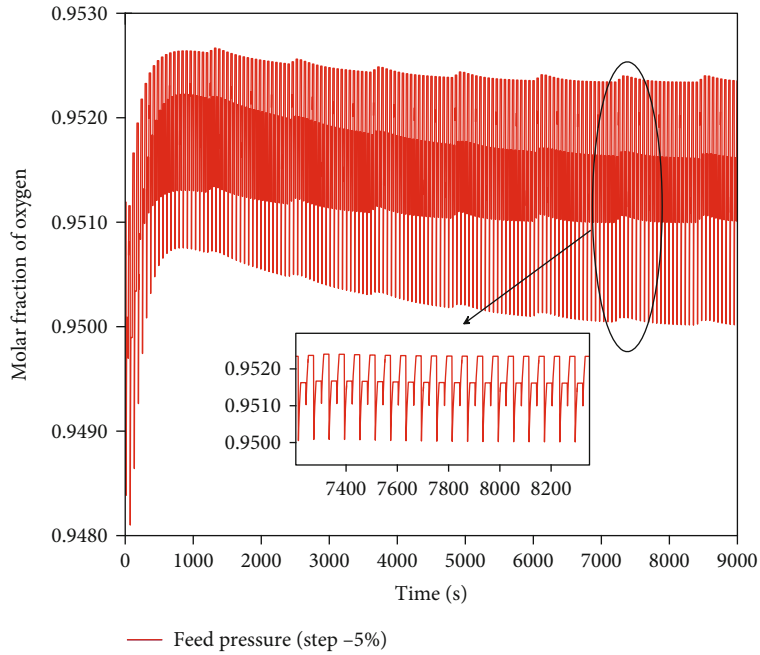

(e) Pressure: 150 kPa to 142.5 kPa; Flow: 0.89436528 kmolh^{-1}; Temperature: 296.15 K; Molar fraction: 0.78 (N_2) and 0.22 (O_2)

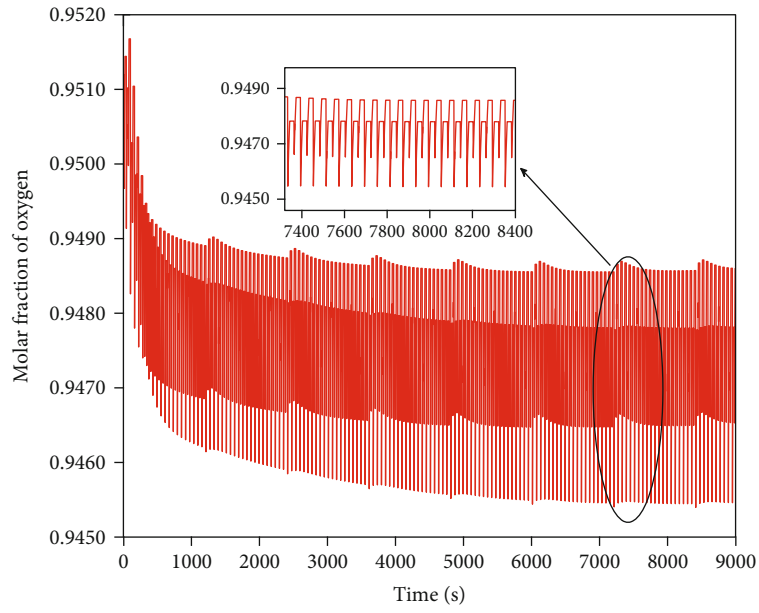

(f) Pressure: 150 kPa to 157.5 kPa; Flow: 0.89436528 kmolh^{-1}; Temperature: 296.15 K; Molar fraction: 0.78 (N_2) and 0.22 (O_2)

Figure 11: Continued.

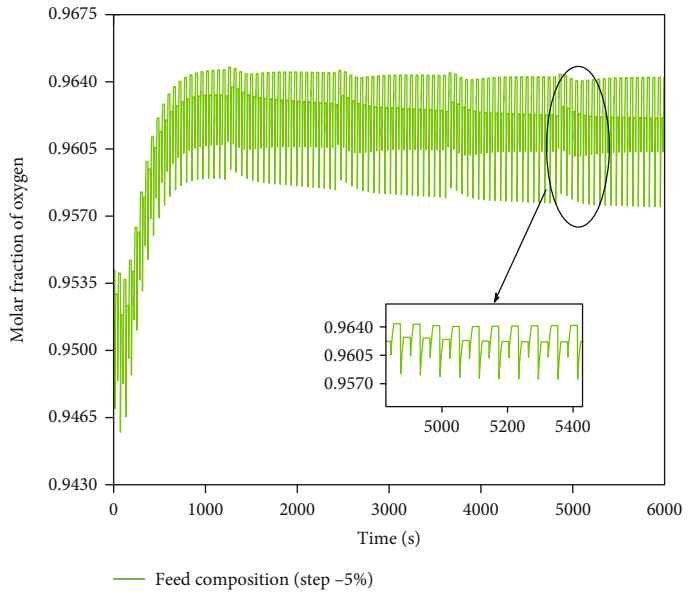

(g) Molar fraction: 0.78 (N_2) and 0.22 (O_2). to 0.741 (N_2) and 0.259 (O_2); Pressure: 150 kPa to 157.5 kPa; Flow: 0.89436528 $kmolh^{-1}$; Temperature: 296.15 K

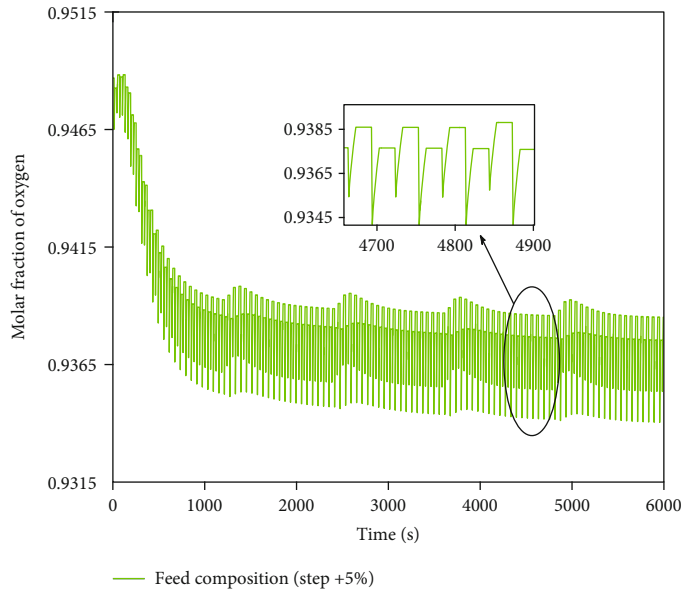

(h) Molar fraction: 0.78 (N_2) and 0.22 (O_2). to 0.819 (N_2) and 0.181 (O_2); Pressure: 150 kPa to 157.5 kPa; Flow: 0.89436528 $kmolh^{-1}$; Temperature: 296.15 K

Figure 11: Sensitivity analysis applied to the PSA process for the production of medical oxygen.

Table 19: Analysis of the possible input variables that have the greatest effect on the purity obtained.

Run	Temperature (K)	Flow $kmolh^{-1}$	Pressure kPa	Composition nitrogen-oxygen	Purity % molar fraction of oxygen	Number of cycles
1	296.15	0.89436528	150	0.78-0.22	95.00	40
2	281.34	0.89436528	150	0.78-0.22	94.90	16
3	310.95	0.89436528	150	0.78-0.22	94.90	16
4	296.15	0.849647016	150	0.78-0.22	95.20	14
5	296.15	0.939083544	150	0.78-0.22	94.80	15
6	296.15	0.89436528	142.5	0.78-0.22	95.30	12
7	296.15	0.89436528	157.5	0.78-0.22	94.60	11
8	296.15	0.89436528	150	0.741-0.259	95.40	9
9	296.15	0.89436528	150	0.819-0.181	94.00	10

Table 20: Comparison of the thermodynamic values of various adsorbents as a function of different temperatures and pressures.

Reference	Adsorbents	Temperature K	Maximum adsorption capacity Q $(g\, g_{ads}^{-1})$	Langmuir constant (bar^{-1})	Pressure Atm
[100]	Silicalite	313.15	0.125 (CO_2)	1.089	5
[5]	NaA zeolite	277	0.228(CO_2)	—	10
	ZSM/C	293	0.139(CO_2)	—	4
	T-type nanoparticles zeolite	288	0.21296(CO_2)	—	1
	13X zeolite	323	0.229(CO_2)	—	1
	SX-[bmim] [TF2N]	298	0.2234(CO_2)	—	20
	BphC18PMOP 1200	298	0.04092(CO_2)	—	1
	APTES@SHEPF	298	0.10516(CO_2)	—	1
	APTMS@PhC12PMO	298	0.03168(CO_2)	—	1
[101]	Silica gel	298.15	0.264(CO_2)	8.609×10^{-6}	1
[102]	CMS-3 K	323	0.1188(CO_2)	12.74×10^{-6}	6.5
	CMS-3 K	308	0.1012(CO_2)	12.74×10^{-6}	6.5
	CMS-3 K	298	0.088(CO_2)	12.74×10^{-6}	6.5
[103]	COSMO zeolite 13X	298	0.1936(CO_2)	0.149	3
	COSMO zeolite 13X	333	0.1364(CO_2)	0.149	3
	UOP zeolite 13X	298	0.2288(CO_2)	0.149	3
	UOP zeolite 13X	333	0.1584(CO_2)	0.149	3
	EIKME zeolite 13X	298	0.22(CO_2)	0.149	3
	EIKME zeolite 13X	333	0.132(CO_2)	0.149	3
	COSMO zeolite 5A	298	0.154(CO_2)	0.149	3
	COSMO zeolite 5A	333	0.1496(CO_2)	0.149	3
	Activated carbon	298	0.1276(CO_2)	0.149	3
	Activated carbon	333	0.0748(CO_2)	0.149	3
[104]	Potassium clinoptilolite N	573	0.00638(CO_2)	—	10
	Potassium clinoptilolite N	573	0.00286(CO_2)	—	11
	Potassium clinoptilolite N	573	0.00308(CO_2)	—	16
	Potassium clinoptilolite N	548	0.00616(CO_2)	—	10
	Potassium clinoptilolite N	548	0.00264(CO_2)	—	10
	Potassium clinoptilolite Z1	548	0.0044(CO_2)	—	10
	Potassium clinoptilolite Z1	523	0(CO_2)	—	—
	Potassium clinoptilolite Z1	523	0.002684(CO_2)	—	12.5
	Potassium clinoptilolite Z1	523	0.00484(CO_2)	—	20
	Potassium clinoptilolite Z1	498	0(CO_2)	—	10
	Potassium clinoptilolite Z2	498	0.003476(CO_2)	—	10
	Potassium clinoptilolite Z2	498	0.0044(CO_2)	—	10
	Potassium clinoptilolite Z2	473	0(CO_2)	—	10
	Potassium clinoptilolite Z2	473	0.00277(CO_2)	—	10
	Potassium clinoptilolite Z2	473	0.0044(CO_2)	—	10
[105]	MOF-508b	296.15	0.083(N_2)	0.12	5
	CMS-3 K	296.15	0.080(N_2)	1.13	5
[106]	Zeolite 13X	313	0.176 (CO_2)	2.93×10^{-10}	1.5
	Zeolite 13X	323	0.0924(CO_2)	2.93×10^{-10}	1.5

Table 21: Works reported on the different configurations of PSA processes for purification of biomethane.

Reference	Experimental/simulated	PSA cycles	Pressure swing (kPa)	Bed regeneration time (min)	Steam feed composition (% molar fraction of CH_4)
[105]	Experimental	2 bed 6 steps	600-800 to 30-15	3.33-11.66	50-75
[102]	Simulated	2 beds 6 steps	650	4.16667	55
[103]	Simulated	1-2 beds 3-6 steps	347-350	2.3-2.55 min	64
[101]	Experimental	2 beds 4 steps	400	1.81667	55
[100]	Simulated	3 beds 10 steps	100	—	60

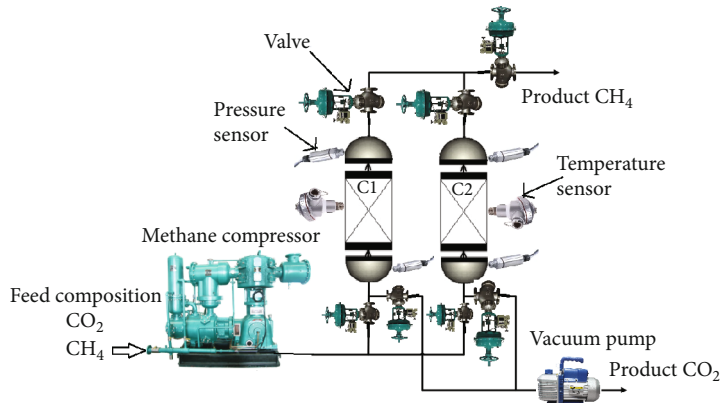

Figure 12: Schematic diagram of the PSA process using 2-beds, 6-steps.

Table 22: Distributed parameter models of the PSA processes for biomethane production.

Reference	Equations governing the PSA process (nonlinear model)	Temperature effects	Pressure effects
[101]	4 PDEs	Consider adsorption isotherms	Consider pressure gradient
[102]	3 PDEs	Consider adsorption isotherms	No pressure gradient
[107]	4 PDEs	Consider adsorption isotherms	Consider pressure gradient
[103]	3 PDEs	Consider adsorption isotherms	No pressure gradient
[100]	4 PDEs	Consider adsorption isotherms	Consider pressure gradient

contaminants such as H_2S, which may be present in the gas with concentrations of CO_2 35-50%, CH_4 50-65%, H_2S up to 4000 ppm, and siloxanes of 0-20 mgm^3. There are several technologies to produce biomethane, some of them are chemical absorption, water washing, membranes, pressure swing adsorption, and cryogenic. However, PSA has better advantages compared to the technologies mentioned, which are lower energy demand, higher biomethane recovery, separation of other possible compounds present in the biogas (N_2 and O_2), and it does not need H_2O.

6.1. Adsorption and Separation for the CH_4, CO_2 with Different Adsorbents. Isotherms for different single components of CO_2, CH_4, or CO were fitted using the BET, Langmuir, Freundlich, single or double-site isotherm. The isotherms are type I, II, and III. (see Figure 2).

There are different adsorbents to separate biogas and purify biomethane, these can be activated carbon, zeolite type 13X, clinoptilolite, etc. Table 20 simplifies the important points of each adsorbent, showing the adsorption parameters and capacities.

In Table 20, it can be seen that the adsorbents that have the highest adsorption capacity are zeolite type 13X, activated carbons and carbon molecular sieves, these zeolites are synthetic, however, clinoptilolite (natural zeolite) has good adsorption capacity despite being tested with high temperatures.

The design and configuration of the PSA for biomethane production depends largely on the properties of the adsorbent: adsorption load and diffusion, pressure, stable temperature, etc.

In Table 21, it can be seen that there are experimental and simulated works related to the production and purification of

Table 23: Governing equations and simplifications for production and purification of biomethane.

The component i mass balance	$-\varepsilon D_{ax}\frac{\partial y_i}{\partial z^2}+\frac{\partial\left(v_g c_i\right)}{\partial z}+\left(\varepsilon_b+(1-\varepsilon_b)\varepsilon_p\right)\frac{\partial c_i}{\partial t}+\rho_p(1-\varepsilon_b)\frac{\partial q_i}{\partial t}=0$
The energy balance	$\left(\left(\varepsilon_b+(1-\varepsilon_b)\varepsilon_p\right)\sum_{i=1}^{N}c_i\left(C_{\mathrm{cpg},i}M_i-R\right)+(1-\varepsilon_b)\rho_s C_{\mathrm{ps}}+(1-\varepsilon_b)\rho_s\sum_{i=1}^{N}q_i\left(c_{\mathrm{pg},i}M_i-R\right)\right)\frac{\partial T}{\partial t}+v_g\rho_g\sum_{i=1}^{N}C_{\mathrm{pg},i}M_i\frac{\partial T}{\partial Z}+\rho_s(1-\varepsilon_b)\sum_{i=1}^{N}\frac{\partial q_i}{\partial t}\Delta H+2h\frac{T-T_W}{R_b}-\left(\varepsilon_b+\varepsilon_p(1-\varepsilon_b)\right)\frac{\partial P}{\partial t}-k_g\frac{\partial^2 T}{\partial Z^2}=0$
The momentum balance	$-\frac{\partial P}{\partial Z}=\frac{150\mu\left(1-\varepsilon_p\right)^2}{\left(2R_p\right)^2\varepsilon_b^3}V_g+1.75\frac{(1-\varepsilon_b)\rho_g}{2R_p\varepsilon_b^3}\left\lvert V_g\right\rvert V_g$
Extended Langmuir equation	$q_i^*=\frac{q_{m,i}b_iP_i}{1+\sum_{i=1}^{n}b_iP_i},\ b_i=b_0\exp^{-(\Delta H_i/R)(1/T-(1/313-15))}$
LDF model	$\frac{\partial q_i}{\partial t}=15\frac{D_{c,i}}{R_p^2}(q_i^*-q_i),\ D_{c,i}=\frac{\varepsilon_p D_{k,i}D_m}{\tau(D_{k,i}+D_m)}$
Boundary and initial conditions	
I. Adsorption step	
(i) $t=0$	$Y_i=\mathrm{inlet}.Y_i,\ T=\mathrm{inlet}.T,\ P=\mathrm{inlet}.P$
(ii) $z=0$	$V_g>0,\ Y_i=\mathrm{inlet}.Y_i,\ T=\mathrm{inlet}.T,\ P=\mathrm{inlet}.P$
(iii) $z=L$	$\frac{\partial Y}{\partial z}=0,\ \frac{\partial T}{\partial z}=0,\ \frac{\partial P}{\partial z}=0$
II. Blowdown step	
(i) $t=0$	$Y_i=Y_i^{(I)},\ T=T^{(I)},\ P=P^{(I)}$
(ii) $z=0$	$\frac{\partial Y}{\partial z}=0,\ \frac{\partial T}{\partial z}=0,\ \frac{\partial P}{\partial z}=0$
(iii) $z=L$	$\frac{\partial Y}{\partial z}=0,\ \frac{\partial T}{\partial z}=0,\ \frac{\partial P}{\partial z}=0$
III. Purge step	
(i) $t=0$	$Y_i=Y_i^{(\mathrm{II})},\ T=T^{(\mathrm{II})},\ P=P^{(\mathrm{II})}$
(ii) $z=0$	$\frac{\partial Y}{\partial z}=0,\ \frac{\partial T}{\partial z}=0,\ \frac{\partial P}{\partial z}=0$
(iii) $z=L$	$\frac{\partial Y}{\partial z}=0,\ \frac{\partial T}{\partial z}=0,\ \frac{\partial P}{\partial z}=0$
IV. Repressurization step	
(i) $t=0$	$Y_i=Y_i^{(\mathrm{III})},\ T=T^{(\mathrm{III})},\ P=P^{(\mathrm{III})}$
(ii) $z=0$	$\frac{\partial Y}{\partial z}=0,\ \frac{\partial T}{\partial z}=0,\ \frac{\partial P}{\partial z}=0$
(iii) $z=L$	$\frac{\partial Y}{\partial z}=0,\ \frac{\partial T}{\partial z}=0,\ \frac{\partial P}{\partial z}=0$

Table 24: Start-up parameters of the PSA process for the purification and production of biomethane.

FEED		
Flow	0.0719	$kmolh^{-1}$
Methane	0.65	$kmolkmol^{-1}$
CO_2	0.35	$kmolkmol^{-1}$
Temperature	298.15	T
Production pressure	1000	kPa
Purge pressure	100	kPa
SIZING		
Bed height	1	m
Bed diameter	0.06	m
Zeolite 13X		
Particle radius	0.00157	m
Bulk solid density	1160.0	$Kg\,m^{-3}$

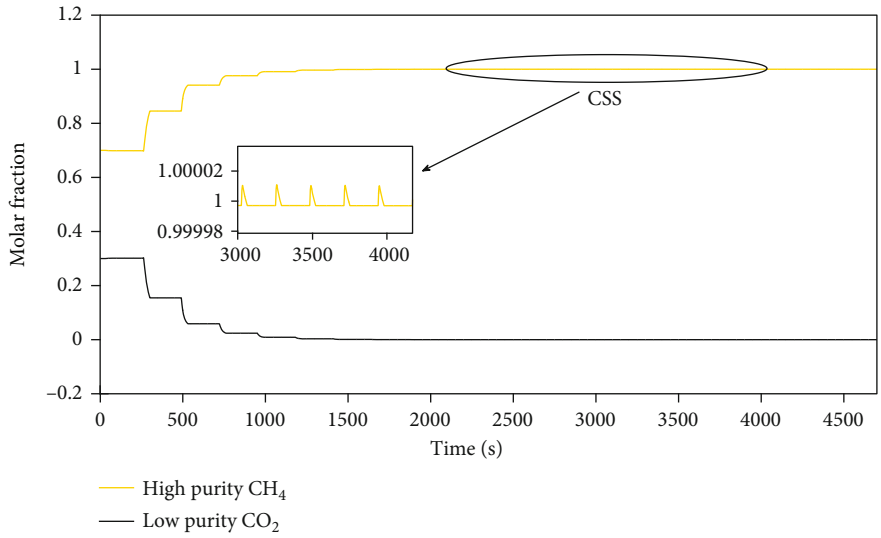

Figure 13: Purification and production of biomethane from the start-up.

biomethane, some of them work with more than two columns; however, the classic configuration is two columns. The pressure values in which the process oscillates are above 300 kPa up to 1000 kPa. Therefore, for the production of biomethane, it is necessary to contemplate pressures above 300 kPa. Regeneration times are longer compared to PSA for the production of medical oxygen and bioethanol.

Figure 12 shows the flow diagram of the PSA process for the production of biomethane. The feed flow is compressed to a specific pressure, then it is injected into the packed columns with selective adsorbents on the CO_2 compound. As a final product, a highly pure CH_4 is obtained. Part of the flow is recirculated through the vacuum pump to purge the column being regenerated. This process continues cyclically until a biomethane purity above 99% is obtained.

There are few works related to the production of biomethane, however, those found in the literature show a great contribution. Most of them are very complete works in describing their equations and propose models that consider both adsorption isotherms and pressure gradients. Table 22 shows some of them.

Table 23 shows a general model of the PSA process for biomethane production. The model was obtained from works the works of Abd et al., Ali et al., and Wu et al. [5, 101, 105]. The PSA cycle applied in this work consists of two integrated beds with four consecutive steps. The scheme of the cycle and its sequence are shown in Table 23. The Roman numerals represent the sequence of the steps, which are: (I) adsorption step; (II) blowdown step; (III) purge step; and (IV) repressurization step.

6.2. Parametric Study of the PSA Process for the Production of Biomethane. The parameters of this PSA process for the production and purification of biomethane are shown in the following Table 24.

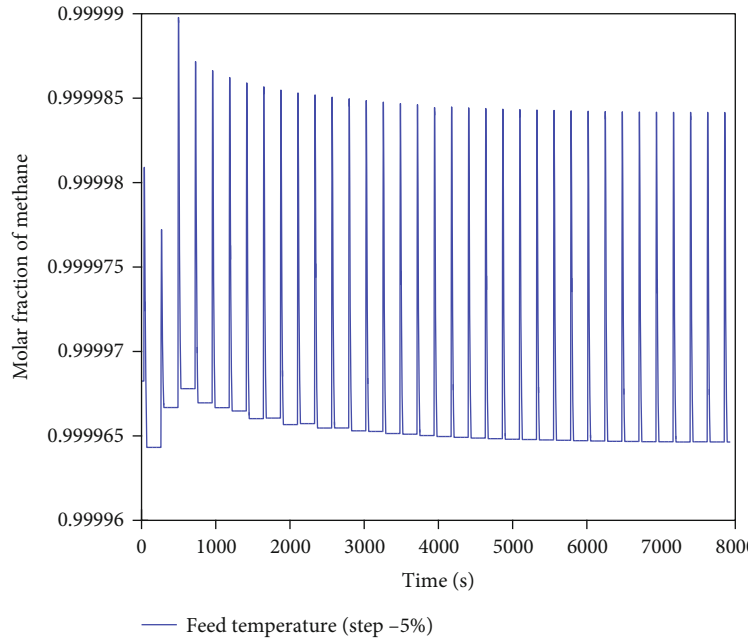

(a) Temperature: 303.15 K to 287.99 K; Flow: 0.0719 $kmolh^{-1}$; Pressure: 400 kPa; Molar fraction: 0.65 (CH_4) and 0.35 (CO_2)

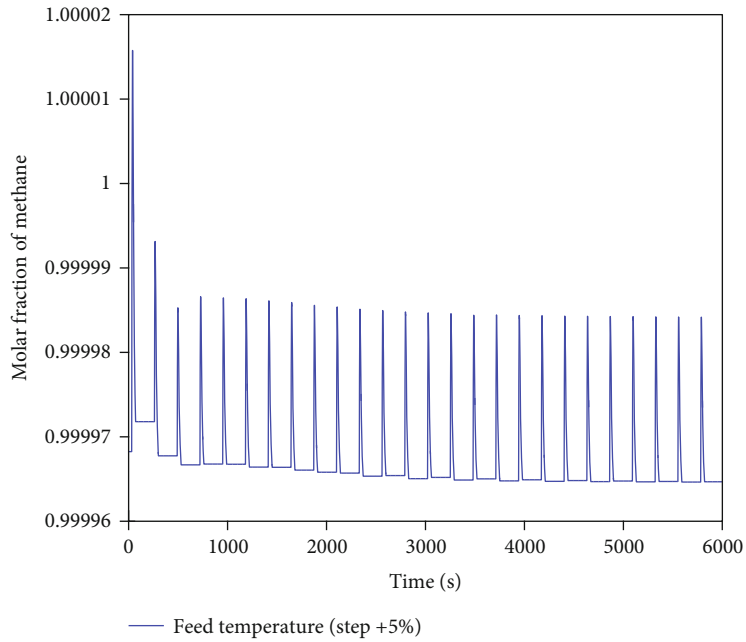

(b) Temperature: 303.15 K to 318.30 K; Flow: 0.0719 $kmolh^{-1}$; Pressure: 400 kPa; Molar fraction: 0.65 (CH_4) and 0.35 (CO_2)

Figure 14: Continued.

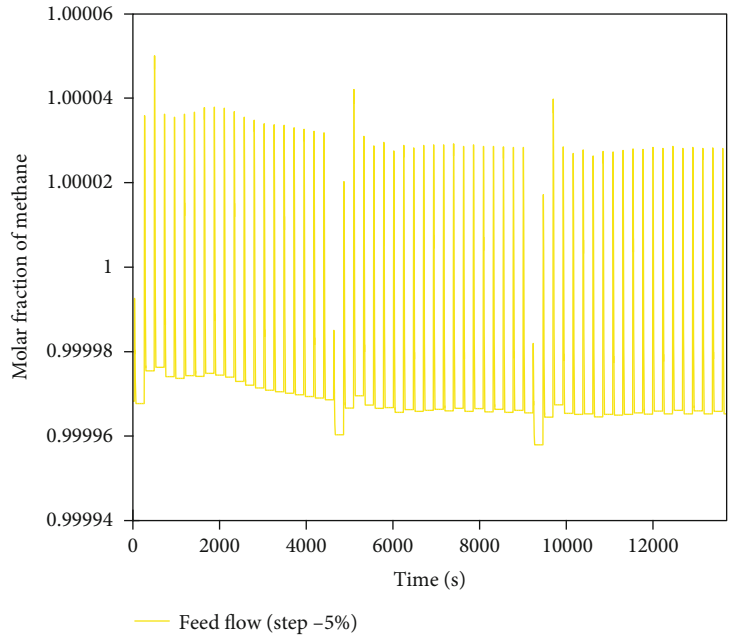

(c) Flow: 0.0719 kmolh^{-1} to 0.0683 kmolh^{-1}; Temperature: 303.15 K; Pressure: 400 kPa; Molar fraction: 0.65 (CH_4) and 0.35 (CO_2)

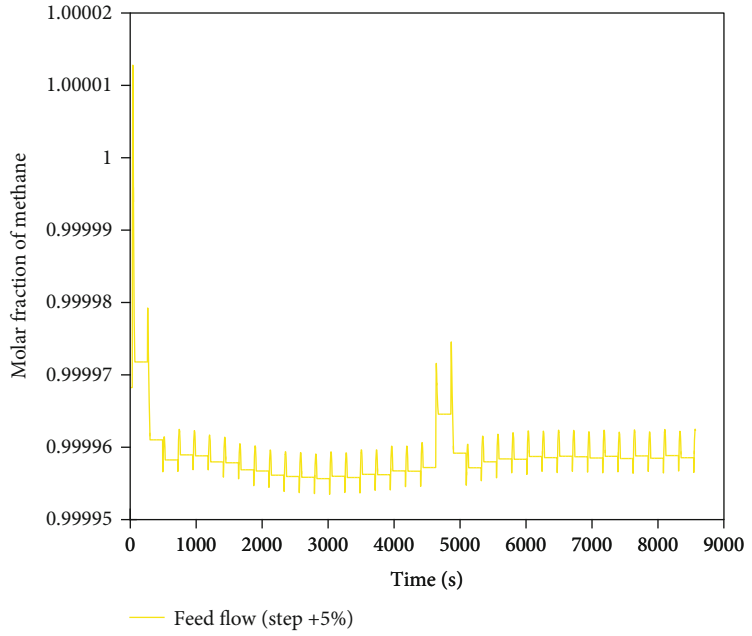

(d) Flow: 0.0719 kmolh^{-1} to 0.0755 kmolh^{-1}; Temperature: 303.15 K; Pressure: 400 kPa; Molar fraction: 0.65 (CH_4) and 0.35 (CO_2)

Figure 14: Continued.

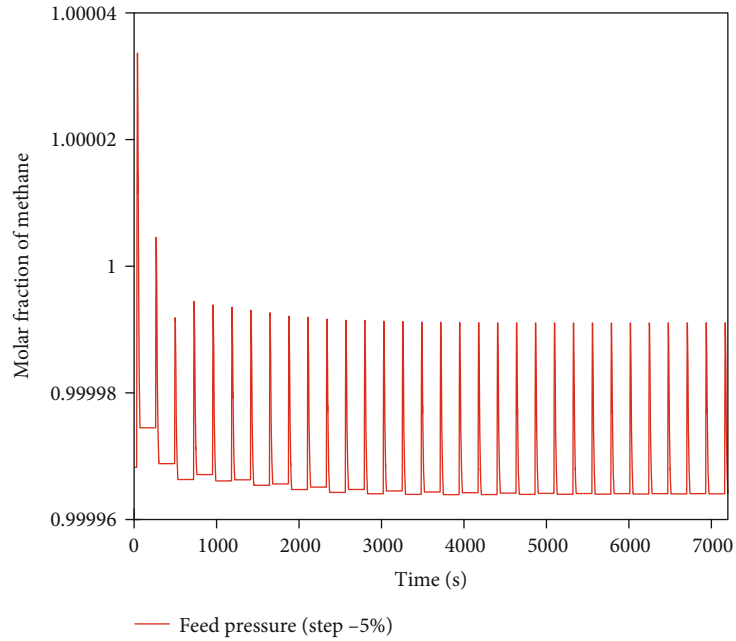

(e) Pressure: 400 kPa to 380 kPa; Flow: 0.0719 kmolh^{-1}; Temperature: 303.15 K; Molar fraction: 0.65 (CH_4) and 0.35 (CO_2)

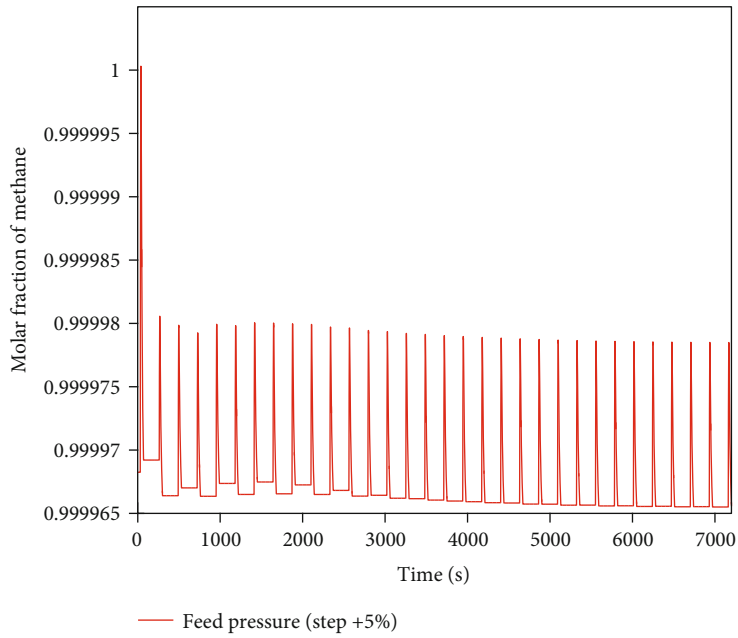

(f) Pressure: 400 kPa to 420 kPa; Flow: 0.0719 kmolh^{-1}; Temperature: 303.15 K; Molar fraction: 0.65 (CH_4) and 0.35 (CO_2)

Figure 14: Continued.

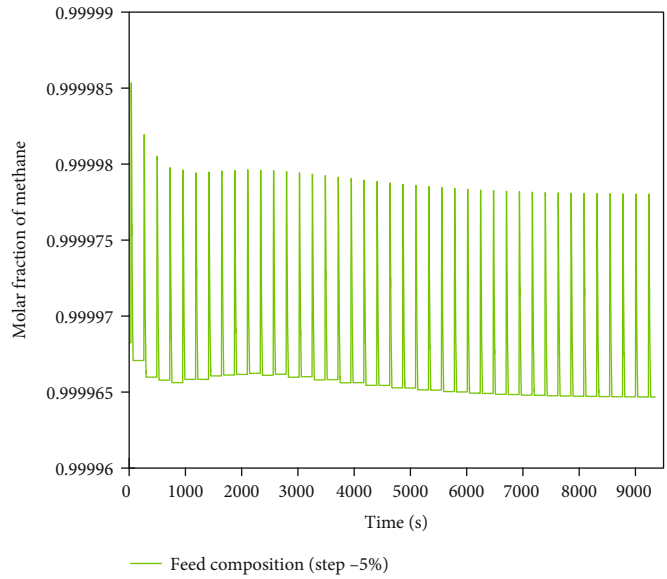

(g) Molar fraction: 0.65 (CO_2) and 0.35 (CO_2) to 0.6175 (CH_4) and 0.3825 (CO_2); Pressure: 400 kPa; Flow: 0.0719 $kmolh^{-1}$; Temperature: 303.15 K

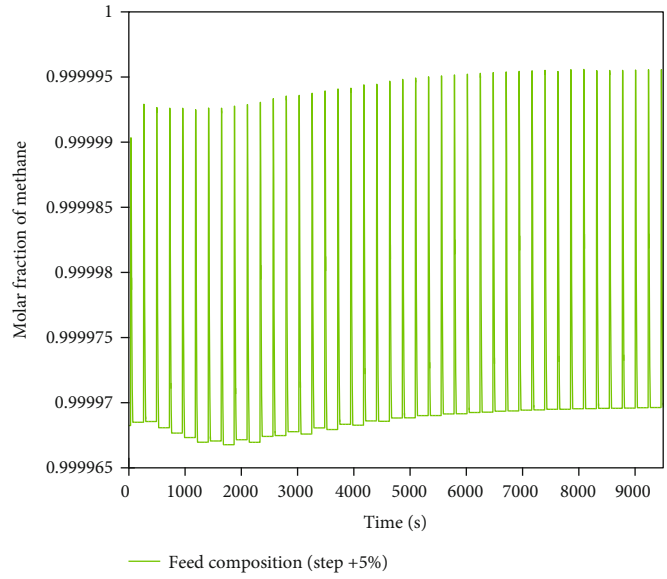

(h) Molar fraction: 0.65 (CH_4) and 0.35 (CO_2) to 0.6825 (CH_4) and 0.175 (CO_2); Pressure: 400 kPa; Flow: 0.0719 $kmolh^{-1}$; Temperature: 303.15 K

Figure 14: Sensitivity analysis applied to the PSA process for the production of biomethane.

Table 25: Analysis of the possible input variables that have the greatest effect on the purity obtained.

Run	Temperature (K)	Flow $kmolh^{-1}$	Pressure kPa	Composition CH_4-CO_2	Purity % molar fraction of CH_4	Number of cycles
1	303.15	0.0719	400	0.65-0.35	99.99	10
2	287.99	0.0719	400	0.65-0.35	99.9965	18
3	318.30	0.0719	400	0.65-0.35	99.997	13
4	303.15	0.0683	400	0.65-0.35	99.998	26
5	303.15	0.0755	400	0.65-0.35	99.996	18
6	303.15	0.0719	380	0.65-0.35	99.997	10
7	303.15	0.0719	420	0.65-0.35	99.9960	11
8	303.15	0.0719	400	0.6175-0.3825	99.9965	20
9	303.15	0.0719	400	0.6825-0.3175	99.9975	21

Figure 13 shows the methane and CO_2 profiles. The molar fraction of the methane rises in the first 3 cycles, this continues until reaching the CSS, which achieves a biomethane purity above 99%. On the other hand, the purity of CO_2 is declining.

Figure 14 shows the results of the sensitivity analysis and it is observed that all the variables have the same effect taking into account a variation of ± 0.05%. The effects shown on biomethane purity are small, but the flow variable can be taken into account as a possible variable to manipulate since it shows more outstanding profiles compared to the other variables. In order to better visualize this performance, it would be convenient to increase the variation value, in order to observe greater effects on biomethane purity.

Table 25 shows the detailed data of the results presented in Figure 14. It shows the cycle times, the purities, and the changes generated by each input variable.

7. Conclusions

The phenomenon of adsorption with molecular sieves has a great contribution to separating atoms or molecules from a gas or mixture, but it has a greater impact and scope using the PSA method. In this contributing review, the importance of the PSA process to purify and produce bioethanol, biohydrogen, medical oxygen, and biomethane is demonstrated.

The tendency to use this process is referred to the scope it has to produce purities above 99%, this scope of purification that this PSA process has is of great importance since they meet international purity standards to be used as fuels.

In this review, the different adsorbents that can be used for the separation and purification of the compounds of ethanol, hydrogen, oxygen, and methane were summarized. The effects of temperature and pressure have a great effect on the adsorption capacity. Synthetic adsorbents show that they have a better adsorption capacity, but natural adsorbents can be a widely used alternative to adsorb different compounds of natural gas or mixture since they have pores of different sizes and this is a great advantage over synthetic adsorbents.

The different configurations and models of the PSA process were shown and analyzed, showing that it is of great importance to contemplate the greatest number of PDEs in order to have general balance data, mass balance moment balance, energy balance, wall balance, thermodynamic balance, and kinetic, this in relation to having an approximation of results to real plants.

A parametric study was carried out, which allowed observing the purity achieved and the cycle times that are reached by varying certain input parameters. These results show that not all variables have the same effect and that they may be insignificant in the effect that is generated on the purity obtained.

Likewise, it can be concluded that the parametric study that was carried out for each case of separation and production of compounds was a great contribution to defining one or two variables that can control the purity obtained as a final product. These variables can also be seen as disturbances since they are at the input of the PSA process and can affect it if not controlled in a secondary way.

As future works, controllers can be designed on these plants to maintain the desired purity stable and meet international standards to be used as fuel. Processes can be optimized based on the results obtained and have greater recovery and production of bioethanol, biohydrogen, medical oxygen, and biomethane.

Data Availability

The simulations data used to support the findings of this study are included in the article.

Conflicts of Interest

The authors declare that they have no conflicts of interest.

References

[1] I. Ihsanullah, "Applications of MOFs as adsorbents in water purification: progress, challenges and outlook," *Current Opinion in Environmental Science Health*, vol. 26, article 100335, 2022.

[2] L. Ansone-bertina, V. Ozols, L. Arbidans et al., "Metal–organic frameworks (MOFs) containing adsorbents for carbon capture," *Energies*, vol. 15, p. 3473, 2022.

[3] A. D. Wiheeb, Z. Helwani, J. Kim, and M. R. Othman, "Pressure swing adsorption technologies for carbon dioxide capture," *Separation & Purification Reviews*, vol. 45, no. 2, pp. 108–121, 2016.

[4] X. Zhu, S. Li, Y. Shi, and N. Cai, "Recent advances in elevated-temperature pressure swing adsorption for carbon capture and hydrogen production," *Progress in Energy and Combustion Science*, vol. 75, article 100784, 2019.

[5] A. A. Abd, M. R. Othman, S. Z. Naji, and A. S. Hashim, "Methane enrichment in biogas mixture using pressure swing adsorption: process fundamental and design parameters," *Materials Today Sustainability*, vol. 11-12, article 100063, 2021.

[6] M. Luberti and H. Ahn, "Review of Polybed pressure swing adsorption for hydrogen purification," *International Journal of Hydrogen Energy*, vol. 47, no. 20, pp. 10911–10933, 2022.

[7] S. S. Hosseini and J. F. Denayer, "Biogas upgrading by adsorption processes: mathematical modeling, simulation and optimization approach - a review," *Journal of Environmental Chemical Engineering*, vol. 10, no. 3, article 107483, 2022.

[8] Y. Shen, Z. Tang, W. Li, and D. Zhang, "A review of numerical research on the pressure swing adsorption process," *Processes*, vol. 10, no. 5, p. 812, 2022.

[9] "Aspen plus|leading process simulation software|Aspentech," https://www.aspentech.com/en/products/engineering/aspen-plus.

[10] A. J. González Hernández, L. Avelino, U. García, A. Uscanga, and L. Solano, "Solución numérica del modelo en el proceso de adsorción para la deshidratación de etanol por medio de zeolitas," *Congreso Nacional de Control Automático*, 2017.

[11] J. Guan and X. Hu, "Simulation and analysis of pressure swing adsorption: ethanol drying process by the electrical analogue, separation and purification technology," *Separation And Purification Technology*, vol. 31, no. 1, p. 31, 2003, http://www.elsevier.com/locate/seppur.

[12] T. Yamamoto, Y. H. Kim, B. C. Kim, A. Endo, N. Thongprachan, and T. Ohmori, "Adsorption characteristics of zeolites for dehydration of ethanol: evaluation of diffusivity of water in porous structure," *Chemical Engineering Journal*, vol. 181-182, pp. 443–448, 2012.

[13] E. Ivanova, D. Damgaliev, and M. Kostova, "Adsorption separation of ethanol-water liquid mixtures by natural clinoptilolite," *Journal of the University of Chemical Technology and Metallurgy*, vol. 44, pp. 267–274, 2009.

[14] J. Y. Rumbo Morales, A. F. Perez Vidal, G. Ortiz Torres et al., "Adsorption and separation of the H2O/H2SO4 and H2O/C2H5OH mixtures: a simulated and experimental study," *Processes*, vol. 8, p. 290, 2020, https://www.mdpi.com/2227-9717/8/3/290/htmhttps://www.mdpi.com/2227-9717/8/3/290.

[15] S. Al-Asheh, F. Banat, and A. A. Fara, "Dehydration of ethanol-water azeotropic mixture by adsorption through phillipsite packed-column," *Separation Science and Technology*, vol. 44, no. 13, pp. 3170–3188, 2009.

[16] P. Huo, Y. Zhang, L. Zhang et al., "Insight into the adsorption process of ethanol and water on the pore structure and surface chemistry properties engineered activated carbon fibers," *Industrial Engineering Chemistry Research*, vol. 60, no. 30, pp. 11141–11150, 2021.

[17] Y. R. Son, S. G. Ryu, and H. S. Kim, "Rapid adsorption and removal of sulfur mustard with zeolitic imidazolate frameworks ZIF-8 and ZIF-67," *Microporous and Mesoporous Materials*, vol. 293, article 109819, 2020.

[18] G. Leo-Avelino, G. Urrea-Garcia, J. Gómez-Rodríguez, S. Perez-Correa, and M. Aguilar-Uscanga, "Natural Mexican clinoptilolite for ethanol dehydration: adsorption–regeneration experimental parameter determination and scaling–up at pilot plant," *Revista Mexicana de Ingeniería Química*, vol. 20, no. 3, pp. 1–11, 2021, http://www.rmiq.org/ojs311/index.php/rmiq/article/view/2358.

[19] H. Chang, X. G. Yuan, H. Tian, and A. W. Zeng, "Experimental study on the adsorption of water and ethanol by cornmeal for ethanol dehydration," *Industrial and Engineering Chemistry Research*, vol. 45, no. 11, pp. 3916–3921, 2006.

[20] Y. Wang, C. Gong, J. Sun, H. Gao, S. Zheng, and S. Xu, "Separation of ethanol/water azeotrope using compound starch-based adsorbents," *Bioresource Technology*, vol. 101, no. 15, pp. 6170–6176, 2010.

[21] J. A. Delgado, M. A. Uguina, J. L. Sotelo, V. I. Águeda, A. García, and A. Roldán, "Separation of ethanol-water liquid mixtures by adsorption on silicalite," *Chemical Engineering Journal*, vol. 180, pp. 137–144, 2012.

[22] S. Karimi, B. Ghobadian, M. R. Omidkhah, J. Towfighi, and M. Tavakkoli Yaraki, "Experimental investigation of bioethanol liquid phase dehydration using natural clinoptilolite," *Journal of Advanced Research*, vol. 7, no. 3, pp. 435–444, 2016.

[23] K. Kupiec, J. Rakoczy, L. Zieliński, and A. Georgiou, "Adsorption-desorption cycles for the separation of vapour phase ethanol/water mixtures," *Adsorption Science Technology*, vol. 26, no. 3, pp. 209–224, 2008.

[24] A. Ricardo and G. Soto, *Síntesis, caracterización y evaluación de un tamiz molecular para la deshidratación de etanol azeotrópico, Ph. D. thesis*, Institutional Repository of Universidad Nacional de Columbia, 2012.

[25] T. Kristóf, É. Csányi, G. Rutkai, and L. Merényi, "Prediction of adsorption equilibria of water–methanol mixtures in zeolite NaA," *Molecular Simulation*, vol. 32, no. 10-11, pp. 869–875, 2007.

[26] M. Carmo and J. Gubulin, "Ethanol-water adsorption on commercial 3A zeolites: kinetic and thermodynamic data," *Brazilian Journal of Chemical Engineering*, vol. 14, no. 3, pp. 217–224, 1997, http://www.scielo.br/j/bjce/a/XnGLp8855JYfV7ckCLvsjzS/?lang=en.

[27] A. Chaibi, Y. Boucheffa, and N. Bendjaballah-Lalaoui, "TGA investigation of water and ethanol adsorption over LTA zeolites," *Microporous and Mesoporous Materials*, vol. 324, article 111285, 2021.

[28] H. J. Huang, S. Ramaswamy, U. W. Tschirner, and B. V. Ramarao, "A review of separation technologies in current and future biorefineries," *Separation and Purification Technology*, vol. 62, no. 1, pp. 1–21, 2008.

[29] M. Simo, S. Sivashanmugam, C. J. Brown, and V. Hlavacek, "Adsorption/desorption of water and ethanol on 3A zeolite in near-adiabatic fixed bed," *Industrial and Engineering Chemistry Research*, vol. 48, no. 20, pp. 9247–9260, 2009.

[30] E. Ebrahimiaqda and K. L. Ogden, "Simulation and cost analysis of distillation and purification step in production of anhydrous ethanol from sweet sorghum," *ACS Sustainable Chemistry and Engineering*, vol. 5, no. 8, pp. 6854–6862, 2017.

[31] J. Y. Morales, G. L. López, V. M. Martínez, F. D. Vázquez, J. A. Mendoza, and M. M. García, "Parametric study and control of a pressure swing adsorption process to separate the waterethanol mixture under disturbances," *Separation and Purification Technology*, vol. 236, article 116214, 2020.

[32] J. Y. Rumbo-Morales, G. Lopez-Lopez, V. M. Alvarado, J. S. Valdez-Martinez, F. D. Sorcia-Vázquez, and J. A. Brizuela-Mendoza, "Simulation and control of a pressure swing adsorption process to dehydrate ethanol," *Revista Mexicana de Ingeniera Quimica*, vol. 17, no. 3, pp. 1051–1081, 2018.

[33] P. Pruksathorn and T. Vitidsant, "Production of pure ethanol from azeotropic solution by pressure swing adsorption," *Korean Journal of Chemical Engineering*, vol. 26, no. 4, pp. 1106–1111, 2009.

[34] M. Simo, C. J. Brown, and V. Hlavacek, "Simulation of pressure swing adsorption in fuel ethanol production process," *Computers and Chemical Engineering*, vol. 32, no. 7, pp. 1635–1649, 2008.

[35] J.-S. Jeong, B.-U. Jang, Y.-R. Kim, B.-W. Chung, and G.-W. Choi, "Production of dehydrated fuel ethanol by pressure swing adsorption process in the pilot plant," *Korean Journal of Chemical Engineering*, vol. 26, no. 5, pp. 1308–1312, 2009.

[36] J. S. Jeong, H. Jeon, K. M. Ko, B. Chung, and G. W. Choi, "Production of anhydrous ethanol using various PSA (pressure swing adsorption) processes in pilot plant," *Renewable Energy*, vol. 42, pp. 41–45, 2012.

[37] D. Gutiérrez-González, G. Urrea-García, G. Luna-Solano, D. Cantú-Lozano, and J. Gómez-Rodriguez, "Numerical solution of adsorption cycle in ethanol dehydration process," *Procedia Manufacturing*, vol. 49, pp. 32–37, 2020.

[38] K. E. Kang, J. S. Jeong, Y. Kim, J. Min, and S. K. Moon, "Development and economic analysis of bioethanol production facilities using lignocellulosic biomass," *Journal of Bioscience and Bioengineering*, vol. 128, no. 4, pp. 475–479, 2019.

[39] J. Y. Morales, J. A. Mendoza, G. O. Torres, F. D. Vázquez, A. C. Rojas, and A. F. Vidal, "Fault-tolerant control implemented to Hammerstein-Wiener model: application to bioethanol dehydration," *Fuel*, vol. 308, article 121836, 2022.

[40] M. Zhang, H. Sui, H. Yang, X. Li, L. He, and J. Liu, "Adsorption–desorption behaviors of methanol and ethyl acetate on silica gel: modeling and experimental tests," *Industrial Engineering Chemistry Research*, vol. 60, no. 4, pp. 1829–1838, 2021.

[41] E. M. Renteria-Vargas, C. J. Zuniga Aguilar, J. Y. Rumbo Morales et al., "Neural network-based identification of a PSA process for production and purification of bioethanol," *IEEE Access*, vol. 10, pp. 27771–27782, 2022.

[42] J.-J. Lee, M.-K. Kim, D.-G. Lee, H. Ahn, M.-J. Kim, and C.-H. Lee, "Heat-exchange pressure swing adsorption process for hydrogen separation," *AICHE Journal*, vol. 54, no. 8, pp. 2054–2064, 2008.

[43] J. Xiao, Y. Peng, P. Bénard, and R. Chahine, "Thermal effects on breakthrough curves of pressure swing adsorption for hydrogen purification," *International Journal of Hydrogen Energy*, vol. 41, no. 19, pp. 8236–8245, 2016.

[44] X. Zhu, Q. Wang, Y. Shi, and N. Cai, "Layered double oxide/activated carbon-based composite adsorbent for elevated temperature H_2/CO_2 separation," *International Journal of Hydrogen Energy*, vol. 40, no. 30, pp. 9244–9253, 2015.

[45] X. Zhu, Y. Shi, N. Cai, S. Li, and Y. Yang, "Techno-economic evaluation of an elevated temperature pressure swing adsorption process in a 540 MW IGCC power plant with CO_2 capture," *Energy Procedia*, vol. 63, pp. 2016–2022, 2014.

[46] X. Zhu, Y. Shi, S. Li, N. Cai, and E. J. Anthony, "CHAPTER 5: system and processes of pre-combustion carbon dioxide capture and separation," in *Pre-combustion Carbon Dioxide Capture Materials*, pp. 281–334, 2018.

[47] R. Kothari, D. Buddhi, and R. Sawhney, "Sources and technology for hydrogen production: a review," *International Journal of Global Energy Issues*, vol. 21, no. 1/2, pp. 154–178, 2004.

[48] N. Akhlaghi and G. Najafpour-Darzi, "A comprehensive review on biological hydrogen production," *International Journal of Hydrogen Energy*, vol. 45, no. 43, pp. 22492–22512, 2020.

[49] G. Balachandar, J. L. Varanasi, V. Singh, H. Singh, and D. Das, "Biological hydrogen production via dark fermentation: a holistic approach from lab-scale to pilot-scale," *International Journal of Hydrogen Energy*, vol. 45, no. 8, pp. 5202–5215, 2020.

[50] W. Liemberger, M. Groß, M. Miltner, and M. Harasek, "Experimental analysis of membrane and pressure swing adsorption (PSA) for the hydrogen separation from natural gas," *Journal of Cleaner Production*, vol. 167, pp. 896–907, 2017.

[51] S. Sircar and T. C. Golden, "Purification of hydrogen by pressure swing adsorption," *Separation Science and Technology*, vol. 35, no. 5, pp. 667–687, 2006.

[52] M.-B. Kim, Y.-S. Bae, H. Ahn, and C.-H. Lee, "Comparison of adsorption dynamics in kinetic and equilibrium beds in hydrogen ternary system," *Separation science and technology*, vol. 39, no. 13, pp. 2951–2976, 2010.

[53] Y. S. Bae and C. H. Lee, "Sorption kinetics of eight gases on a carbon molecular sieve at elevated pressure," *Carbon*, vol. 43, no. 1, pp. 95–107, 2005.

[54] N. Zhang, P. Bénard, R. Chahine, T. Yang, and J. Xiao, "Optimization of pressure swing adsorption for hydrogen purification based on box-Behnken design method," *International Journal of Hydrogen Energy*, vol. 46, no. 7, pp. 5403–5417, 2021.

[55] W. Tao, S. Ma, J. Xiao, P. Bénard, and R. Chahine, "Simulation and optimization for hydrogen purification performance of vacuum pressure swing adsorption," *Energy Procedia*, vol. 158, pp. 1917–1923, 2019.

[56] B. Silva, I. Solomon, A. M. Ribeiro et al., "H2 purification by pressure swing adsorption using CuBTC," *Separation and Purification Technology*, vol. 118, pp. 744–756, 2013.

[57] J. Xiao, L. Fang, P. Bénard, and R. Chahine, "Parametric study of pressure swing adsorption cycle for hydrogen purification using cu-BTC," *International Journal of Hydrogen Energy*, vol. 43, no. 30, pp. 13962–13974, 2018.

[58] M. Yavary, H. A. Ebrahim, and C. Falamaki, "The effect of number of pressure equalization steps on the performance of pressure swing adsorption process," *Chemical Engineering and Processing: Process Intensification*, vol. 87, pp. 35–44, 2015.

[59] S. G. Subraveti, K. N. Pai, A. K. Rajagopalan et al., "Cycle design and optimization of pressure swing adsorption cycles for pre- combustion CO_2 capture," *Applied Energy*, vol. 254, article 113624, 2019.

[60] B. Ohs, M. Falkenberg, and M. Wessling, "Optimizing hybrid membrane-pressure swing adsorption processes for biogenic hydrogen recovery," *Chemical Engineering Journal*, vol. 364, pp. 452–461, 2019.

[61] R. F. Moreira, J. L. Soares, G. L. Casarin, and A. E. Rodrigues, "Adsorption of CO2 on hydrotalcite-like compounds in a fixed bed," *Separation Science And Technology*, vol. 41, no. 2, pp. 341–357, 2007.

[62] A. Harale, H. T. Hwang, P. K. Liu, M. Sahimi, and T. T. Tsotsis, "Experimental studies of a hybrid adsorbent-membrane reactor (HAMR) system for hydrogen production," *Chemical Engineering Science*, vol. 62, no. 15, pp. 4126–4137, 2007.

[63] J. R. Hufton, S. Mayorga, and S. Sircar, "Sorption-enhanced reaction process for hydrogen production," *AICHE Journal*, vol. 45, no. 2, pp. 248–256, 1999.

[64] Y. Ding and E. Alpay, "Equilibria and kinetics of CO_2 adsorption on hydrotalcite adsorbent," *Chemical Engineering Science*, vol. 55, no. 17, pp. 3461–3474, 2000.

[65] K. B. Lee, A. Verdooren, H. S. Caram, and S. Sircar, "Chemisorption of carbon dioxide on potassium-carbonate-promoted hydrotalcite," *Journal of Colloid and Interface Science*, vol. 308, no. 1, pp. 30–39, 2007.

[66] S.-I. Yang, D.-Y. Choi, S.-C. Jang, S.-H. Kim, and D.-K. Choi, "Hydrogen separation by multi-bed pressure swing adsorption of synthesis gas," *Adsorption*, vol. 14, no. 4, pp. 583–590, 2008.

[67] B. Li, G. He, X. Jiang, Y. Dai, and X. Ruan, "Pressure swing adsorption/membrane hybrid processes for hydrogen purification with a high recovery," *Frontiers of Chemical Science and Engineering*, vol. 10, no. 2, pp. 255–264, 2016.

[68] P. Hao, Y. Shi, S. Li, X. Zhu, and N. Cai, "Correlations between adsorbent characteristics and the performance of pressure swing adsorption separation process," *Fuel*, vol. 230, pp. 9–17, 2018.

[69] J. Schell, N. Casas, D. Marx, and M. Mazzotti, "Precombustion CO2Capture by pressure swing adsorption (PSA): comparison of laboratory PSA experiments and simulations," *Industrial and Engineering Chemistry Research*, vol. 52, no. 24, pp. 8311–8322, 2013.

[70] D. K. Moon, Y. Park, H. T. Oh, S. H. Kim, M. Oh, and C. H. Lee, "Performance analysis of an eight-layered bed PSA

process for H_2 recovery from IGCC with pre-combustion carbon capture," *Energy Conversion and Management*, vol. 156, pp. 202–214, 2018.

[71] D. K. Moon, D. G. Lee, and C. H. Lee, "H_2 pressure swing adsorption for high pressure syngas from an integrated gasification combined cycle with a carbon capture process," *Applied Energy*, vol. 183, pp. 760–774, 2016.

[72] M. Martínez García, J. Y. Rumbo Morales, G. O. Torres et al., "Simulation and state feedback control of a pressure swing adsorption process to produce hydrogen," *Mathematics*, vol. 10, no. 10, p. 1762, 2022.

[73] S. Suzuki, G. M. Eastwood, N. J. Glassford et al., "Conservative oxygen therapy in mechanically ventilated patients," *Critical Care Medicine*, vol. 42, no. 6, pp. 1414–1422, 2014, https://okayama.pure.elsevier.com/en/publications/conservative-oxygen-therapy-in-mechanica-\lly-ventilated-patients-a.

[74] L. A. Munro, "A modification of the pyrogallol method for determining the amount of oxygen in the air," *Journal of Chemical Education*, vol. 5, no. 6, pp. 741-742, 1928.

[75] P. Todur, S. Chaudhuri, M. Eeshwar, D. Teckchandani, and R. Venkateswaran, "Oxygen sources and delivery devices: essentials during COVID-19," *Indian Journal of Respiratory Care*, vol. 10, no. 2, p. 171, 2021.

[76] S. W. Chai, M. V. Kothare, and S. Sircar, "Rapid pressure swing adsorption for reduction of bed size factor of a medical oxygen concentrator," *Industrial and Engineering Chemistry*, vol. 50, no. 14, pp. 8703–8710, 2011.

[77] S. Qadir, D. Li, Y. Gu et al., "Experimental and numerical analysis on the enhanced separation performance of a medical oxygen concentrator through two-bed rapid pressure swing adsorption," *Industrial and Engineering Chemistry Research*, vol. 60, no. 16, pp. 5903–5913, 2021.

[78] C. W. Wu, R. R. Vemula, M. V. Kothare, and S. Sircar, "Experimental study of a novel rapid pressure-swing adsorption based medical oxygen concentrator: effect of the adsorbent selectivity of N2 over O2," *Industrial and Engineering Chemistry Research*, vol. 55, no. 16, pp. 4676–4681, 2016.

[79] T. Banaszkiewicz and M. Chorowski, "Energy consumption of air-separation adsorption methods," *Entropy*, vol. 20, no. 4, p. 232, 2018.

[80] X. Jin, A. Malek, and S. Farooq, "Production of argon from an oxygen-argon mixture by pressure swing adsorption," *Industrial and Engineering Chemistry Research*, vol. 45, no. 16, pp. 5775–5787, 2006.

[81] M. B. Kim, J. G. Jee, Y. S. Bae, and C. H. Lee, "Parametric study of pressure swing adsorption process to purify oxygen using carbon molecular sieve," *Industrial and Engineering Chemistry Research*, vol. 44, no. 18, pp. 7208–7217, 2005.

[82] D. M. Ruthven and S. Farooq, "Air separation by pressure swing adsorption," *Gas Separation Purification*, vol. 4, no. 3, pp. 141–148, 1990.

[83] V. Rama Rao, S. Farooq, and W. B. Krantz, "Design of a two-step pulsed pressure-swing adsorption-based oxygen concentrator," *AICHE Journal*, vol. 56, no. 2, pp. 354–370, 2009.

[84] R. S. Todd, J. He, P. A. Webley, C. Beh, S. Wilson, and M. A. Lloyd, "Fast finite-volume method for PSA/VSA cycle simulation experimental validation," *Industrial and Engineering Chemistry Research*, vol. 40, no. 14, pp. 3217–3224, 2001.

[85] J. C. Santos, P. Cruz, T. Regala, F. D. Magalhães, and A. Mendes, "High-purity oxygen production by pressure swing adsorption," *Industrial and Engineering Chemistry Research*, vol. 46, no. 2, pp. 591–599, 2007.

[86] S. Sircar and W. C. Kratz, "A pressure swing adsorption process for production of 23–50 air," *Separation Science and Technology*, vol. 23, no. 4-5, pp. 437–450, 2006.

[87] X. Zhu, Y. Liu, X. Yang, and W. Liu, "Study of a novel rapid vacuum pressure swing adsorption process with intermediate gas pressurization for producing oxygen," *Adsorption*, vol. 23, no. 1, pp. 175–184, 2017.

[88] M. Xu, H. C. Wu, Y. S. Lin, and S. Deng, "Simulation and optimization of pressure swing adsorption process for high-temperature air separation by perovskite sorbents," *Chemical Engineering Journal*, vol. 354, pp. 62–74, 2018.

[89] X. Zheng, Y. Liu, and W. Liu, "Two-dimensional modeling of the transport phenomena in the adsorber during pressure swing adsorption process," *Industrial and Engineering Chemistry Research*, vol. 49, no. 22, pp. 11814–11824, 2010.

[90] C. S. Chang, S. H. Ni, H. S. Yang, and C. T. Chou, "Simulation study of separating oxygen from air by pressure swing adsorption process with semicylindrical adsorber," *Journal of the Taiwan Institute of Chemical Engineers*, vol. 120, pp. 67–76, 2021.

[91] C. T. Chou and W. C. Huang, "Simulation of a four-bed pressure swing adsorption process for oxygen enrichment," *Industrial and Engineering Chemistry Research*, vol. 33, no. 5, pp. 1250–1258, 1994.

[92] J. G. Jee, M. B. Kim, and C. H. Lee, "Pressure swing adsorption processes to purify oxygen using a carbon molecular sieve," *Chemical Engineering Science*, vol. 60, no. 3, pp. 869–882, 2005.

[93] Y. Liu, Q. Zhang, Y. Cao et al., "Effect of intermittent purge on O2 production with rapid pressure swing adsorption technology," *Adsorption*, vol. 27, no. 2, pp. 181–189, 2020.

[94] S. A. Skvortsov, E. I. Akulinin, O. O. Golubyatnikov, D. S. Dvoretsky, and S. I. Dvoretsky, "Mathematical modelling of cyclic pressure swing adsorption processes," *Journal of Physics: Conference Series*, vol. 1015, no. 3, article 032002, 2018.

[95] J. C. Santos, A. F. Portugal, F. D. Magalhães, and A. Mendes, "Simulation and optimization of small oxygen pressure swing adsorption units," *Industrial and Engineering Chemistry Research*, vol. 43, no. 26, pp. 8328–8338, 2004.

[96] S. Sircar and B. F. Hanley, "Production of oxygen enriched air by rapid pressure swing adsorption," *Adsorption*, vol. 1, no. 4, pp. 313–320, 1995.

[97] X. Zhu, Y. Liu, and R. T. Yang, "Effects of operating temperature on the performance of small scale rapid cycle pressure swing adsorption air separation process," *Adsorption*, vol. 27, no. 2, pp. 205–212, 2020.

[98] M. D. Urich, R. R. Vemula, and M. V. Kothare, "Multi-model predictive control of a novel rapid pressure swing adsorption system," in *Proceedings of the American Control Conference*, pp. 4392–4397, Seattle, WA, USA, 2017.

[99] P. A. Webley and J. He, "Fast solution-adaptive finite volume method for PSA/VSA cycle simulation; 1 single step simulation," *Computers Chemical Engineering*, vol. 23, no. 11-12, pp. 1701–1712, 2000.

[100] C. Yin, W. Sun, H. Yang, and D. Zhang, "Optimization of three-bed VPSA system for biogas upgrading," *Chemical Engineering Science*, vol. 135, pp. 100–108, 2015.

[101] A. Ali Abd and M. Roslee Othman, "Biogas upgrading to fuel grade methane using pressure swing adsorption: parametric sensitivity analysis on an industrial scale," *Fuel*, vol. 308, article 121986, 2022.

[102] B. Kottititum, T. Srinophakun, N. Phongsai, and Q. T. Phung, "Optimization of a six-step pressure swing adsorption process for biogas separation on a commercial scale," *Applied Sciences*, vol. 10, no. 14, p. 4692, 2020, https://www.mdpi.com/2076-3417/10/14/4692/htmhttps://www.mdpi.com/2076-3417/10/14/4692.

[103] Y. F. Chen, P. W. Lin, W. H. Chen, F. Y. Yen, H. S. Yang, and C. T. Chou, "Biogas upgrading by pressure swing adsorption with design of experiments," *Processes*, vol. 9, p. 1325, 2021, https://www.mdpi.com/2227-9717/9/8/1325/htmhttps://www.mdpi.com/2227-9717/9/8/1325.

[104] R. García Franco, M. Á. Hernández, R. Portillo Reyes et al., "Adsorciód de CO2, H2 y CH4 en zeolitas naturales de poro agosto," *Revista Internacional De Contaminación Ambiental*, vol. 34, no. 4, pp. 685–696, 2018, http://www.scielo.org.mx/scielo.php?script=sci_arttextpid=S0188-49992018000400685lng=esnrm=isotlng=eshttp://www.scielo.org.mx/scielo.php?script=sci_abstractpid=S0188-49992018000400685 lng=es nrm=isotlng=es.

[105] B. Wu, X. Zhang, Y. Xu, D. Bao, and S. Zhang, "Assessment of the energy consumption of the biogas upgrading process with pressure swing adsorption using novel adsorbents," *Journal of Cleaner Production*, vol. 101, pp. 251–261, 2015.

[106] M. Patrícia, S. Santos, R. Alírio, and C. Grande, *Advanced modelling of PSA processes for biogas upgrading Ph.D. thesis*, Faculdade de Engenharia Universidade do Porto, 2011.

[107] A. A. Norani, A. Ahmad, T. A. Abdullah, and A. Ripin, "Parametric study of CO2 separation using carbon molecular sieve, zeolite and silica gel," *IOP Conference Series: Materials Science and Engineering*, vol. 808, no. 1, article 012041, 2020.